To the Graduate Council:

I am submitting herewith a thesis written by Brant E. Kanak entitled "Analysis of a Gas Absorption System with Soluble Carrier Gas and Volatile Solvent." I recommend that it be accepted in partial fulfillment of the requirements for the degree of Master of Science, with a major in Chemical Engineering.

Joseph J. Perona, Major Professor

We have read this thesis
and recommend its acceptance:

H. W. Haw

J. D. Watson

Accepted for the Council:

Vice Chancellor
Graduate Studies and Research

3

ANALYSIS OF A GAS ABSORPTION SYSTEM WITH SOLUBLE CARRIER GAS AND VOLATILE SOLVENT

A Thesis

Presented for the

Master of Science

Degree

The University of Tennessee, Knoxville

Brant E. Kanak

August 1979

ACKNOWLEDGMENTS

This work was performed at the Oak Ridge Gaseous Diffusion Plant by Union Carbide Corporation for the U. S. Department of Energy under U. S. Government Contract W-7405 eng-26.

The author would like to express his appreciation to several people who contributed to the success of this work. Dr. Joe Perona served as the author's major advisor and patiently provided overall direction during this long project. The program manager, Dr. Mike Stephenson, provided continual guidance and encouragement and is largely responsible for the thoroughness of this work. The generous contribution of Jane Higdon in the typing and editing of this manuscript is evident throughout. Dr. Bob Merriman reviewed this report as it progressed and kept the author on the straight and narrow. Jeff Patton was of great assistance in the experimental work. Finally, the author would like to thank his parents, Florence and Ervin Kanak, for raising him to have confidence in his abilities.

ABSTRACT

The effects of column diameter, carrier gas coabsorption, and solvent vaporization on the performance of a packed gas absorption column are examined. The system investigated employs dichlorodifluoromethane as a solvent to remove krypton from a nitrogen stream and is characterized by substantial nitrogen coabsorption.

Three columns with diameters of 2, 3, and 4 inches were constructed and packed with 34.5 inches of Goodloe packing. In addition to the more conventional data, the experimental evaluation of these columns included the use of a radioisotope and a gamma scanning technique which provided direct measurement of the columns' molar krypton profiles. A multicomponent gas absorption model was developed, based on the two-film mass transfer theory, that allows the fluxes of all species to interact. Verification of this model was achieved through comparison of the calculated results with experimental data.

With the feed gas flow rate between 6 and 36 lb moles/hr-ft^2 and the solvent feed rate between 40 and 400 lb moles/hr-ft^2, column diameter was found to have no significant impact on the mass transfer efficiency of this system when carried out in columns with diameters of 2 inches or greater. The absorption of krypton was found to be enhanced and inhibited, respectively, by carrier gas coabsorption and solvent vaporization. An injector system to add gaseous solvent to the feed gas stream prior to its introduction into the packed bed was proposed to eliminate the detrimental effects of solvent vaporization. Using this injector to supersaturate the feed gas stream with solvent enhanced absorber performance in the same manner as carrier gas coabsorption.

TABLE OF CONTENTS

LIST OF TABLES

LIST OF FIGURES

FIGURE PAGE

FIGURE PAGE

FIGURE PAGE

FIGURE PAGE

CHAPTER I

INTRODUCTION

A. BACKGROUND

Irradiation of nuclear fuels results in the production of substantial quantities of the radioactive isotope of krypton, Kr^{85}. A typical light water nuclear power reactor, for example, will produce 400,000 curies of Kr^{85} per gigawatt-year of electric power generated.[12] Some of this, less than 1%, is leaked to the reactor cooling circuit from faulty fuel rods, but most is released when the fuel is sheared and dissolved during reprocessing.[21] Although nontoxic, Kr^{85} has a half-life of 10.7 years, and in response to the increasing concern over the possible long-term effects of radioactive emissions, the Environmental Protection Agency has stipulated that the total release of Kr^{85} must be limited to 50,000 curies per gigawatt-year of electric power generated after 1983.[13] This then requires the nuclear fuel reprocessor to remove approximately 90% of all fission product krypton from the reprocessing plant off-gas and store it in a suitable repository.

In 1959, Steinberg[41, 42] suggested that krypton could be selectively absorbed from the gaseous wastes of a reprocessing plant by using dichlorodifluoromethane (R-12) as a solvent. A pilot plant was built in 1967 at the Oak Ridge Gaseous Diffusion Plant (ORGDP) to determine the general feasibility of the fluorocarbon-based process. This plant proved operable and successfully contained greater than 99.9% of the krypton present in the process feed. Based on an analysis of the

overall performance of this pilot plant[46] and the experience gained through its operation, a second generation facility was designed in 1972 and put into operation in late 1974.[44] This plant, shown in Figure I-1, has greater flexibility, tighter control, and more sophisticated analytical equipment than did the original test facility and is providing the data necessary for a thorough engineering analysis of the fluorocarbon process.

The ongoing development effort at ORGDP has identified the fluorocarbon selective absorption process as one of the most versatile of the proposed off-gas processing schemes for krypton retention. This work will culminate with the detailed design criteria for the construction of a demonstration off-gas treatment facility.

B. PROCESS DESCRIPTION

The role of the selective absorption process in a nuclear fuel reprocessing plant is to remove Kr^{85} from the plant's gaseous waste stream and subsequently concentrate the krypton for long-term radioactive waste storage. Three operations, absorption, fractional stripping, and final stripping, are needed to accomplish these two objectives. Each of these steps performs a separation by exploiting the prevailing solubility difference between nitrogen and krypton in the process solvent, R-12. Figure I-2 is a schematic of the selective absorption process.

The primary separation is accomplished in the absorber. The process feed gas, a nitrogen stream containing small amounts of krypton, is compressed, cooled, and passed into the bottom of a packed gas

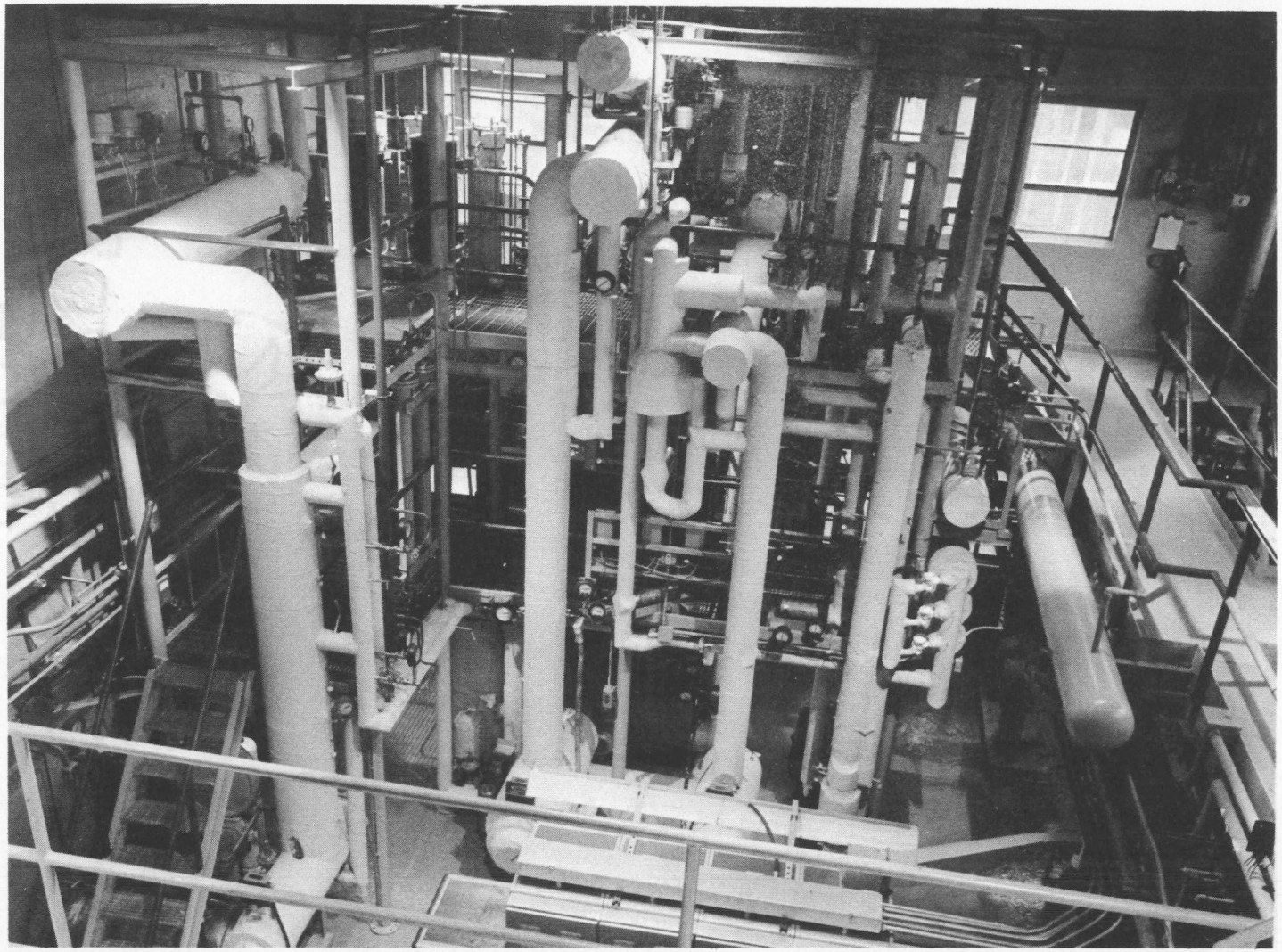

Figure I-1
OVERVIEW OF THE ORGDP PILOT PLANT

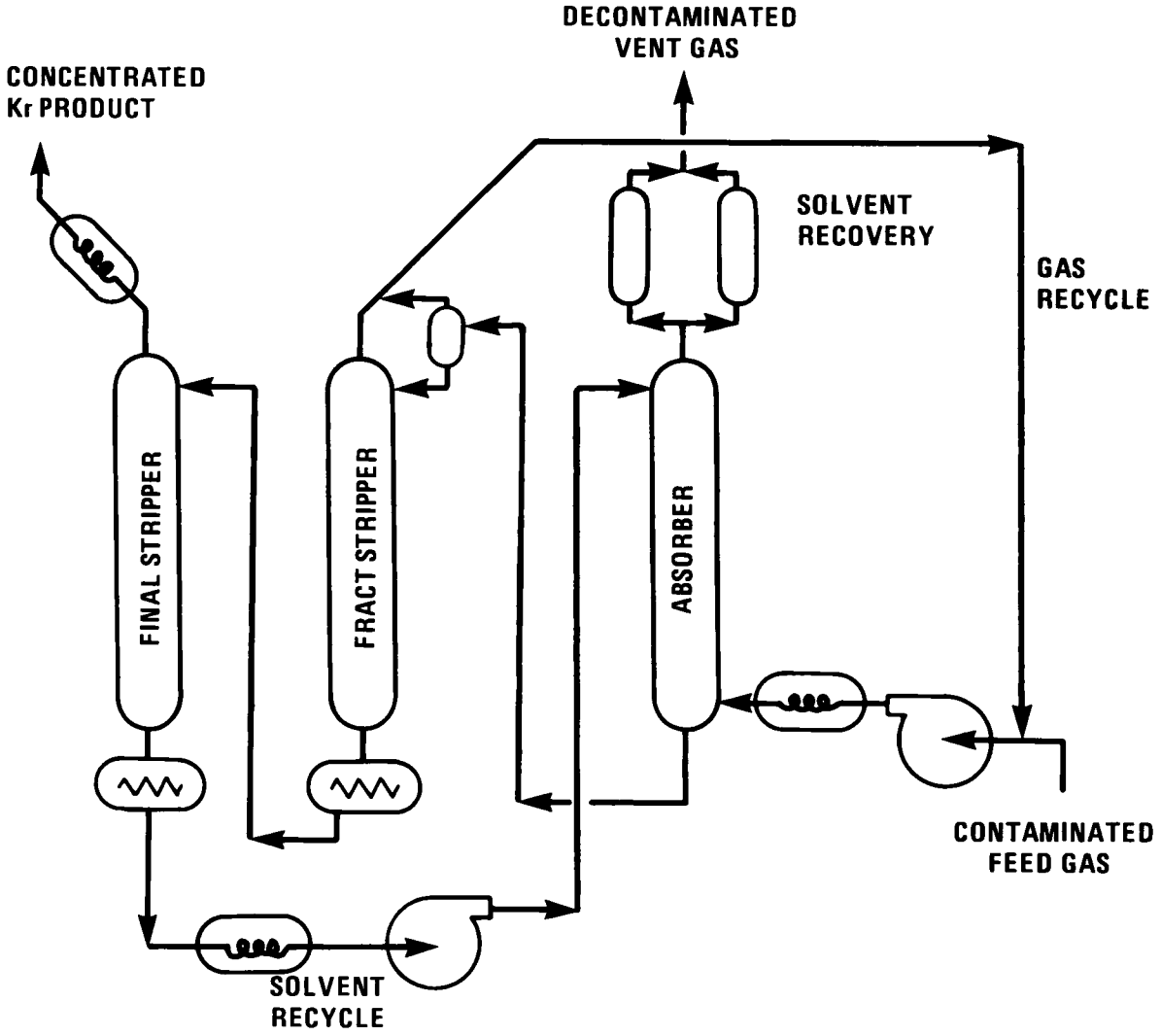

Figure I-2

SCHEMATIC OF THE FLUOROCARBON PROCESS

absorption column. Regenerated solvent is cooled and pumped into the top of the absorber. The column is typically operated with the pressure between 100 and 300 psig and the temperature between -5 and -30°F. Within these limits, most of the krypton can be absorbed. However, at the conditions necessary to affect this krypton absorption, a large amount of nitrogen will also be dissolved. The off-gas from this column is nearly saturated with R-12 which must be removed before the gas can be vented. The loaded solvent leaving the absorber is passed on to the intermediate stripping stage.

Fractional stripping is carried out to desorb the nitrogen dissolved in the absorber and enrich the remaining dissolved gas in krypton. This stage contains a flash chamber and a packed column with a reboiler that are operated at a pressure substantially less than that of the absorber, normally 35 to 50 psig. The reboiler is kept at the saturation temperature of the solvent, which is 52°F for a column pressure of 50 psig. As the loaded solvent from the absorber enters the flash chamber, a large portion of the nitrogen desorbs. The solvent then enters the packed column where another fraction of the nitrogen is driven off. Since a perfect cut is not possible, the off-gas from this stage contains some krypton and is therefore recycled back to the absorber where it is mixed with the process feed at the suction of the gas compressor. The solvent withdrawn from the stripper's reboiler contains dissolved gas that is highly enriched in krypton.

The final stripping operation serves to recover the krypton and regenerate the process solvent. This stage, which consists of a packed column with a reboiler and condenser, is operated at an even lower pressure, usually 15 psig. The remaining dissolved gas is driven off in

this operation and collected as the concentrated gaseous product. Essentially pure R-12 is pulled from the reboiler, cooled, and pumped back to the absorber for reuse.

The primary process components of the ORGDP pilot plant can be identified in Figure I-1 and are, from right to left, the absorber, intermediate stripper, and final stripper. The column on the far left of Figure I-1 is a solvent distillation column which can be used to separate the R-12 from any high-boiling component that may collect in the reboiler of the final stripper. A detailed description of the ORGDP selective absorption pilot plant is given by Stephenson, Eby, and Huffstetler.[45]

C. PROBLEM STATEMENT

Engineering design of a commercial scale demonstration facility requires packed column scale-up data in addition to the usual pilot plant performance information. Previous pilot plant work has yielded only the performance data. The primary purpose of this thesis is to examine absorber performance as a function of column diameter. This work required the construction of three interchangeable test absorbers and the operation and analysis of these columns as an integral part of the ORGDP selective absorption pilot plant.

Carrier gas coabsorption has been shown to have a significant impact on the dissolution of krypton in the fluorocarbon process absorber.[26] This work has demonstrated that the flux of the solvent can also strongly effect krypton absorption. These interactions, although usually neglected in the analysis of gas absorbers, must be considered in a thorough engineering analysis of this absorption system.

Absorption data from the first generation pilot facility has been subjected to three types of analysis through the course of the ORGDP development program. Each effort presented a significant improvement over the previous attempt by incorporating more detail and more accurately representing the physical situation. Although none of these approaches accounted for interaction between the fluxes of all three components, the latest, done in 1975 by Merriman, did account for the effect carrier gas absorption has on the absorption of krypton.[26] It should be noted that these investigators did not have use of the relatively newly developed packed column gamma scanner[43] and were primarily limited to end-point analysis. These works were also hampered by relatively limited flow measurement and control instrumentation.[34]

This thesis contains a more general engineering model of the fluorocarbon process absorber. The derivation of this model included allowances for the flux of krypton, the carrier gas, and solvent and the interaction of these fluxes. The improved analytical techniques employed in the present pilot plant provided the data necessary to fit this model to the performance of the three test absorbers. This work represents the final design model of the fluorocarbon process absorber. Stephenson[43] has completed models of the intermediate and final strippers. Together, these models will be used to establish the design criteria for the construction of a full-scale facility.

CHAPTER II

THEORY

Gas absorption is an operation in which a gas mixture is contacted with a liquid for the purpose of selectively dissolving one or more components of the gas and to provide a solution of these in the liquid. The formulation of the differential equations governing gas absorption is relatively straightforward. Determining solutions to these equations, however, can present formidable difficulties unless certain simplifying assumptions can be made. In this chapter, these differential equations are developed, and several commonly used assumptions and their respective solutions are presented. The applicability of these solutions to the fluorocarbon process absorber is discussed in the following chapter.

A. DEVELOPMENT OF GOVERNING EQUATIONS

The equations describing gas absorption can be developed around the differential column section depicted in Figure II-1. The gas phase continuity equation for species j can be written over this volume as

$$\frac{\partial C_j}{\partial t} + \frac{1}{r}\frac{\partial}{\partial r}(r\, N_{jr}) + \frac{1}{r}\frac{\partial N_{j\theta}}{\partial \theta} + \frac{\partial N_{jz}}{\partial z} = R_j, \qquad \text{II-1}$$

where C_j = molar concentration of j in gas phase, lb moles/ft^3,

N_{jr} = molar flux of j in radial direction, lb moles/hr-ft^2,

$N_{j\theta}$ = molar flux of j in angular direction, lb moles/hr-ft^2,

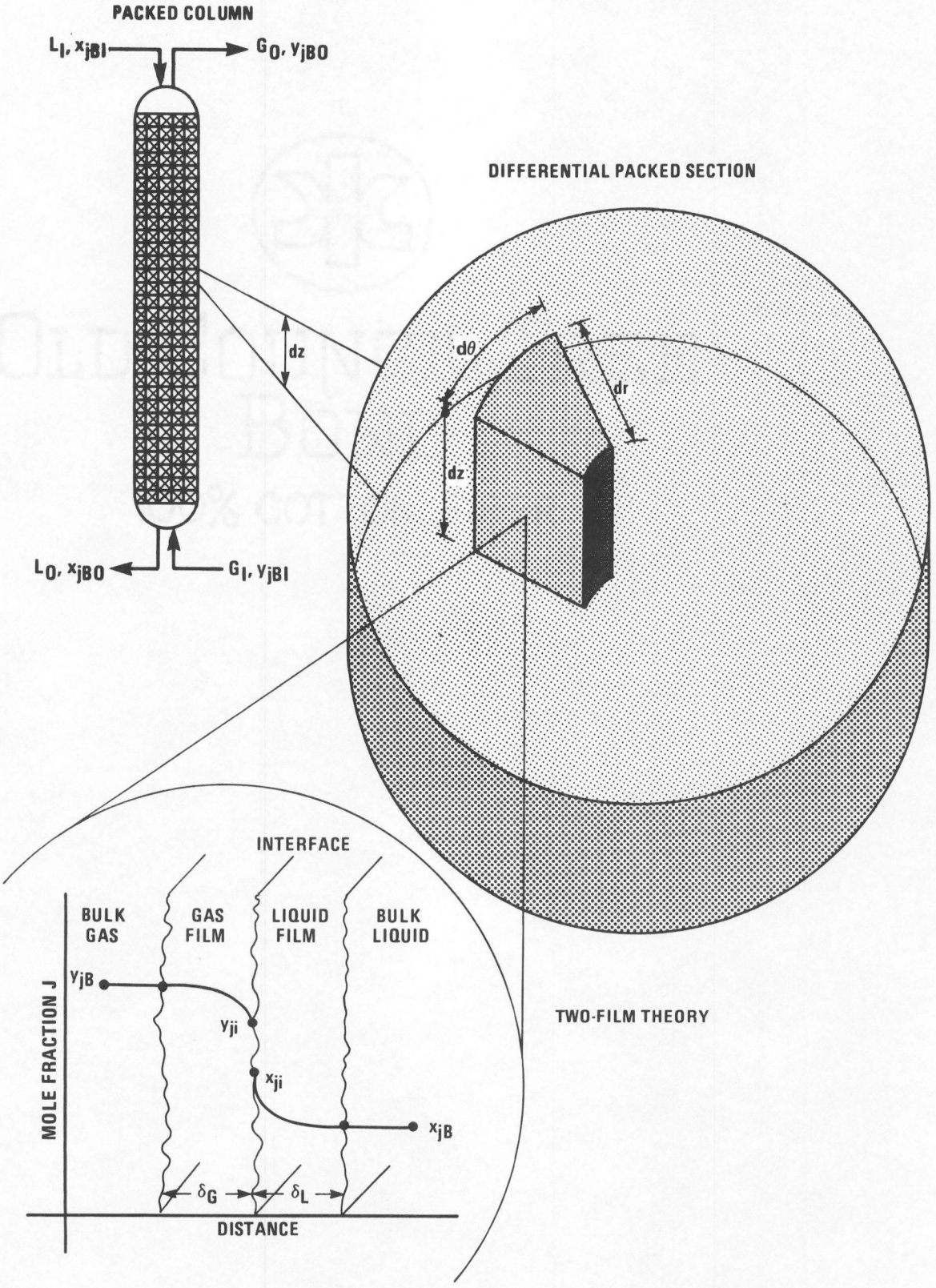

Figure II-1
DIFFERENTIAL PACKED SECTION AND TWO-FILM THEORY

N_{jz} = molar flux of j in axial direction, lb moles/hr-ft^2, and

R_j = rate of depletion of j from gas phase, lb moles/hr-ft^3.

At steady state, if the radial and angular fluxes are assumed to be negligible, equation II-1 reduces to

$$\frac{dN_{jz}}{dz} = R_j. \qquad \text{II-2}$$

According to the plug-flow model, neglecting axial dispersion, the axial flux can be expressed as

$$N_{jz} = Gy_{jB}, \qquad \text{II-3}$$

where G = molar bulk gas flow rate, lb moles/hr-ft^2, and

y_{jB} = bulk gas mole fraction of j.

This further reduces the species continuity equation to

$$\frac{d(Gy_{jB})}{dz} = R_j. \qquad \text{II-4}$$

In gas absorption, the rate at which the gas phase is depleted of component j, R_j, is the rate at which j is absorbed by the liquid. The Whitman two-film theory[49] is commonly used to describe this interphase mass transfer. According to this model, thin gas and liquid films separate the bulk gas from the bulk liquid. All the resistance to mass transfer and, correspondingly, the only concentration gradients present are confined within these films. Transport through the films occurs by molecular diffusion. At the gas-liquid interface, it is assumed that the gas and liquid compositions are in equilibrium. Figure II-1

demonstrates the application of this theory to the differential column section under consideration. Although some experimental evidence does not support this model, in most cases, equilibrium does exist at the interface and the two-film theory can be used to successfully predict interphase mass transfer.[48]

As these films are very thin compared to the radius of any curvature present, they will be assumed to have slab geometry with concentration gradients existing only in the direction perpendicular to the gas-liquid interface. Flux across the gas film can then be described by the one-dimensional representation of Fick's law of diffusion for ideal solutions.

$$N_{ji} = y_j \sum_k N_{ki} - D_{jM} C_T \frac{dy_j}{d\ell}, \qquad \text{II-5}$$

where N_{ji} = molar flux of j across the gas film perpendicular to the gas-liquid interface, lb moles/hr-ft^2 interfacial area,

y_j = gas phase mole fraction of j,

D_{jM} = molecular diffusivity, ft^2/hr,

C_T = total molar concentration, lb moles/ft^3, and

ℓ = distance in the gas film, ft.

At steady state, if the diffusivity and total molar concentration are assumed constant, integration of equation II-5 from the bulk gas, across the gas film, to the gas liquid interface, yields

$$N_{ji} = Q_j \frac{D_{jM} C_T}{\delta_G} \ln \left(\frac{Q_j - y_{ji}}{Q_j - y_{jB}} \right), \qquad \text{II-6}$$

where δ_G = thickness of gas film, ft,

y_{ji} = interfacial gas mole fraction of j, and

$Q_j = N_{ji}/\Sigma_k N_{ki}$.

This relation strictly applies only to stagnant film diffusion. In order to apply equation II-6 to turbulent systems, the grouping $D_{jM}C_T/\delta_G$ is replaced with F_{Gj}, the Colburn-Drew mass transfer coefficient.[10] This parameter, a function of the physical properties of the system and the conditions of flow, accounts for the additional transport due to turbulence and has the same units as the terms it replaced, lb moles/hr-ft^2. Thus,

$$N_{ji} = Q_j F_{Gj} \ln \left(\frac{Q_j - y_{ji}}{Q_j - y_{jB}}\right). \qquad \text{II-7}$$

As N_{ji} is the interphase transfer per effective interfacial surface area, the product of N_{ji} and a, the effective interfacial surface area per unit volume, is the rate of gas phase depletion of j, or

$$N_{ji}\, a = R_j. \qquad \text{II-8}$$

Substitution of equations II-4 and II-8 into equation II-7 gives

$$d(Gy_{jB}) = W_j F_{Gj} a \ln \left(\frac{W_j - y_{ji}}{W_j - y_{jB}}\right) dz, \qquad \text{II-9}$$

where $W_j = d(Gy_{jB})/dG$.

A similar development based on the liquid phase leads to

$$d(Lx_{jB}) = V_j F_{Lj} a \ln \left(\frac{V_j - x_{jB}}{V_j - x_{ji}}\right) dz, \qquad \text{II-10}$$

where $V_j = d(Lx_{jB})/dL$,

L = molar bulk liquid flow rate, lb moles/hr-ft^2,

x_{jB} = bulk liquid mole fraction of j,

F_{Lj} = Colburn-Drew liquid phase mass transfer coefficient for j, lb moles/hr-ft^2 interfacial area, and

x_{ji} = interfacial liquid mole fraction of j.

Equations II-9 and II-10 show the interaction between the interfacial fluxes of the different species present. If the bulk flux, dG, is large and positive, the absorption of species j will be enhanced, exhibiting greater flux than would be expected from inspection of just its concentration gradient. On the other hand, if the bulk flux is large and negative, indicating bulk movement into the gas phase, the absorption of j will be inhibited. If this negative flux is large enough, species j can be caused to move against its concentration gradient. Toor and Sebulsky[47] termed this last effect "reverse diffusion." These interactions can be of considerable importance in the analysis of a gas absorber, but unfortunately, are usually ignored.

B. ABSORPTION OF ONE COMPONENT

If it can be assumed that only species j will undergo interphase transport,

$$dG = d(Gy_{jB}), \qquad \text{II-11}$$

and equation II-9 simplifies to

$$d(Gy_{jB}) = F_{Gj} a \ln \left(\frac{1 - y_{ji}}{1 - y_{jB}}\right) dz. \qquad \text{II-12}$$

Although G will vary with column position, G_C, the molar flow rate of insoluble gas(es), will not. Since

$$G_C = (1 - y_{jB})\ G, \qquad \text{II-13}$$

$$d(Gy_{jB}) = G_C\ d\left(\frac{y_{jB}}{1 - y_{jB}}\right) = G_C\ \frac{dy_{jB}}{(1 - y_{jB})^2} = G\ \frac{dy_{jB}}{1 - y_{jB}}. \qquad \text{II-14}$$

Substituting this into equation II-12, rearranging, and integrating,

$$Z = \int_{y_{jBO}}^{y_{jBI}} \frac{G\ dy_{jB}}{F_{Gj}a\ (1 - y_{jB})\ \ln\left(\frac{1 - y_{ji}}{1 - y_{jB}}\right)}, \qquad \text{II-15}$$

where Z = depth of packing, ft,

y_{jBI} = inlet bulk gas mole fraction of j, and

y_{jBO} = outlet bulk gas mole fraction of j.

Since

$$y_{jB} - y_{ji} = (1 - y_{ji}) - (1 - y_{jB}), \qquad \text{II-16}$$

equation II-15 can be rewritten as

$$Z = \int_{y_{jBO}}^{y_{jBI}} \left(\frac{G}{F_{Gj}a}\right) \frac{[(1 - y_{ji}) - (1 - y_{jB})]\ dy_{jB}}{(1 - y_{jB})\ (y_{jB} - y_{ji})\ \ln\left(\frac{1 - y_{ji}}{1 - y_{jB}}\right)} \qquad \text{II-17}$$

or

$$Z = \int_{y_{jBO}}^{y_{jBI}} \left(\frac{G}{F_{Gj}a}\right) \frac{(1 - y_j)_{iBM}}{(1 - y_{jB})(y_{jB} - y_{ji})} dy_{jB}, \qquad \text{II-18}$$

where $(1 - y_j)_{iBM}$ = log - mean of $(1 - y_{ji})$ and $(1 - y_{jB})$.

Although G, F_{Gj}, and a are all expected to vary along the packed bed, the ratio $G/F_{Gj}a$ is usually assumed to be constant, removed from the integral, and defined as H_{TG}, the height of a gas transfer unit. Equation II-18 can now be expressed as

$$Z = H_{TG} \int_{y_{jBO}}^{y_{jBI}} \frac{(1 - y_j)_{iBM}\, dy_{jB}}{(1 - y_{jB})(y_{jB} - y_{ji})}. \qquad \text{II-19}$$

The remaining integral, defined as the number of gas transfer units, N_{TG}, can be further simplified by substitution of the arithmetic mean for the log-mean to the form

$$N_{TG} = \int_{y_{jBO}}^{y_{jBI}} \frac{dy_{jB}}{(y_{jB} - y_{ji})} + \frac{1}{2} \ell n \left(\frac{1 - y_{jBO}}{1 - y_{jBI}}\right), \qquad \text{II-20}$$

which can be graphically integrated.

An analogous set of expressions can be derived by the same procedure from the liquid phase continuity equation.

C. OVERALL COEFFICIENTS

Overall mass transfer coefficients are often used to avoid the difficulties involved in determining interfacial compositions. The gas

phase overall mass transfer coefficient is defined such that

$$d(Gy_{jB}) = W_j \, F_{OGj} a \, \ell n \left(\frac{W_j - y_j^*}{W_j - y_{jB}}\right) dz, \qquad \text{II-21}$$

where F_{OGj} = overall gas phase mass transfer coefficient for species j, lb moles/hr-ft^2 interfacial area, and

y_j^* = gas phase mole fraction of j that would exist in equilibrium with the bulk liquid.

If, again, it can be assumed that only one component is absorbed, $G/F_{OGj}a$ is constant, and the arithmetic mean can be substituted for the log-mean, a development identical to that shown previously can be used to reduce equation II-21 to

$$Z = H_{OG} \, N_{OG}, \qquad \text{II-22}$$

where $H_{OG} = G/F_{OGj}a$, height of an overall gas transfer unit, ft, and

$$N_{OG} = \int_{y_{jBO}}^{y_{jBI}} \frac{dy_{jB}}{(y_{jB} - y_j^*)} + \frac{1}{2} \ell n \left(\frac{1 - y_{jBO}}{1 - y_{jBI}}\right), \qquad \text{II-23}$$

number of overall gas transfer units.

In dilute solutions, the last term in equation II-23 is negligible and may be omitted. Also, the gas and liquid flow rates become nearly constant in dilute solutions, so a mass balance on the absorbing species, j, around a section of column which includes the top can be written as

$$x_{jB} = x_{jBI} - \frac{G}{L} (y_{jBO} - y_{jB}). \qquad \text{II-24}$$

If it can be further assumed the equilibrium distribution curve can be approximated by a straight line over the region of interest,

$$y_j^* = m\, x_{jB} + b, \qquad \text{II-25}$$

an expression can be derived for y_j^* which does not contain x_{jB}. Substitution of this relation into equation II-23 yields

$$N_{OG} = \int_{y_{jBO}}^{y_{jBI}} \frac{dy_{jB}}{y_{jB} - [(y_{jB} - y_{jBO})\frac{G}{L} + x_{jBI}]\, m - b}, \qquad \text{II-26}$$

which can be integrated to the form

$$N_{OG} = \frac{1}{1 - \frac{mG}{L}} \ln \left[\frac{(y_{jBI} - m\, x_{jBI} - b)}{(y_{jBO} - m\, x_{jBI} - b)} \left(1 - \frac{mG}{L}\right) + \frac{mG}{L}\right]. \qquad \text{II-27}$$

Assuming that Henry's law applies (b = 0) and defining the ratio $\frac{mG}{L}$ as A, the absorption factor, equation II-27 becomes

$$N_{OG} = \frac{1}{1 - A} \ln \left[\left(\frac{y_{jBI} - m\, x_{jBI}}{y_{jBO} - m\, x_{jBI}}\right) (1 - A) + A\right], \qquad \text{II-28}$$

which is Colburn's[9] integrated form of the design equation, probably the most commonly used relation in the analysis of gas absorbers.

D. EQUIMOLAR COUNTERDIFFUSION

The special case of equimolar counterdiffusion cannot be evaluated through use of the previously derived expressions. As the molar

flow rates do not change (dL = dG = 0), equations II-9, II-10, page 12, and II-21 become undefined. It is therefore necessary to reevaluate equation II-5,

$$N_{ji} = y_j \sum_k N_k - D_{jM} C_T \frac{dy_j}{d\ell}. \qquad \text{II-5}$$

As the flux across the gas-liquid interface from the gas to the liquid is equal to the flux in the opposing direction,

$$\sum_k N_k = 0, \qquad \text{II-29}$$

which simplifies equation II-5 to

$$N_{ji} = -D_{jM} C_T \, dy_j/d\ell. \qquad \text{II-30}$$

Integration across the gas film followed by substitution of equations II-4, page 10, and II-8, page 12, into the result yields

$$d(Gy_{jB}) = \frac{D_{jM} C_T}{\delta_G} a \, (y_{jB} - y_{ji}) \, dz. \qquad \text{II-31}$$

As was done earlier, the quantity $D_{jM}C_T/\delta_G$ is replaced with a mass transfer coefficient giving

$$d(Gy_{jB}) = k_{Gj} a \, (y_{jB} - y_{ji}) \, dz, \qquad \text{II-32}$$

where k_{Gj} = the equimolar counterdiffusion gas phase mass transfer coefficient for species j, lb moles/hr-ft^2 interfacial area.

Overall coefficients are also used in this situation to avoid determining interfacial compositions. The gas phase coefficient is defined such that

$$d(Gy_{jB}) = k_{OGj}a\ (y_{jB} - y_j^*)\ dz, \qquad \text{II-33}$$

where k_{OGj} = the overall equimolar counterdiffusion gas phase mass transfer coefficient for species j, lb moles/hr-ft^2 interfacial area.

Even though equations II-32 and II-33 are strictly valid only in the case of equimolar counterdiffusion, because of the simplicity of these relationships, they are often used in the evaluation of other situations. In order to apply mass transfer coefficients determined in this fashion to nonidentical situations, it is necessary to convert the k-type coefficient to an F-type coefficient. This is done by equating the appropriate flux equations, solving for the F-type coefficient in terms of the k-type, and applying the F-type coefficient with the more general flux equation to the new conditions.

E. THEORETICAL PLATES

This method of absorber analysis evaluates the packed column with stage-wise contactor theory. A theoretical plate is defined as a height of packing where the gas stream leaving is in equilibrium with the liquid stream leaving the section. At the top of the column, with the solvent feed and column off-gas fully defined, a mass balance around the top theoretical plate and the applicable equilibrium relations may be solved to yield the magnitude and composition of the gas stream

entering and the liquid stream leaving the top plate. This procedure will provide the information necessary to repeat the calculation for the second theoretical plate. By continuing down the column in this fashion until the given composition change is realized, the number of theoretical plates required will be determined. The product of the number of theoretical plates and the height of packing equivalent to a theoretical plate (HETP) is then the depth of packing needed.

Unfortunately, the HETP must be determined experimentally, and varies with the size and type of packing used, the gas and liquid flow rates, and for a particular system, the composition of both the gas and liquid streams. In order to use this method an enormous amount of experimental data is needed. This difficulty, caused by the fundamental difference between tray and packed columns, has caused this method of analysis to be largely abandoned.

CHAPTER III

PREVIOUS WORK AND PRESENT APPROACH

The performance of the fluorocarbon process absorber has been analyzed by three different methods since the inception of the ORGDP development effort. In 1970, pilot plant absorption data were evaluated using both Colburn's equation and theoretical plate approach. A more detailed incremental model was constructed and fit to the experimental data in 1975. In this chapter, these methods will be reviewed and the more general approach adopted for this work will be presented.

The results of the first two of these methods were published by Stephenson, Merriman, and Dunthorn.[46] Initially, Colburn's integrated form of the design equation, equation II-28, was used in conjunction with experimental absorber end-point data to determine the number of overall gas transfer units for a variety of operating conditions. These values of N_{OG} were then divided into the depth of packing, yielding an H_{OG} for each case. However, as shown in the previous chapter, equation II-28 is built on the assumptions that only one component is transferring phases, and the gas and liquid flow rates are constant throughout the column. The experimental data, on the other hand, indicated that the flow rates, in particular the gas flow, changed appreciably due to carrier gas coabsorption. As this approach cannot handle such variations, averages of the inlet and outlet flows were used in these calculations. The H_{OG}'s that were determined were then correlated to these average flow rates. As the authors pointed out, there is no way of knowing *a priori* what these averages will be, so they developed a correlation between the feed flow rates and the averages to be used.

A theoretical plate approach was the second of these two efforts. The number of theoretical plates was calculated for each set of data using the method outlined in Chapter II. The HETP for each case was found by dividing the packed depth by the N_{TP}. This analysis represented an improvement over the first approach as it allows flow rate variations and the flux of all species to be taken into account. As in the first analysis, the HETP's were correlated to averages of the gas and solvent flow rates.

Both of these methods provided adequate correlations of the experimental data. However, although the average flow rates are a function of the feed rates, they are also a function of several other parameters, including contacting area and thus the column's dimensions. In the design of larger columns, extrapolation of these feed flow rates to stage height correlations would be highly questionable. From a theoretical standpoint, as Colburn's equation will not account for the flux of more than one species, and the theoretical plate approach treats the packed bed as a stage-wise contactor, these methods of analysis do not accurately represent the physical situation.

The third model described the fluorocarbon process absorber much more thoroughly. Merriman[26] developed and applied a rather unique approach which accounted for not only the flux of krypton, but also the carrier gas flux and the interaction of these fluxes. In addition to predicting absorber krypton removal, this model was then capable of predicting the load to be placed on the intermediate stripper.

Merriman quantified the nitrogen flux through the use of the liquid phase counterpart of equation II-33,

$$d(Lx_{NB}) = k_{OLN}a\ (x_N^* - x_{NB})\ dz. \qquad \text{III-1}$$

This was intergrated over the packed depth assuming x_N^* to be constant at $1/m_N$. The result of this integration depends upon the assumption made as to the variation of $k_{OLN}a$ with L. Merriman found that in any given test L varied only slightly and $k_{OLN}a$ was not significantly dependent on L. Equation III-1 was therefore integrated assuming $k_{OLN}a$ to be constant and L to be constant at the feed value. The resultant expression was evaluated with experimental end-point data and provided an average value of $k_{OLN}a$ for each set of experimental data. These were then correlated to the average Schmidt and Reynolds numbers.

The total krypton flux was divided into two separate components, flux due to diffusion and flux due to bulk movement,

$$N_K^T = N_K^D + N_K^B. \qquad \text{III-2}$$

The total and diffusive fluxes were described with equation II-33 as

$$N_K^T = d(Gy_{KB}) = k_{OGK}^T a\ (y_{KB} - y_K^*)\ dz, \qquad \text{III-3}$$

and

$$N_K^D = k_{OGK}a\ (y_{KB} - y_K^*)\ dz, \qquad \text{III-4}$$

while the flux due to bulk movement was described as

$$N_K^B = y_{KB} \sum_k N_k = y_{KB}\ dG. \qquad \text{III-5}$$

Considering the two components nitrogen and krypton,

$$\sum_k N_k = k^T_{OGK}a\ (y_{KB} - y^*_K)\ dz + k_{OLN}a\ (x^*_N - x_{NB})\ dz. \qquad \text{III-6}$$

In the case where y_{KB} is small, substitution of equations III-3 through III-6 into equation III-2 yields

$$k^T_{OGK}a = k_{OGK}a + k_{OLN}a\ [\frac{y_{KB}\ (x^*_N - x_{NB})}{(y_{KB} - y^*_K)}]. \qquad \text{III-7}$$

According to this approach, if one can evaluate $k_{OGK}a$ and $k_{OLN}a$ and calculates the bracketed term using the expected averages of the end-point conditions, equation III-7 will provide the effective average overall mass transfer coefficient which accounts for both transport mechanisms.

A correlation for $k_{OGK}a$ is needed to apply equation III-7. Substitution of equations III-3, III-4, and III-5 into equation III-2 shows that

$$k_{OGK}a\ (y_{KB} - y^*_K)\ dz = d(Gy_{KB}) - y_{KB}\ dG = G\ dy_{KB}. \qquad \text{III-8}$$

This expression can be used to determine $k_{OGK}a$ provided the gas flow rate is known. For each set of data, Merriman calculated the change in the gas flow rate in incremental steps over the packed depth with equation III-1, using the correlation for average $k_{OLN}a$ to provide local mass transfer coefficients. This gas flow profile was then used with equation III-8 to determine y_{KB} at incremental positions across the column. A value of $k_{OGK}a$ was found for each set of data such that the

calculated ratio y_{KBI}/y_{KBO} matched that of the experimental data. These values were correlated in the same fashion as were the values of $k_{OLN}a$.

Merriman tested the validity of this approach by determining $k^{T}_{OGK}a$ for each data set from equation III-3 using the same procedure that was used to determine $k_{OGK}a$ from equation III-8. These values compared very favorably to those predicted by equation III-6.

This model was not developed to accommodate any solvent flux. However, at the time this work was done, the absorber feed gas stream was essentially saturated with R-12, so no driving force existed for any solvent flux. Even if the feed gas stream had not been saturated with R-12, the absorber was being operated at approximately 25 atm and -25°F. At these conditions, the equilibrium gas phase mole fraction of R-12 is less than 0.01, and the small amount of solvent flux that would occur could safely be ignored. Currently, the absorber is being operated with a feed gas that is not saturated with solvent and at the much lower pressure of 8 atm where R-12 represents almost 5% of an equilibrium gas phase. Higher temperatures have also been considered to reduce the refrigeration requirements of the process, and, in particular, the experimental portion of this work was conducted at approximately -15°F where an equilibrium gas phase consists of 11% R-12. Clearly, in these cases, the movement of the solvent into a subsaturated feed gas should be considered.

Rather than incorporate the flux of R-12 into Merriman's model, for this work, it was decided to take a more conventional approach. Equation II-21, page 16, its liquid phase counterpart, and equations II-9 and II-10, page 12, are all capable of describing the flux of each of the three components and the interaction of these fluxes. Because of

the ease with which interfacial compositions can be determined for this system, and to be consistent with Stephenson's intermediate and final stripper models,[43] the model contained herein is based on equation II-9,

$$d(Gy_{jB}) = W_j \, F_{Gj} a \, \ell n \left(\frac{W_j - y_{ji}}{W_j - y_{jB}}\right) dz, \qquad \text{II-9}$$

and equation II-10,

$$d(Lx_{jB}) = V_j \, F_{Lj} a \, \ell n \left(\frac{V_j - x_{jB}}{V_j - x_{ji}}\right) dz. \qquad \text{II-10}$$

CHAPTER IV

EXPERIMENTAL APPARATUS AND PROCEDURES

Use of a gas absorber model based on equations II-9 and II-10, page 12, requires specific knowledge concerning the mass transfer coefficients $F_{Gj}a$ and $F_{Lj}a$ for the system of interest. As this information was not available for the fluorocarbon process absorber, experimental pilot plant data were needed so that correlations for these quantities could be developed. In order to identify any effects attributable to column diameter, it was necessary to collect performance data from several absorption columns. Additional pilot plant absorber performance data were required to permit the accuracy of the model's predictions to be judged against experimental observations. These data were provided by an absorber test loop equipped with interchangeable columns that was designed, built, and operated as an integral part of the ORGDP selective absorption pilot plant. The equipment and procedures used in this experimental effort are described in this chapter.

A. PROCESS PIPING

The absorber test loop was designed to provide quality data on the mass transfer occurring within the fluorocarbon process absorber. The loop was constructed in parallel with the existing pilot plant absorber and replaced it in the flow scheme of the ORGDP pilot plant for the duration of this experimental campaign. A schematic of this loop is shown in Figure IV-1. Three test columns were fabricated for installation in the loop. The four process lines were flanged to allow these

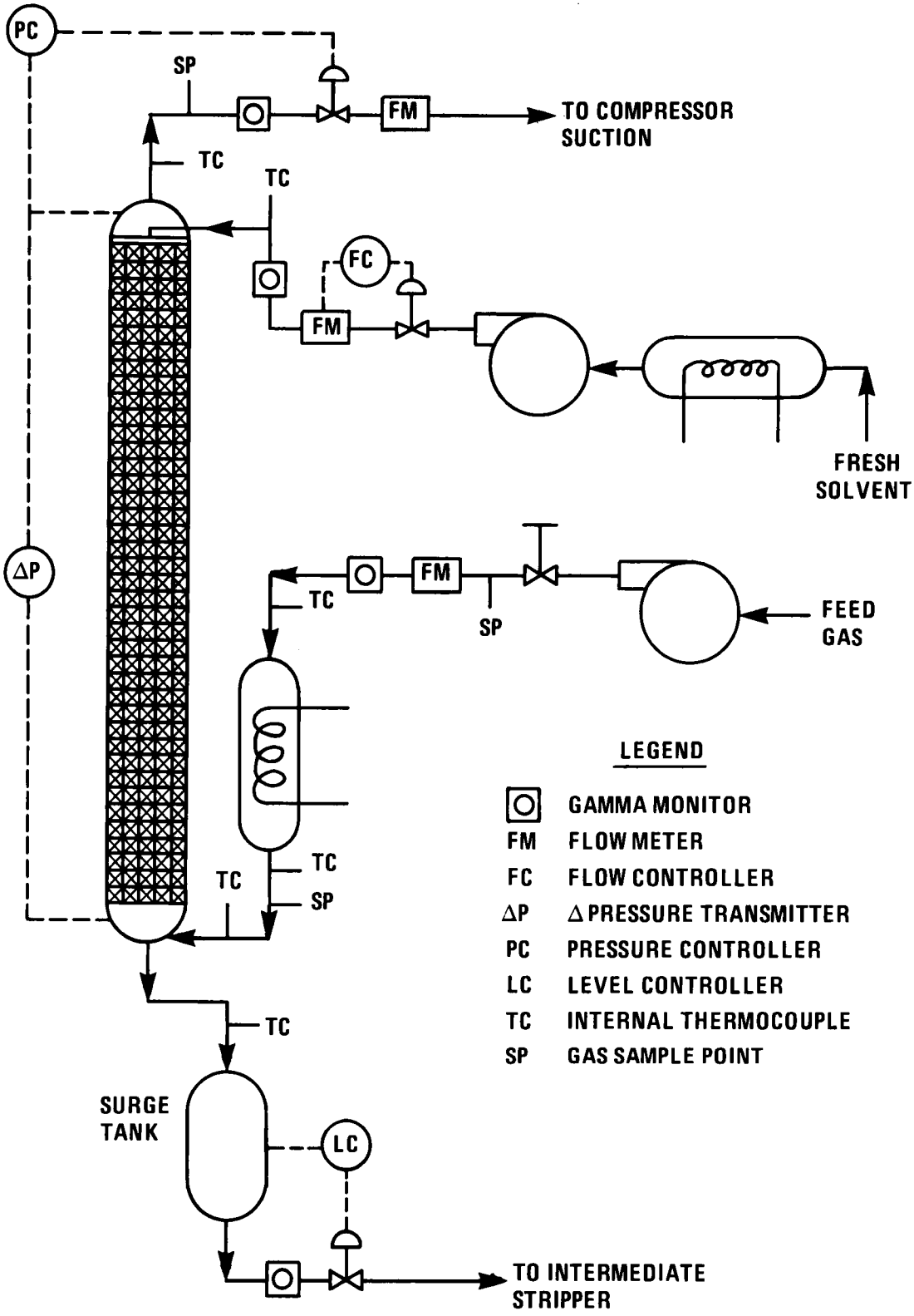

Figure IV-1
SCHEMATIC OF ABSORBER TEST LOOP

packed beds to be easily interchanged. Auxiliary pilot plant equipment supplied the test loop with feed gas flow rates ranging from 7 to 17 scfm and solvent feed rates of 0.5 to 1.5 gpm. The process piping and test columns were insulated with 2 to 3 inches of polyurethane foam and covered with mastic sealer.

Goodloe packing had been chosen for use in the fluorocarbon process and was therefore used in this work. This rolled wire mesh packing, shown in Figure IV-2, was selected on the basis of its large surface area to volume ratio and high throughput. The operating characteristics of Goodloe packing[28] and the flow rate capabilities of the pilot plant limited the test columns to diameters ranging from 2 to 4 inches. Consequently, the three columns were constructed with diameters of 2, 3, and 4 inches, providing a fourfold range in cross-sectional area for examination.

Three feet of packing was used in each of the test columns. Previous pilot plant experience with Goodloe indicated that a depth of 3 feet would provide detectable compositional changes across the bed yet leave measurable amounts of krypton in the column off-gas. In addition, this depth is not sufficient to lead to segregation of the phases so redistributors were not required.

As the three columns were constructed to be interchangeable, they are nearly identical. The packed section of each column was flanged to allow inspection of the packing and permit the columns to be used in future studies involving different packing materials. The packed section of the 4-inch-diameter column is shown in Figure IV-3. This segment of each column consists of a 40-inch piece of Schedule 40 304L stainless steel pipe with flanges welded flush with both ends. As recommended by

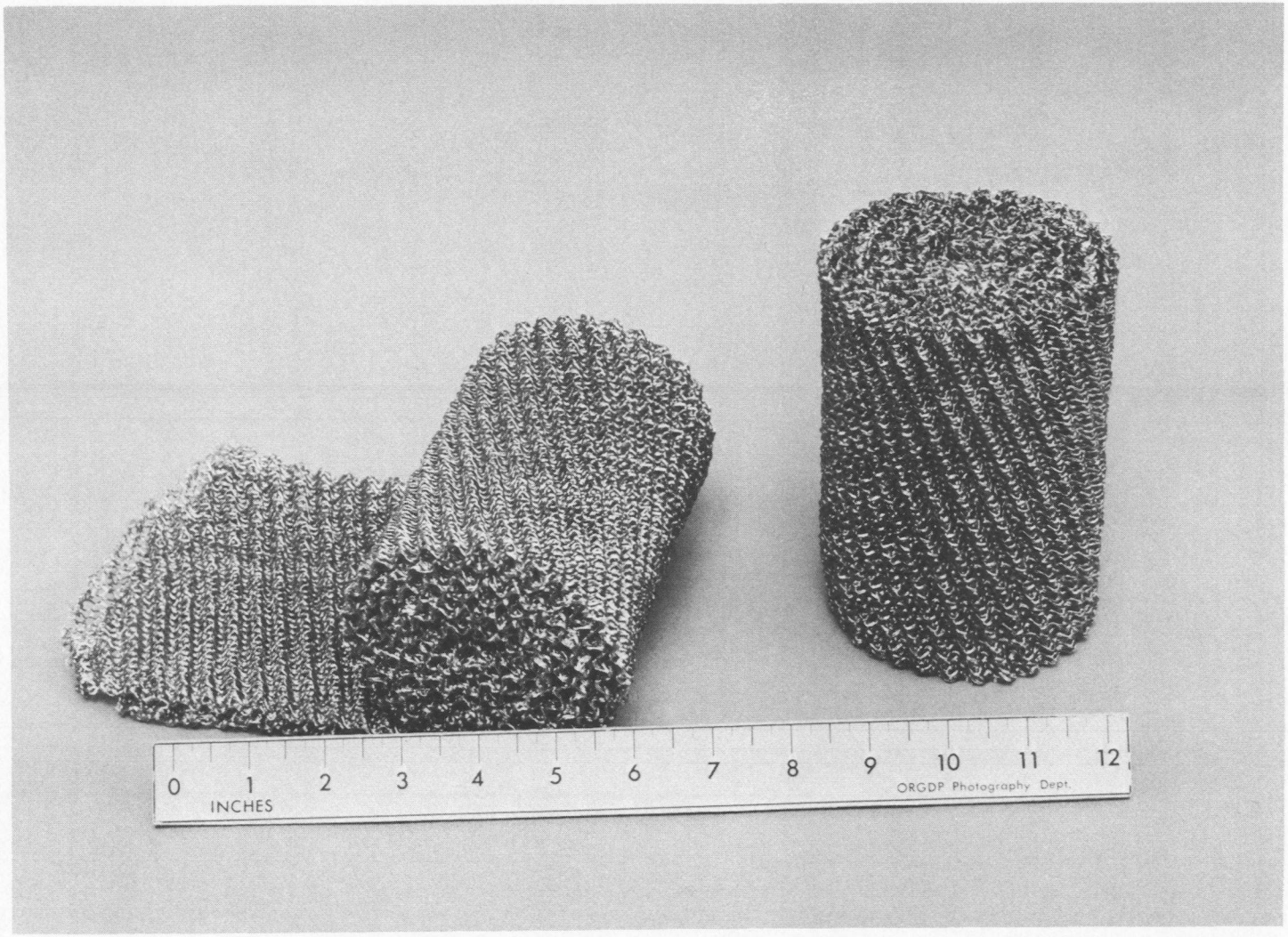

Figure IV-2
THREE-INCH-DIAMETER SECTIONS OF GOODLOE PACKING

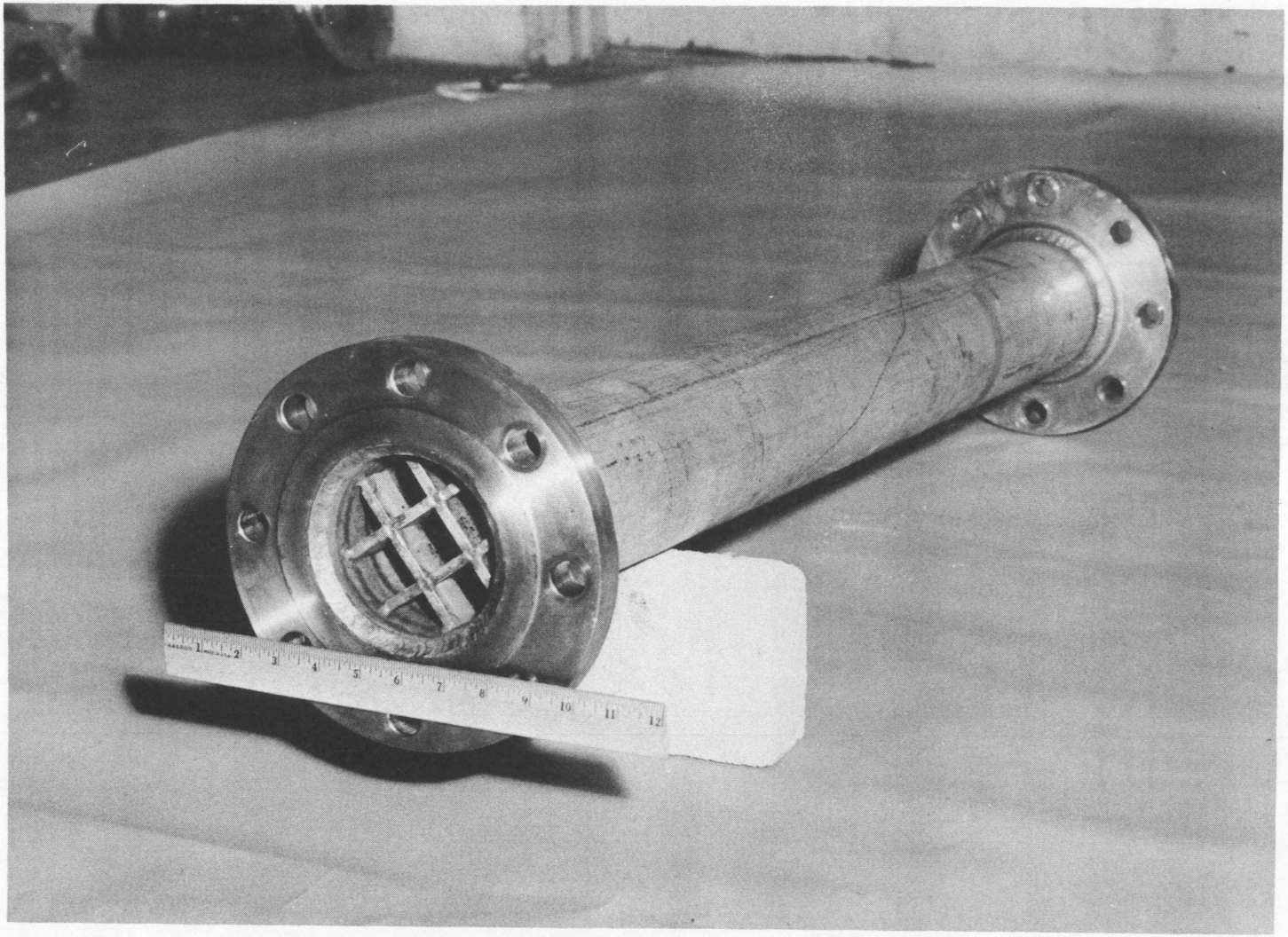

Figure IV-3
PACKED SECTION OF FOUR-INCH-DIAMETER COLUMN

Metex Corporation,[28] the manufacturer of Goodloe packing, a subway-grating-type packing support was fabricated and installed in the pipe an inch from one end. In addition to providing support for the packing, this structure helped distribute the gas flow and align it perpendicular to the face of the packing. In none of the columns did the area of this support exceed 40% of the total cross-sectional area. Following the packing instructions provided by Metex,[29] six pieces of 316 stainless steel Goodloe packing were installed in each of the three sections, giving each column a total packed depth of 34.5 inches.

Top and bottom sections, shown in Figure IV-4, that flanged to both the packed section and the process streams were constructed for each column. Pressure taps consisting of 1/8-inch Schedule 40 pipe were installed in each of these sections. The liquid distributor, mounted in the top section, was adjusted to seat directly on top of the packing so as to minimize the amount of mass transfer occurring above the packing and, in addition, to serve as a packing restrainer.

Teflon gaskets were placed between the three sections which were then bolted together and hydrostatically pressure-checked at 150 psig. The assembled 4-inch-diameter column is shown in Figure IV-5. Figure IV-6 shows the same column insulated and installed in the test loop.

B. PROCESS INSTRUMENTATION

The process instrumentation was designed to both control the process and provide the data needed for analysis. All control loops operated in the feedback mode and employed indicating PID controllers. Hard copies of the values of all required process parameters were

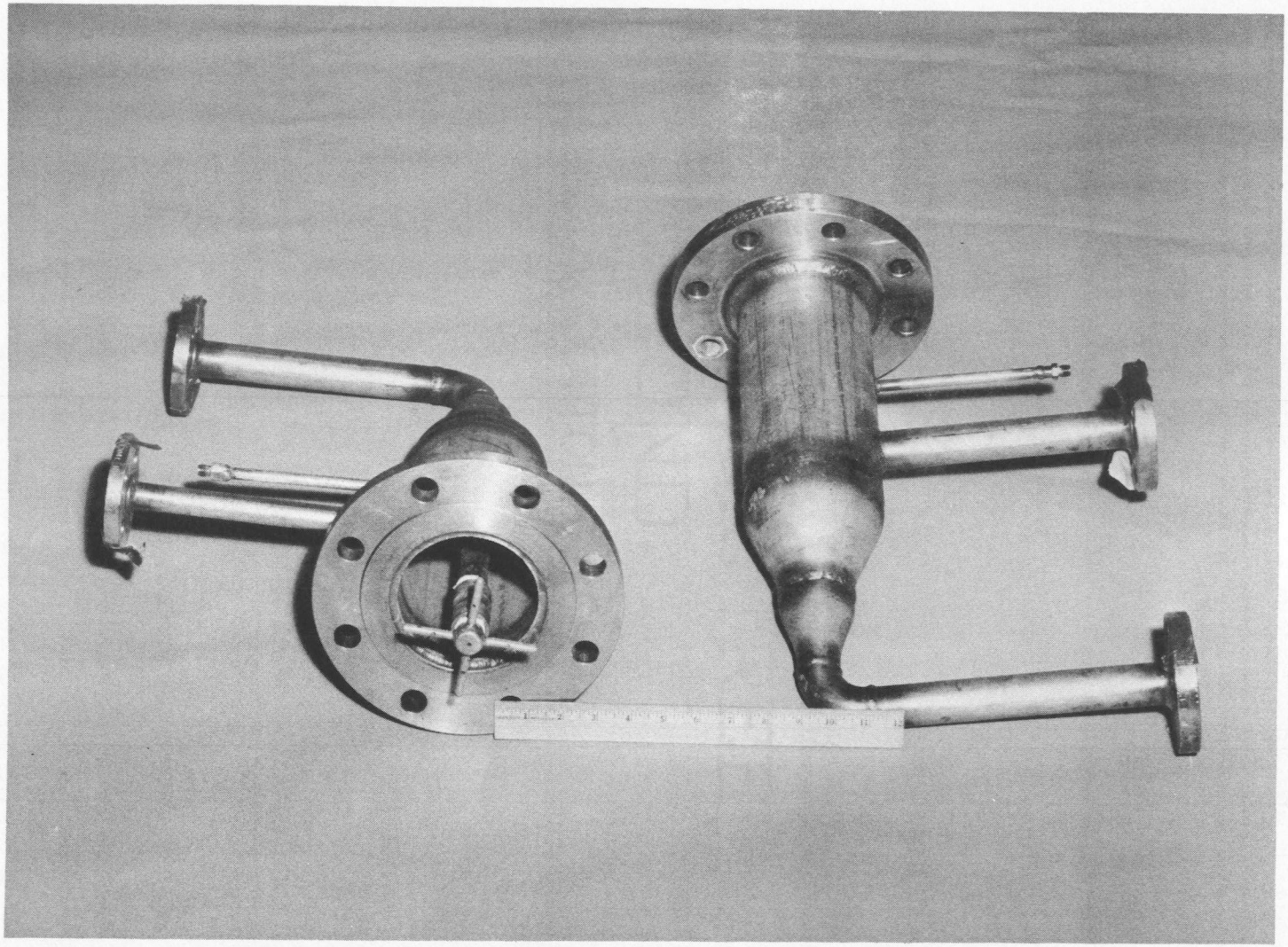

Figure IV-4
TOP AND BOTTOM SECTIONS OF FOUR-INCH-DIAMETER COLUMN

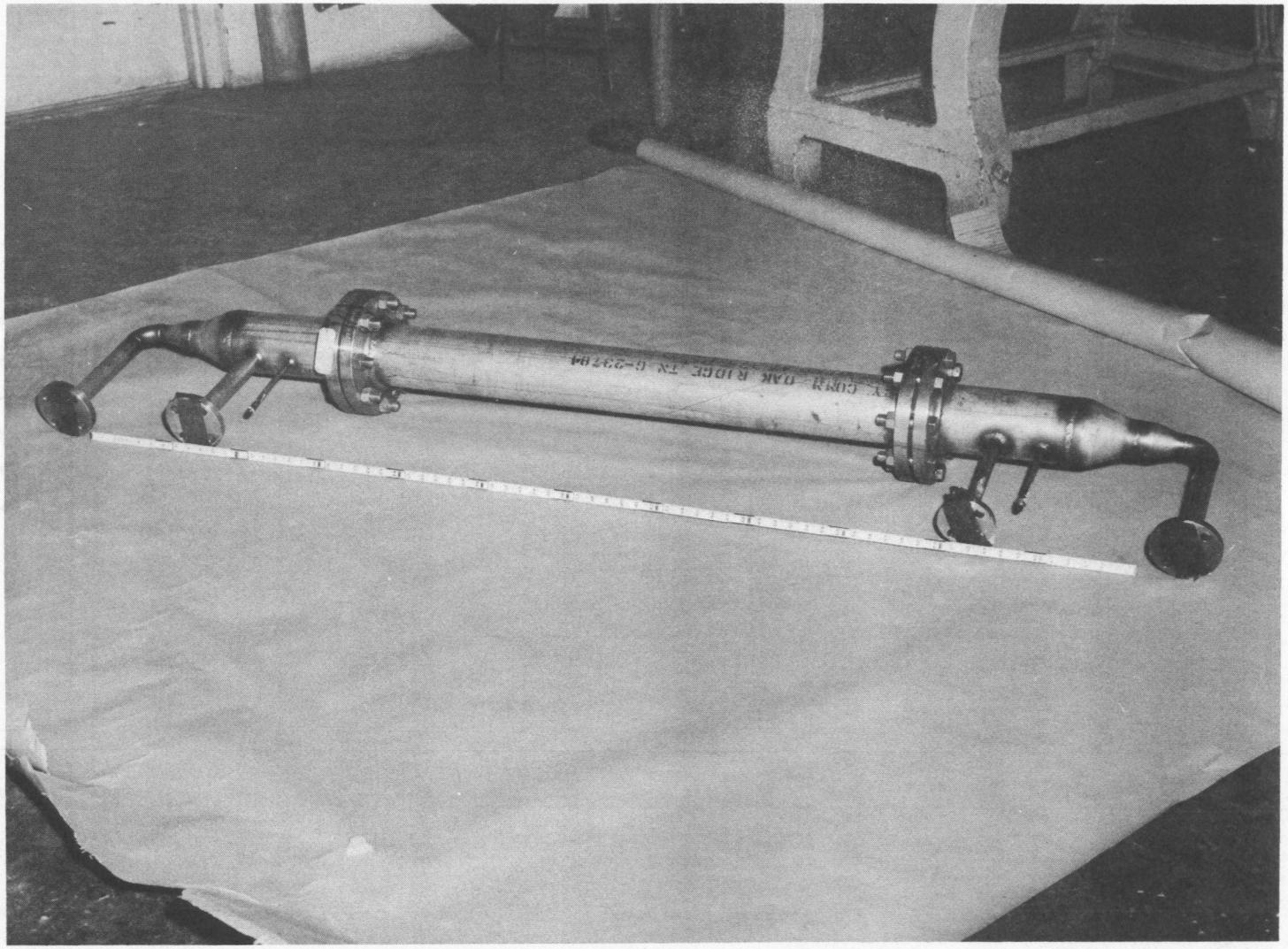

Figure IV-5
ASSEMBLED FOUR-INCH-DIAMETER COLUMN

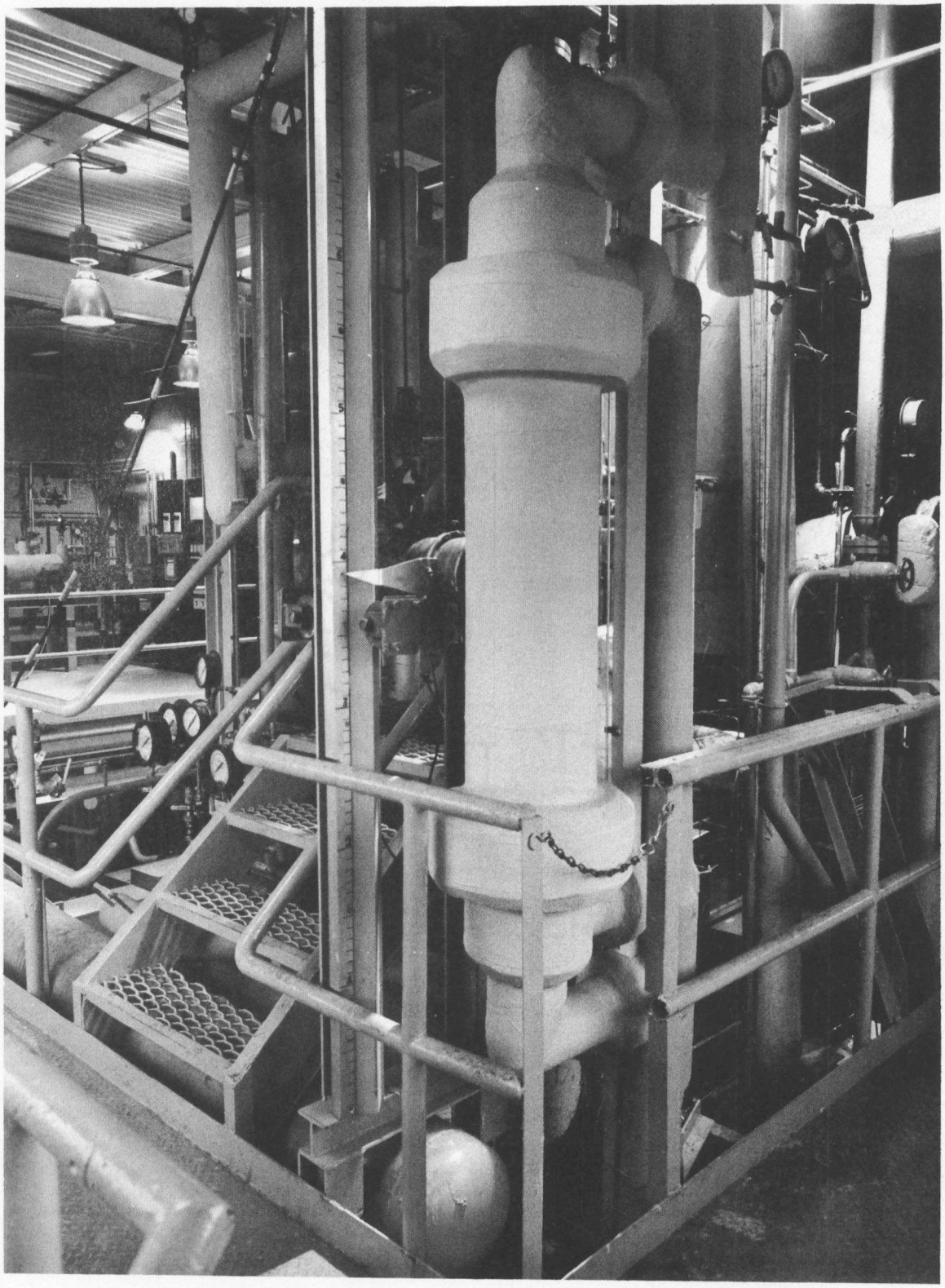

Figure IV-6
FOUR-INCH-DIAMETER COLUMN INSTALLED IN TEST LOOP AND INSULATED

periodically generated by a digital recorder. The process instrumentation is shown schematically on Figure IV-1, page 28.

The solvent flow rate to the test column was measured with a rotameter and controlled with a liquid control valve. The level in the solvent surge pot situated between the absorber and intermediate stripper was monitored with a capacitance probe and maintained with another liquid control valve. A hand-operated needle valve was used to control the feed gas flow rate. The gas flow rates in and out of the test column were measured with linear thermal mass flowmeters. The pressure taps on the columns were connected to a differential pressure transmitter which yielded the pressure drop across the bed. The top pressure tap and a regulated gas supply header were connected across another differential pressure transmitter to determine the total column pressure. A control valve located on the absorber off-gas stream was used to maintain the column pressure. Copper-constantan thermocouples were installed in each of the four process streams approximately 6 inches from the point the test column flanged into the loop. Sample withdrawal ports were situated in both gas lines.

All process instrumentation was designed to be accurate to within ±1% and was calibrated immediately prior to the experimental campaign. Thermocouple readings were determined to be accurate within ±0.5°F. Stephenson, et al.,[45] have prepared a detailed description of the ORGDP selective absorption pilot plant instrumentation.

C. ANALYTICAL METHODS

Two analytical methods were used to obtain data not provided by the process instrumentation. Mass spectrometry was used to analyze

samples of the inlet and outlet gas streams, and a radioisotope tracer technique, developed by Stephenson,[43] was used to obtain operating krypton profiles of the test columns. As tracer techniques are not commonly used in the chemical processing industry, and since such a method was heavily relied upon in this work, it will be discussed in some detail.

Radioisotope Tracer Techniques

Although the use of radioisotope tracer techniques is not widespread, such methods can be of particular value in mass transfer studies as they are highly sensitive and can be performed without the disruptive effects inherent in sampling techniques.

Radiotracer techniques have previously been used in several engineering applications. Notz and Meservey,[32] Ackley and Notz,[1] and Schaffer[37] used radiation detection equipment to measure the equilibrium solubilities of various gases in liquid CO_2 and R-12. Fulham and Hulbert,[14] Jones and Jones,[20] and McCaw[24] discuss the use of an external gamma scanning technique to study sieve tray damage. A gamma source and detector were mounted on opposing sides of a column. A density profile of the column was determined by raising and lowering the source and detector in unison along the face of the column and noting the variation of the detected count rate. From these attenuation profiles, sieve tray damage and liquid holdup were deduced. Markas and Beckman[23] used a radiotracer technique to study flow patterns in a toluene-water extraction column. In this work, the toluene was tagged with I^{131}, and an external gamma detector was used to determine entrance effects and flow distribution problems.

In order to perform radioisotope tracer analysis, an appropriate isotope and detection equipment must be available. The isotope chosen must behave as the species or phase under study. The necessary detection equipment consists of a detector sensitive to the energy of the isotope, an amplifier, a pulse height analyzer, and a timed pulse counter.

A thorough description of radiation detection equipment is provided by Chase.[7] For detection of gamma radiation, a thallium activated sodium iodide crystal is commonly used. When struck by a gamma photon, this crystal emits a pulse of light of an intensity proportional to the photon's energy. This light pulse is converted to an electrical signal via a photomultiplier tube. The resultant electrical signal is amplified and fed to the pulse height analyzer which discriminates between the energy levels of the signals and routes only those in the region of interest to the counter. The counter accepts and totals these pulses for a preset time interval.

It is possible that the detector will be struck by more than one photon within the resolving time of the equipment in which case the counter will register less than the actual number of counts. The resolving power of the detection system depends on the decay constant of the detection crystal and the time constants of the associated electronics. The true count rate can be expressed as

$$\eta_G = \eta_o/(1 - \eta_o\tau), \qquad \text{IV-1}$$

where η_G = true gross count rate,

η_o = observed count rate, and

τ = resolving time.

In most cases, the experiment and equipment are designed such that $\eta_o\tau < 0.01$ and η_o is essentially η_G.

In most environments, η_G includes not only radiation from the source, but ambient background radiation as well. This background radiation must be determined and separated out, usually by counting with the intended source removed from the view of the detector. The net count rate is then

$$\eta_N = \eta_G - \eta_B, \qquad \text{IV-2}$$

where η_N = true net count rate, and

η_B = background count rate.

The true net count rate is related to the number of moles of tracer present in the counting volume by

$$n_j = \eta_N/\varepsilon V_c A_j, \qquad \text{IV-3}$$

where n_j = moles of j in counting volume,

ε = counting yield,

V_c = counting volume, and

A_j = specific molar activity of j, disintegrations/g mole-min.

The counting yield is defined by the physical relationship between the source and detector. This value, fixed for a given system and geometry, consists of the detector efficiency and any attenuation by material situated between the source and detector. The quantity εV_c can be considered a system calibration factor to be experimentally evaluated.

A useful quantity and one much used in this work is the ratio of the moles of tracer at one point to that at another,

$$n_{j2}/n_{j1} = \left(\frac{\eta_{N2}}{\eta_{N1}}\right)\left(\frac{\varepsilon V_{c1}}{\varepsilon V_{c2}}\right). \qquad \text{IV-4}$$

When using this ratio, the calibration factor $\varepsilon V_{c1}/\varepsilon V_{c2}$ can be determined by ratioing the true net count rates of a common standard taken at each position.

As radioactive decay is a random phenomenon, there is a certain amount of error inherent in any single measurement. It is usually assumed that the actual value is within one standard deviation, σ, of the measured value. As the best available estimate of the actual value is the measured value itself, the best estimate of the standard deviation is

$$\sigma(\eta_G) = (\eta_G)^{1/2}. \qquad \text{IV-5}$$

If the calibration factor $\varepsilon V_{c1}/\varepsilon V_{c2}$ were determined by counting a standard and taking background readings, through use of the relations

$$\sigma(A\text{-}B) = [\sigma^2(A) + \sigma^2(B)]^{1/2} \qquad \text{IV-6}$$

and

$$\sigma(D/E) = \frac{D}{E}\left[\left(\frac{\sigma(D)}{D}\right)^2 + \left(\frac{\sigma(E)}{E}\right)^2\right]^{1/2}, \qquad \text{IV-7}$$

it can be seen that σ of the resultant molar ratio of equation IV-4 can be expressed as

$$\sigma(n_{j2}/n_{j1}) = \left(\frac{\eta_{G2} - \eta_{B2}}{\eta_{G1} - \eta_{B1}}\right)\left(\frac{\eta_{cG1} - \eta_{cB1}}{\eta_{cG2} - \eta_{cB2}}\right)\left[\frac{\eta_{G2} + \eta_{B2}}{(\eta_{G2} - \eta_{B2})^2}\right.$$

$$+ \frac{\eta_{G1} + \eta_{B1}}{(\eta_{G1} - \eta_{B1})^2} + \frac{\eta_{cG2} + \eta_{cB2}}{(\eta_{cG2} - \eta_{cB2})^2}$$

$$\left. + \frac{\eta_{cG1} + \eta_{cB1}}{(\eta_{cG1} - \eta_{cB1})^2}\right]^{1/2}, \qquad \text{IV-8}$$

where the subscript c indicates counting rates taken in the determination of the calibration factor. Gardner and Ely[15] present a thorough discussion on the statistical handling of radioisotope measurements.

Pilot Plant Gamma Analysis

The feed to the fluorocarbon process from a nuclear fuel reprocessing facility is expected to contain 1-10 ppm krypton. Pilot plant work in such a low concentration range required an analytical tool of high sensitivity. A radiotracer method was chosen as it provided the needed sensitivity and could be performed without disturbing the system.

The choice of isotope was obvious in this case, and Kr^{85} itself was used. Although Kr^{85} is a 99.59% beta emitter and only a 0.41% gamma emitter, beta is completely attenuated by metals and a beta detector would have to be placed inside the process piping. In addition, beta is strongly attenuated by the process solvent which would severely confound the analysis. Gamma emissions, on the other hand, can be monitored external to the system and are not appreciably attenuated by R-12.[43] It was therefore decided to monitor the gamma emissions of Kr^{85}.

Stationary gamma counting positions are located on each of the four process streams connecting to the test absorber. These are indicated on Figure IV-1, page 28. At each position a 1.5- to 2-inch-thick lead shield encases the process piping to reduce the ambient radiation. When placed inside this shielding, the detector is held perpendicular to and in contact with the pipe.

A portable gamma scanner was constructed to provide operating krypton profiles of the test columns. The scanner is shown schematically in Figure IV-7, and the actual unit can be seen in Figure IV-8. A 2-inch-thick lead shield was mounted on a carriage that rode up and down the side of the column on vertical tracks, being lifted by an overhead electrical hoist. A pointer installed on the carriage indicated its position on a scale inscribed on one of the tracks. A 1-inch-diameter hole was bored through the shield to provide a window between the column and the detector. By using this scanner to determine count rates at various column positions, it was possible to determine the molar krypton profile of the column without disturbing it. Such profiles were an invaluable source of information in this work. Stephenson[43] has applied this scanning technique to a variety of unit operations with great success.

D. EXPERIMENTAL PROCEDURES

A series of experiments were conducted at the ORGDP pilot plant using the absorber test loop to obtain the required performance data. The experimental campaign ran from October 1977 through February 1978. During this period, the pilot plant was operated 24 hours a day, 4 days a week. In total, 55 tests were completed, approximately 18 per column,

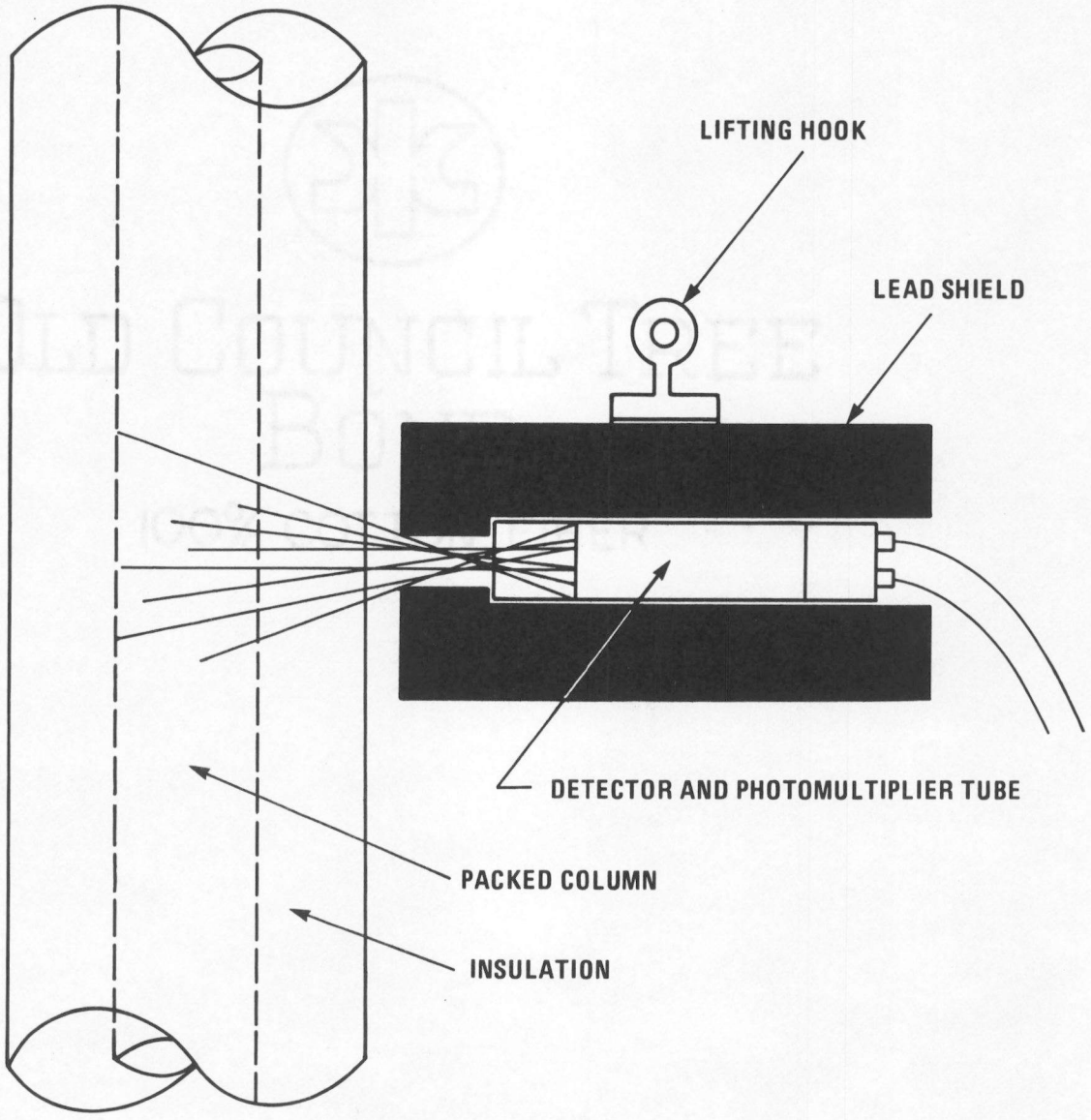

Figure IV-7

SCHEMATIC OF PORTABLE GAMMA SCANNER

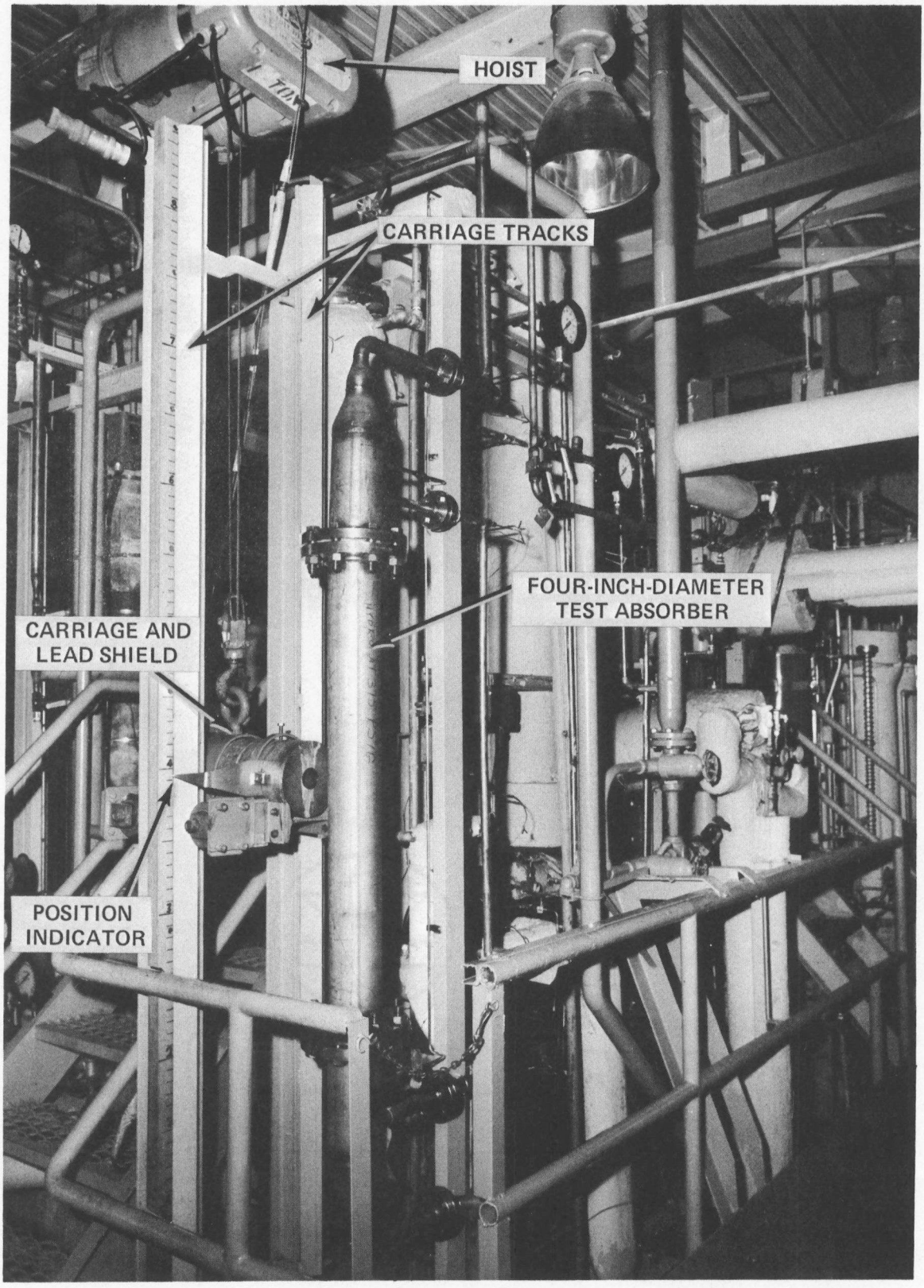

Figure IV-8
TEST ABSORBER WITH GAMMA SCANNER

encompassing the largest possible range of flow rates. Most of these were conducted near -15°F and 8.3 atm. The 4-inch-diameter column was the first evaluated in the test loop, followed by the 3-inch, and then the 2-inch column.

After a column was installed and insulated, the gamma calibration factors were determined. The gas compressors were started and nitrogen was circulated through the test loop. One to two curies of Kr^{85} were then added to the system. The krypton content of the absorber feed gas was monitored with the gamma detection equipment, and the flow rate was recorded at 10-minute intervals. After about 3 hours, these parameters stabilized indicating that the krypton had been evenly distributed throughout the system. A gamma scan of the column was then taken with 1-minute readings being made every 2 inches. The background radiation was determined by repeating the scan with a 1.5-inch-thick lead plug inserted in the window of the lead shield. With no solvent present, the krypton concentration was constant throughout the column, and any differences between the net count rates at the various positions were attributable to the calibration factor εV_c. By subtracting out the background and ratioing the net counts at the bottom of the column to those at each column position, the factor $\varepsilon V_{c1}/\varepsilon V_{c2}$, for use in equation IV-4, page 40, was determined for each position on the particular column relative to the bottommost position.

Once these calibration factors were determined, the solvent pump was started, and the remainder of the process was brought on-line. Controller set points were established, and the process parameters were recorded at 1/2-hour intervals. The krypton content of the inlet and outlet gas streams was periodically checked. When these values

stabilized, data were collected and new set points were initiated. Steady state was reached approximately 7 hours after start-up or following a change in the liquid flow rate. The system responded much quicker to changes in the gas flow rate attaining equilibrium after about 3 hours.

Data were collected after the process had convincingly demonstrated its stability. The process parameters were recorded at 10-minute intervals, and several gamma readings were made on the inlet and outlet gas streams. The radiation detection equipment was also used to verify the purity of the solvent feed. A gamma scan of the column with background readings was then completed in the same fashion as described earlier. These data, along with equation IV-4, page 40, and the previously determined calibration factors, provided profiles of the relative amount of krypton present in the column. Following the scan, the process variables and the count rates of the process streams were re-examined for fluctuations. If none had occurred, samples of the absorber off-gas, absorber feed gas, and process feed gas were respectively pulled into evacuated Monel cylinders for laboratory mass spectrometry analysis. New set points were instituted, and the recorders were reset to 1/2-hour intervals. Figure IV-9 shows a typical set of data. The error bands on the krypton profile were calculated with equation IV-8, page 41, and showed no significant variation from test to test. Several of the data sets are shown in the next chapter with the remainder being listed in Appendix B.

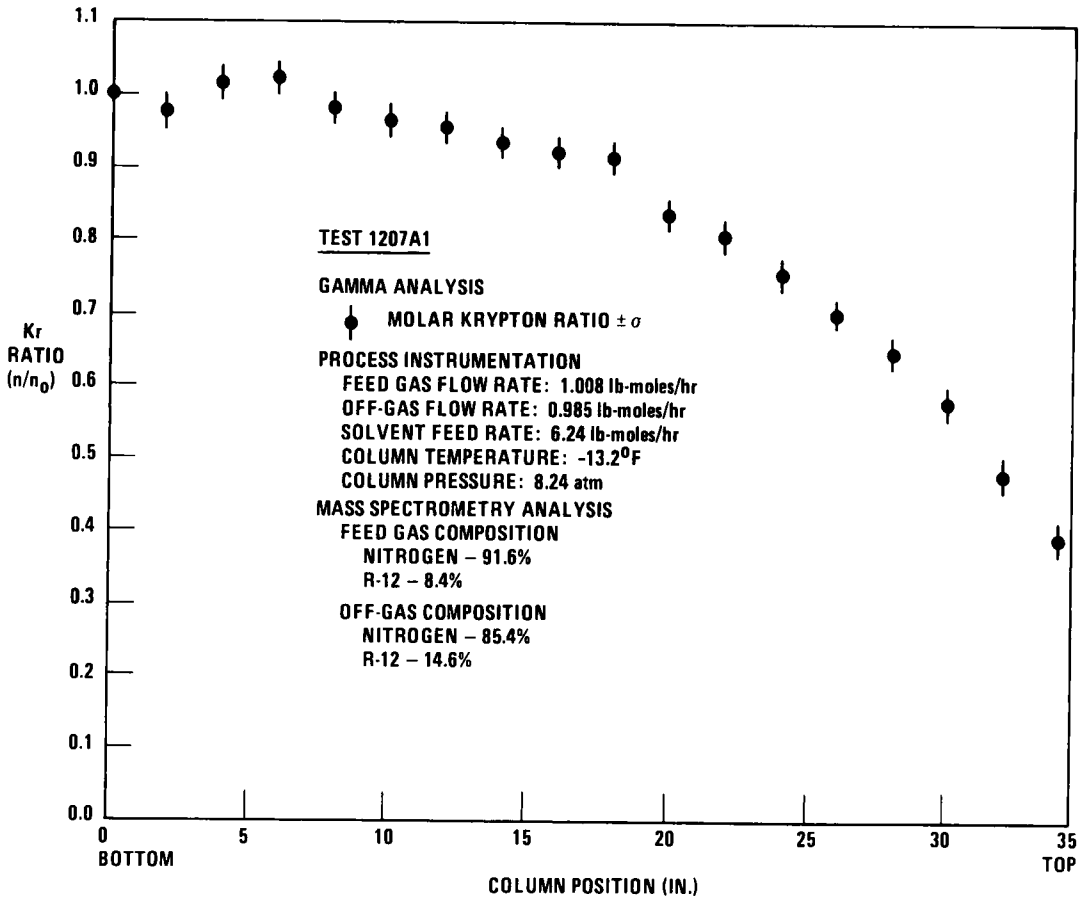

Figure IV-9

COMPLETE SET OF DATA FROM A TYPICAL TEST

CHAPTER V

SOLUTION OF MODEL EQUATIONS AND COMPARISON OF RESULTS

A computer code based on equations II-9,

$$d(Gy_{jB}) = W_j \, F_{Gj} a \, \ell n \left(\frac{W_j - y_{ji}}{W_j - y_{jB}}\right) dz, \qquad \text{II-9}$$

and II-10,

$$d(Lx_{jB}) = V_j \, F_{Lj} a \, \ell n \left(\frac{V_j - x_{jB}}{V_j - x_{jk}}\right) dz, \qquad \text{II-10}$$

was developed to predict the performance of the fluorocarbon process absorber. This required the determination of correlations for $F_{Gj}a$ and $F_{Lj}a$. In this chapter, the techniques used to find solutions to the model equations are described, and the correlations found for the mass transfer coefficients are presented. The predictions of the model are then compared to experimental absorber performance data to verify the validity of the model.

A. SOLUTION OF MODEL EQUATIONS

Given the flow rates and compositions at one surface of a differential slab of packing, the model calculates the values of these variables at the other surface. The information provided is used to solve equations II-9 and II-10 for the flux of each component occurring within the increment. Mass balances around the section are then solved

utilizing these fluxes to yield the flow rates and compositions at the opposing surface. The code was arbitrarily constructed to start at the top of the packed bed and work its way down, using the results of the last calculation as the starting point for the next. The calculations are performed over a 0.01-foot-deep packed section. This choice of increment size is discussed in Appendix D. Figure V-1 is a flow chart of the model. A Fortran code is listed in Appendix E.

Interfacial Concentrations of Nitrogen and R-12

In order to calculate the flux from equations II-9 and II-10, it is necessary to obtain the mass transfer coefficients, the interfacial area, and the interfacial compositions. The interfacial concentrations of nitrogen and R-12 are determined by taking advantage of the low concentration of krypton. As the krypton concentration is below 10 ppm,

$$y_{Ri} + y_{Ni} \tilde{=} 1.0 \qquad \text{V-1}$$

and

$$x_{Ri} + x_{Ni} \tilde{=} 1.0, \qquad \text{V-2}$$

where the subscripts R and N refer respectively to R-12 and nitrogen. This reduces the problem to one of determining the equilibrium mole fractions in a two-phase binary system. These values are calculated through simultaneous solution of equations V-1 and V-2, with Henry's law for nitrogen and Raoult's law for R-12. The Henry's law constant used for nitrogen and the expression used for the vapor pressure of R-12 are presented in Appendix A. As the absorber is assumed to be isothermal, and

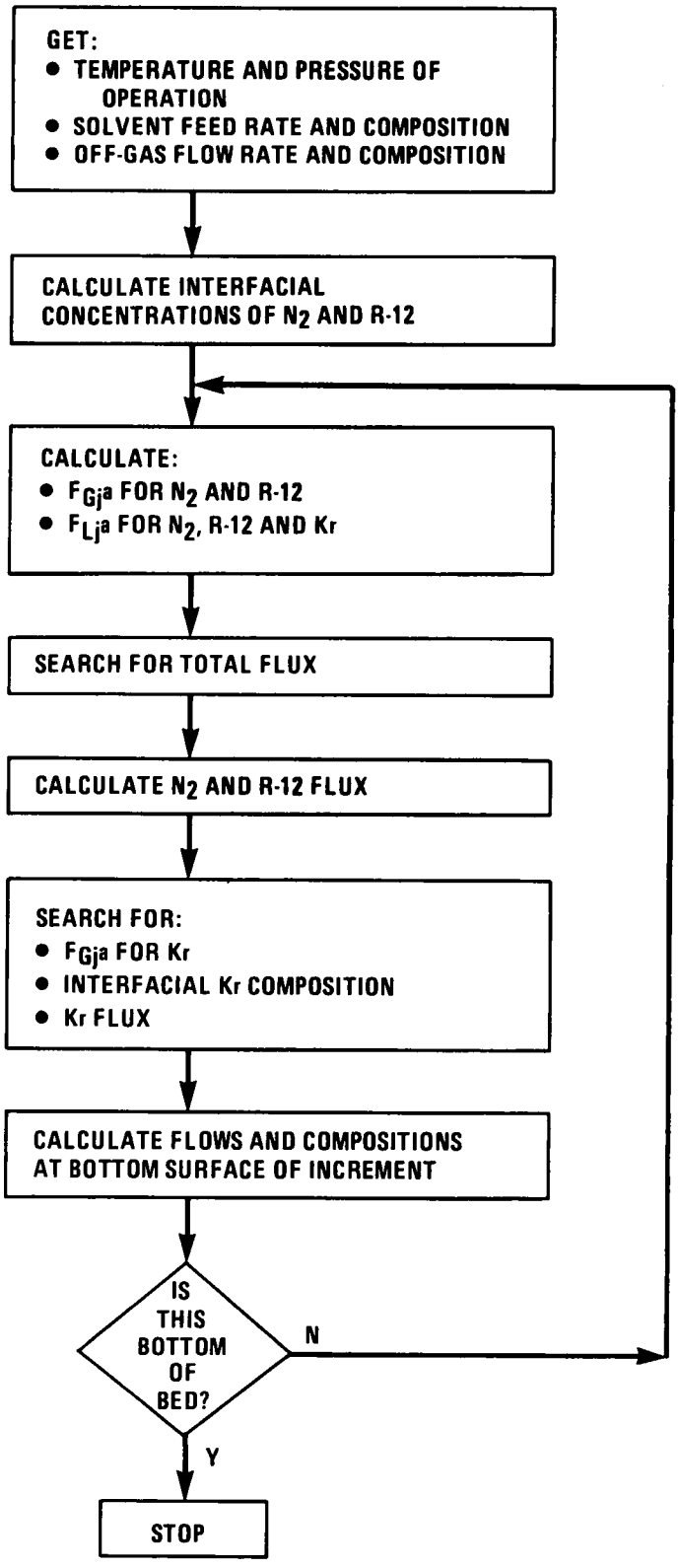

Figure V-1
FLOW SCHEME OF ABSORBER MODEL

these constants are functions of only temperature and pressure, the interfacial concentrations of nitrogen and R-12 are fixed throughout the column by the temperature and pressure of operation.

Calculation of Mass Transfer Coefficients and Interfacial Area

As the correlations for the mass transfer coefficients and the interfacial area will be discussed later, let it suffice to say at this point that these values are calculated from an expression of the form

$$Sh_j a = C_1 \, Re_G^{C_2} Re_L^{C_3} Sc_j^{C_4}, \qquad V\text{-}3$$

where Sh_j = Sherwood number of component j in specified phase, $F_j \ell M_A / D_{jM} \rho$,

Re_G = gas phase Reynolds number, $\ell G M_{AG} / \mu_G$,

Re_L = liquid phase Reynolds number, $\ell L M_{AL} / \mu_L$,

Sc_j = Schmidt number of component j in specified phase, $\mu / \rho D_{jM}$,

ℓ = characteristic length, ft,

M_A = average molecular weight of specified phase, lb/lb mole,

ρ = density of given phase, lb/ft^3,

μ = viscosity of given phase, lb/ft-hr,

C_1, C_2, C_3, and C_4 = constants of the correlation.

The evaluation of equation V-3 requires a substantial amount of physical data for each species. The physical properties used in this work are listed in Appendix A.

The characteristic length, ℓ, tends to be a rather ambiguous quantity for a packing like Goodloe. In cases of this type, Treybal[48] suggests using the diameter of a sphere with the same surface area to

volume ratio as the packing. Shulman[38] suggests incorporating the operating void fraction of the packing. In this work, the characteristic length is defined as

$$\ell = 6/A_p(1 - \varepsilon_o), \qquad \text{V-4}$$

where A_p = surface area to volume ratio of the dry packing, 585 ft^2/ft^3 for Goodloe,[22] and

ε_o = operating void fraction of the packing.

The operating void fraction is determined by a method Stephenson[43] developed based on the operating and static liquid hold-ups. This calculation is described in Appendix C.

As only small amounts of krypton are present, the viscosity of the gas phase is calculated as the viscosity of a nitrogen-R-12 mixture. This value is determined with Wilke's correlation,

$$\mu_G = \sum_{i=1}^{N} (y_i\mu_i / \sum_{j=1}^{N} y_j\Phi_{ij}), \text{ lb/ft-hr}, \qquad \text{V-5}$$

where $\Phi_{ij} = \frac{1}{2\sqrt{2}} \frac{[1 + (\mu_i/\mu_j)^{1/2}(M_j/M_i)^{1/4}]^{2.0}}{(1 + M_i/M_j)^{1/2}}$. (5)

The viscosity of the liquid phase is assumed to be that of liquid R-12.

The average molecular weight of each phase is the mole fraction weighted average of the weights of nitrogen and R-12. The gas density, ρ_G, is the mole fraction weighted average of the densities of R-12 and nitrogen, each being determined from its equation of state. The density of liquid R-12 is used as the density of the liquid phase.

The diffusivity is the only factor that will cause the mass transfer coefficients calculated with equation V-3 to differ between the species in a given phase. In the gas phase, as a molecule of R-12 or nitrogen will rarely encounter another molecule of anything but R-12 or nitrogen, the binary diffusivity of these two components is used for both. In the absence of experimental data on this system, the correlation of Hirschfelder, Curtiss, and Bird is used with the improvement offered by Wilke and Lee,[36]

$$D_{ij} = \frac{B\, T^{3/2}\, [(M_i + M_j)/(M_i M_j)]^{1/2}}{P\, \sigma_{ij}^{\,2}\, \Omega}, \text{ cm}^2/\text{sec} \qquad \text{V-6}$$

where $B = 0.00214 - 0.000492\, [(M_i + M_j)/M_i M_j]^{1/2}$,

T = temperature, °K,

P = pressure, atm,

σ_{ij} = Lennard-Jones force constant, Å, $(\sigma_i + \sigma_j)/2$,[36]

Ω = collision integral, $1.06036/T'^{0.1561} + 0.193/e^{0.47635T'} + 1.03587/e^{1.52996T'} + 1.76474/e^{3.89411T'}$,[31]

$T' = T/\varepsilon_{ij}$, and

ε_{ij} = Lennard-Jones force constant, °K, $(\varepsilon_i \varepsilon_j)^{1/2}$.[36]

As $D_{ij} = D_{ji}$, $F_{GR}a$ and $F_{GN}a$ have the same value. To determine the diffusivity of krypton in the gas phase, all three components must be considered. As this calculation requires the flux occurring within the increment, its description will be deferred.

In the liquid phase, as in the gas phase, the binary nitrogen-R-12 diffusivity is used for both species. For krypton, the binary

krypton-R-12 diffusivity is used. Both of these are calculated with the correlation of Wilke and Chang,[36]

$$D_{ij} = 7.4 \cdot 10^{-8} \frac{M_R^{1/2} T}{\mu_L V_b^{0.6}}, \text{ cm}^2/\text{sec}, \qquad \text{V-7}$$

where μ_L = viscosity of the solution, centipoise, and

V_b = molal volume of the solute at its normal boiling point, $\text{cm}^3/\text{g-mole}$.

After the above calculations have been performed, values of $F_{GN}a$, $F_{GR}a$, $F_{LN}a$, $F_{LR}a$, and $F_{LK}a$ are available for use.

Determination of Nitrogen and R-12 Fluxes

With the bulk flow rates and compositions known, and values of the mass transfer coefficients, interfacial area, and interfacial concentrations having been calculated for nitrogen and R-12, equations II-9 and II-10, page 12, can be solved for the total flux occurring within the current increment. Since

$$d(Gy_{jB}) = d(Lx_{jB}) \qquad \text{V-8}$$

and

$$dL = dG, \qquad \text{V-9}$$

equations II-9 and II-10, page 12, can be equated and rearranged to the form

$$dG - \left(\frac{1}{1/F_{Gj}a\ dz + 1/F_{Lj}a\ dz}\right) \ln\left[\frac{(y_{jB} - x_{jB})\ e^{(dG/F_{Gj}a\ dz)}}{(y_{jB} - x_{ji})}\right.$$

$$\left. + \frac{(y_{ji} - x_{ji})\ e^{(dG/F_{Lj}a\ dz)} - y_{ji} + x_{jB}}{(y_{jB} - x_{ji})}\right] = 0. \qquad \text{V-10}$$

As the properties of nitrogen are known better than those of R-12, equation V-10 is written for nitrogen and searched with a bisection routine for the total flux, dG.

Once the total flux has been found, the individual fluxes of nitrogen and R-12 are calculated. Equation II-9, page 12, rewritten to the form

$$d(Gy_{jB}) = \frac{y_{ji}\ dG - y_{jB}\ dG\ e^{(dG/F_{Gj}a\ dz)}}{1 - e^{(dG/F_{Gj}a\ dz)}}, \qquad \text{V-11}$$

is used to calculate $d(Gy_{NB})$ and $d(Gy_{RB})$.

Determination of Krypton Flux

The flux of krypton is also calculated with equation V-II. However, before this can be done, it is necessary to know y_{Ki} and $F_{GK}a$. Through rearrangement of equation V-10, it can be seen that

$$y_{Ki} = \frac{[y_{KB} - x_{KB} - y_{KB}\ e^{(dG/F_{LK}a\ dz)}]\ e^{(dG/F_{GK}a\ dz)} + x_{KB}}{[(1/m_K - 1 - (1/m_K)e^{(dG/F_{GK}a\ dz)}]e^{(dG/F_{LK}a\ dz)} + 1.0}. \qquad \text{V-12}$$

Therefore, if $F_{GK}a$ can be determined with equation V-3, the flux of krypton can be obtained. In order to calculate $F_{GK}a$, D_{KM} is required, and, as was mentioned earlier, this diffusivity should be that of krypton in a nitrogen-R-12 mixture. This is calculated as an effective binary diffusivity[5] with

$$1/D_{KM} = \frac{\sum_{j=1}^{N} [x_{jB}d(Gy_{KB}) - x_{KB}d(Gy_{jB})]/D_{Kj}}{d(Gy_{KB}) - x_{KB}\sum_{j=1}^{N} d(Gy_{jB})}, \qquad \text{V-13}$$

where the required binary diffusivities, D_{KR} and D_{KN}, are determined with equation V-6. As D_{KM} is a function of $d(Gy_{KB})$, equations V-13, V-3, page 51, V-12, and V-11 must be solved in an iterative fashion. The flux of krypton, $d(Gy_{KB})$, is determined from this system of equations by a method of progressive substitution with the variation in the value of D_{KM} being used as the convergence criteria. When convergence is obtained, all the fluxes occurring within the current increment have been determined.

Conditions at the Bottom Surface

Given the flow rates and compositions at the top surface of a differential slab of packing, and having determined the fluxes occurring within the increment, the conditions at the bottom surface are easily calculated. A mass balance around the increment yields

$$G_{Bottom} = G_{Top} + dG, \qquad \text{V-14}$$

$$L_{Bottom} = L_{Top} + dL, \qquad \text{V-15}$$

$$y_{jB\ Bottom} = \frac{G_{Top}\ (y_{jB\ Top}) + d(Gy_{jB})}{G_{Bottom}}, \qquad \text{V-16}$$

and

$$x_{jB\ Bottom} = \frac{L_{Top}\ (x_{jB\ Top}) + d(Lx_{jB})}{L_{Bottom}}.$$

If the current increment is not the bottommost of the packed bed, the results of equations V-14 through V-17 are used as the starting point for the calculations on the next increment.

B. CORRELATIONS FOR THE MASS TRANSFER COEFFICIENTS AND INTERFACIAL AREA

The published correlations for mass transfer coefficients can often be expressed in the form

$$Sh_j = C_1\ Re^{C_2} Sc_j^{C_3}. \text{(35)} \qquad \text{V-18}$$

Some values of the constants C_1, C_2, and C_3, reported for gas transfer, are listed in Table V-1. Table V-2 contains some of the values published for liquid phase transfer. The expression

$$a = C_1'\ G^{C_2'}\ L^{C_3'} \qquad \text{V-19}$$

is often used to report the interfacial area.[48] In this work, it was felt that the data were not sufficient to independently determine correlations for F_j and a. Instead, correlations for the product $Sh_j a$ were developed.

TABLE V-1

GAS PHASE CORRELATING CONSTANTS FOR EQUATION V-18[38]

Author	Packing	C_1	C_2	C_3
Ju Chin Chu	Spheres and Cylinders	1.48	0.56	1/3
Shulman	Raschig Rings and Berl Saddles	∿0.45	0.64	1/3
Aerov and Umnik	Spheres, Slabs, and Rings	0.395	0.64	1/3
Giĺdenblat	Dumped Rings	0.407	0.655	1/3

TABLE V-2

LIQUID PHASE CORRELATING CONSTANTS FOR EQUATION V-18[38]

Author	Packing	C_1	C_2	C_3
Van Krevelen	Rings	0.00595	0.67	0.33
Tsiparis	Rings	0.0021	0.75	0.50
Onda, Sada, and Murase	Rings	0.0107	0.49	0.50
Onda, Sada, and Otubo	Rings	0.00625	0.50	0.50
Sherwood and Holloway	Rings	0.00333	0.65	0.50
	Saddles	0.00258	0.72	0.50
Ramm and Chagina	Dumped Rings	0.00216	0.77	0.50
	Pall Rings	0.00236	0.77	0.50
	Stacked Rings	0.00192	0.77	0.50
	Tubes	0.00177	0.77	0.50
	Blocks	0.0019	0.77	0.50

Rather than attempt to obtain relations of the form

$$Sh_j a = C_1 C_1' Re^{C_2} Sc_j^{C_3} G^{C_2'} L^{C_3'}, \qquad V\text{-}20$$

it was decided to let the Reynolds numbers absorb the flow rate dependencies of the interfacial area. In addition, as the temperature and pressure were not varied significantly in the experimental portion of this work, no attempt was made to determine C_3, but rather the values most commonly reported were used. Thus, the correlating forms,

$$Sh_{Gj} a = C_1 Re_G^{C_2} Re_L^{C_3} Sc_{Gj}^{1/3} \qquad V\text{-}21$$

and

$$Sh_{Lj} a = C_1' Re_G^{C_2'} Re_L^{C_3'} Sc_{Lj}^{0.50} \qquad V\text{-}22$$

were assumed.

Three sets of experimental data from each column, covering a wide range of flow conditions, were used to determine the constants in equations V-21 and V-22. Acceptable model fits to these experimental data sets were obtained through use of the expressions

$$Sh_{Gj} a = 2.3 Re_G^{1.005} Sc_{Gj}^{1/3} \qquad V\text{-}23$$

and

$$Sh_{Lj} a = 8.0 Re_G^{0.605} Re_L^{0.45} Sc_{Lj}^{0.50} \qquad V\text{-}24$$

for each species in the given phase.

The krypton profiles generated by the model and the above relationships are compared with the nine experimental profiles in Figures V-2 through V-10. In tests 125A1 and 201P1, Figures V-9 and V-10, the calculated and experimental profiles are offset. This discrepancy is attributable to the method used to acquire the experimental profiles. The calibration factor for the bottommost position was determined from a reading made with the detector centered at the top edge of the packing support. If when collecting a data set the reading at the bottom position was made with the detector slightly lower, the detector would see more of the packing support, which more strongly attenuates gamma radiation than does the packing, and an artifically low reading would be obtained. As the remainder of the readings are ratioed to this value, the entire profile will be shifted upwards. Conversely, if the bottommost reading was taken with the detector positioned too high, the profile would be lowered. Unfortunately, no means of reproducing the required position was provided other than the scale inscribed on the tracks. The same offset can occur at the topmost point due to the liquid distributor, but in this case only the topmost point would be affected.

This shift will not, however, affect the overall shape of the profiles, and agreement between the shapes of the experimental and calculated profiles indicates that the model is accurately describing the behavior of the column. The shapes of the calculated and experimental profiles agree quite well in all nine cases even though the experimental profiles were obtained from three different columns and cover a wide range of flow conditions.

As the model starts at the top of the column and works its way down, using the results of the current increment as the starting point

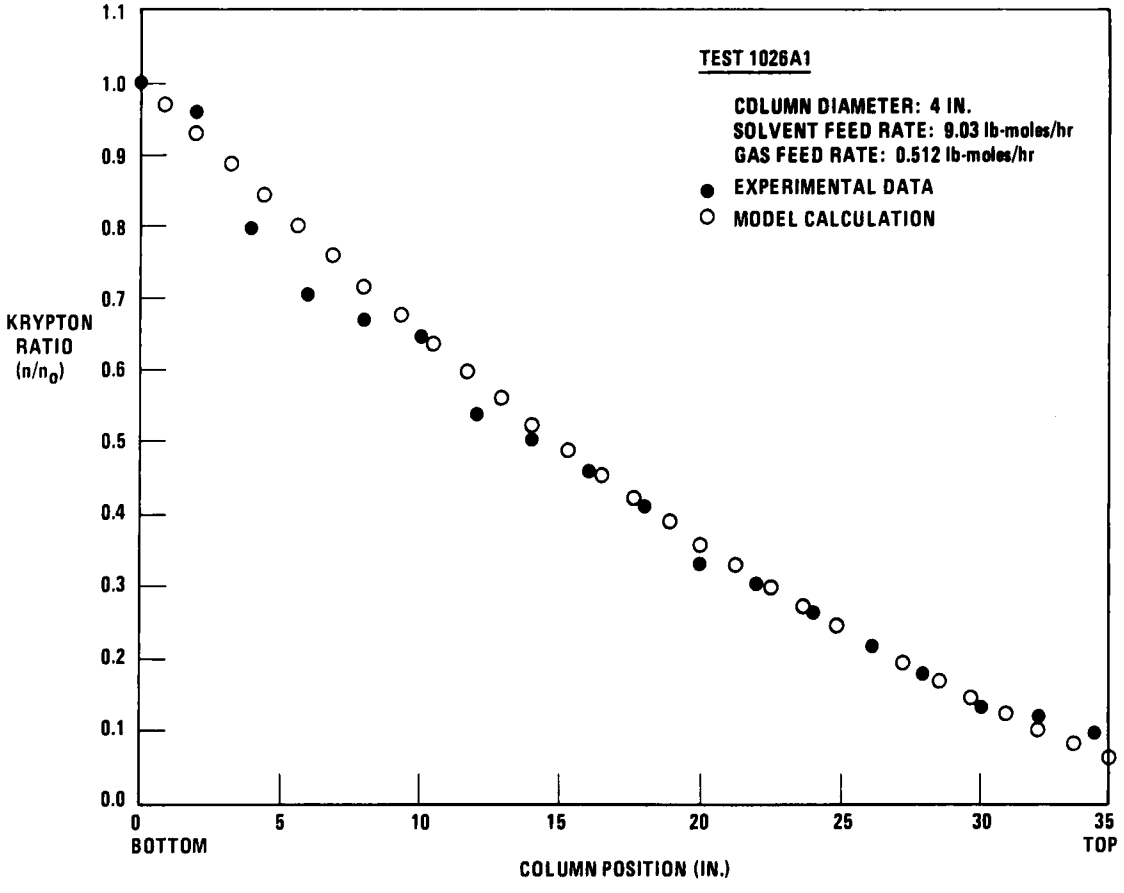

Figure V-2

EXPERIMENTAL AND CALCULATED KRYPTON PROFILES
FOR TEST 1026A1

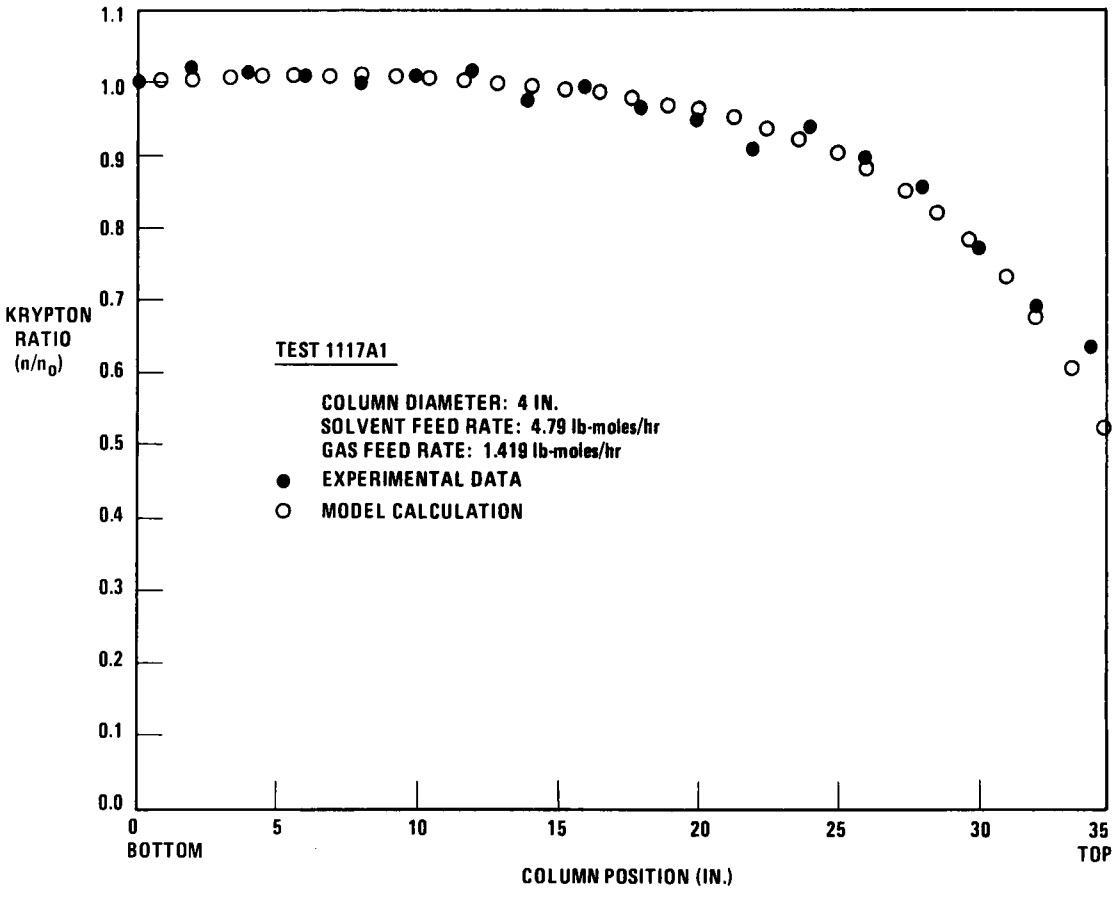

Figure V-3

EXPERIMENTAL AND CALCULATED KRYPTON PROFILES
FOR TEST 1117A1

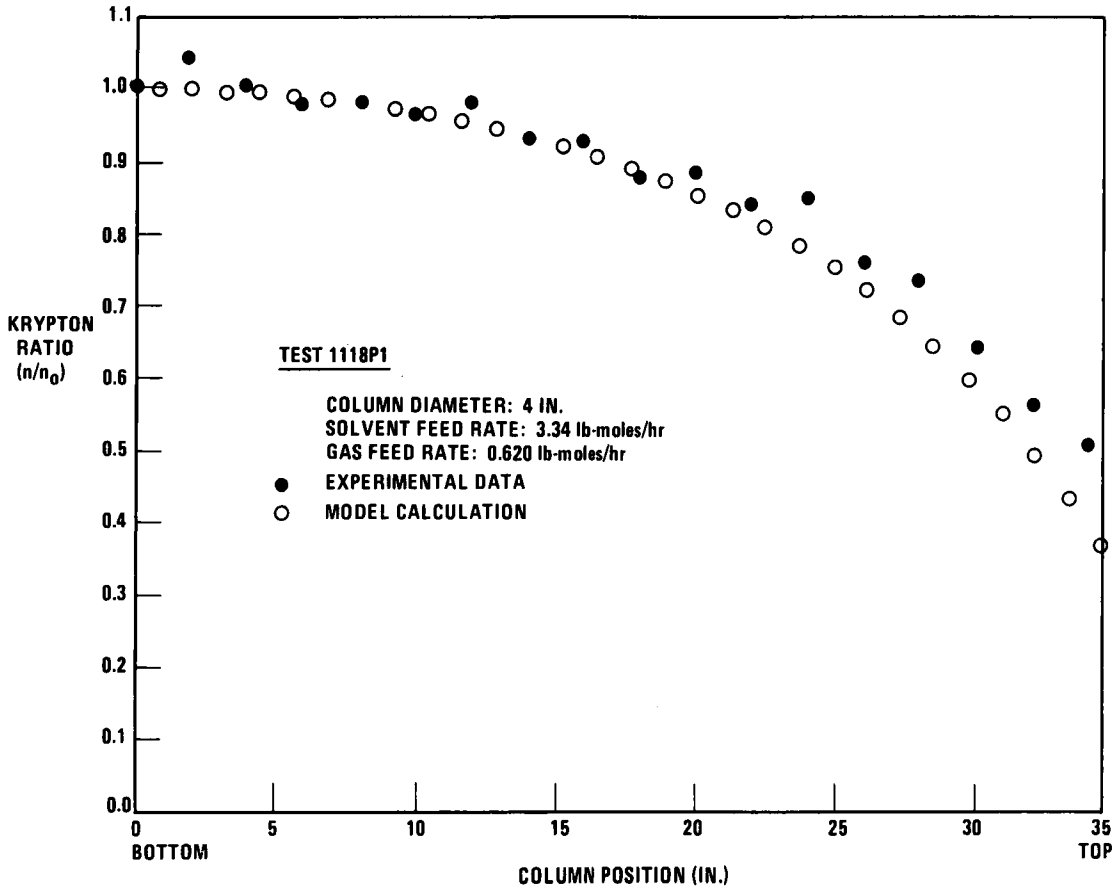

Figure V-4

EXPERIMENTAL AND CALCULATED KRYPTON PROFILES
FOR TEST 1118P1

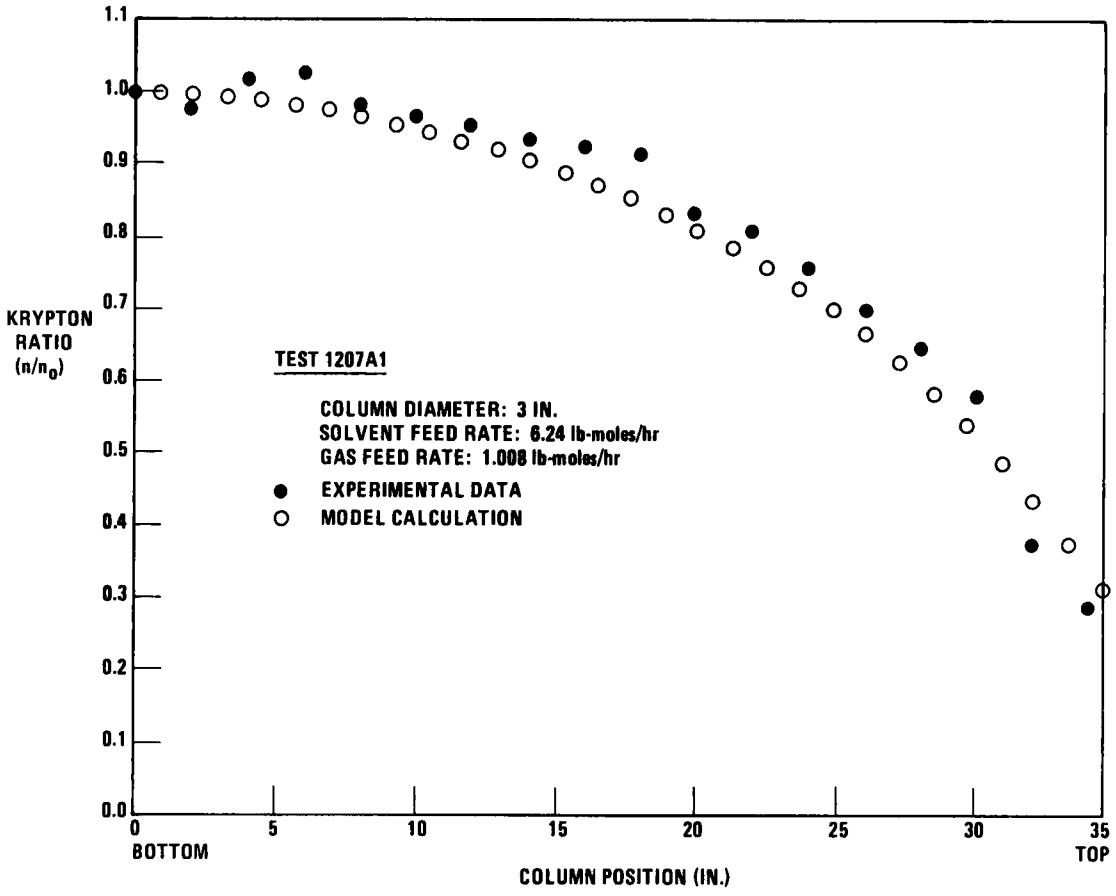

Figure V-5

EXPERIMENTAL AND CALCULATED KRYPTON PROFILES
FOR TEST 1207A1

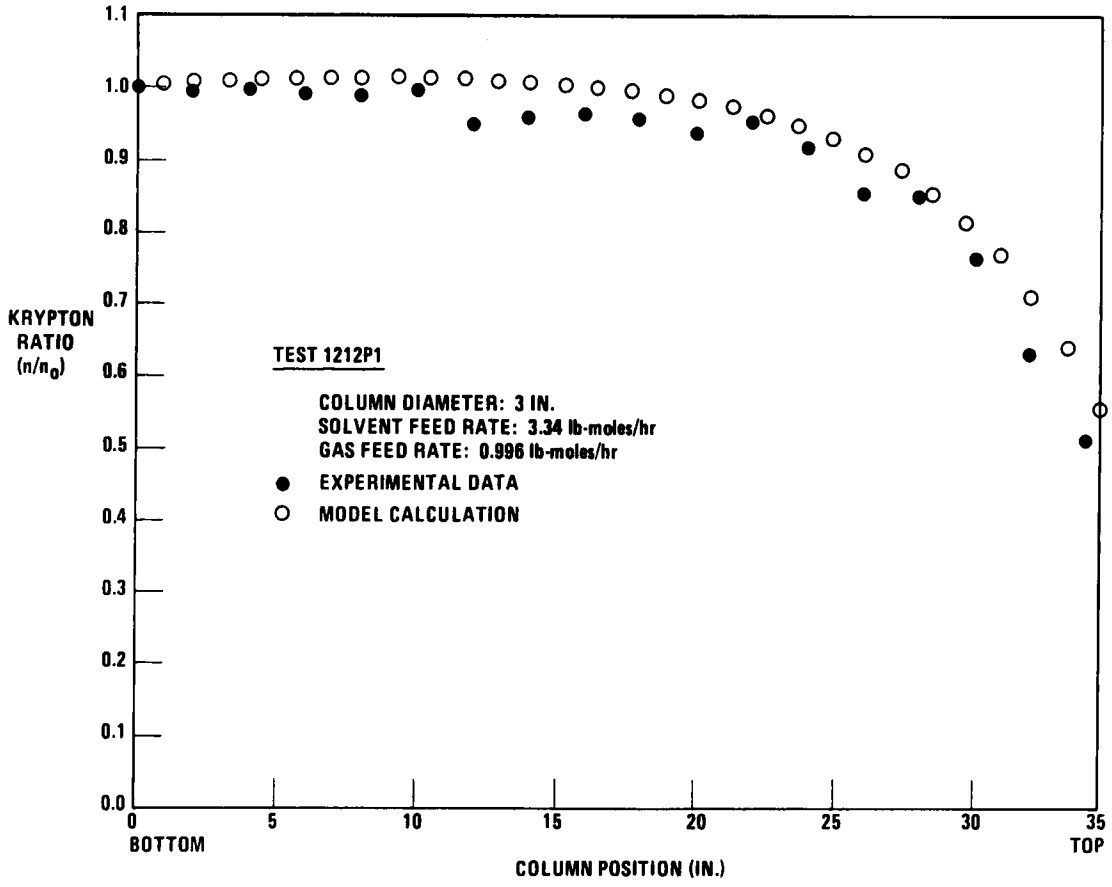

Figure V-6

EXPERIMENTAL AND CALCULATED KRYPTON PROFILES
FOR TEST 1212P1

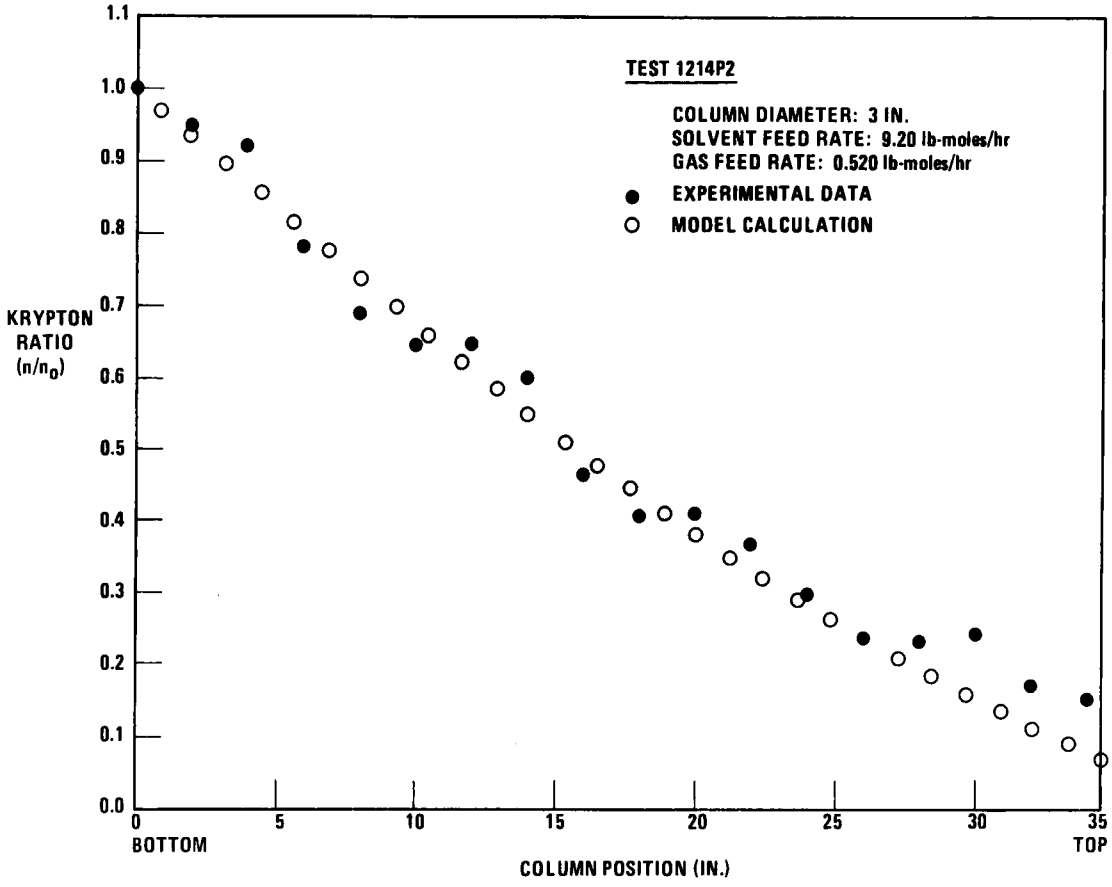

Figure V-7

EXPERIMENTAL AND CALCULATED KRYPTON PROFILES
FOR TEST 1214P2

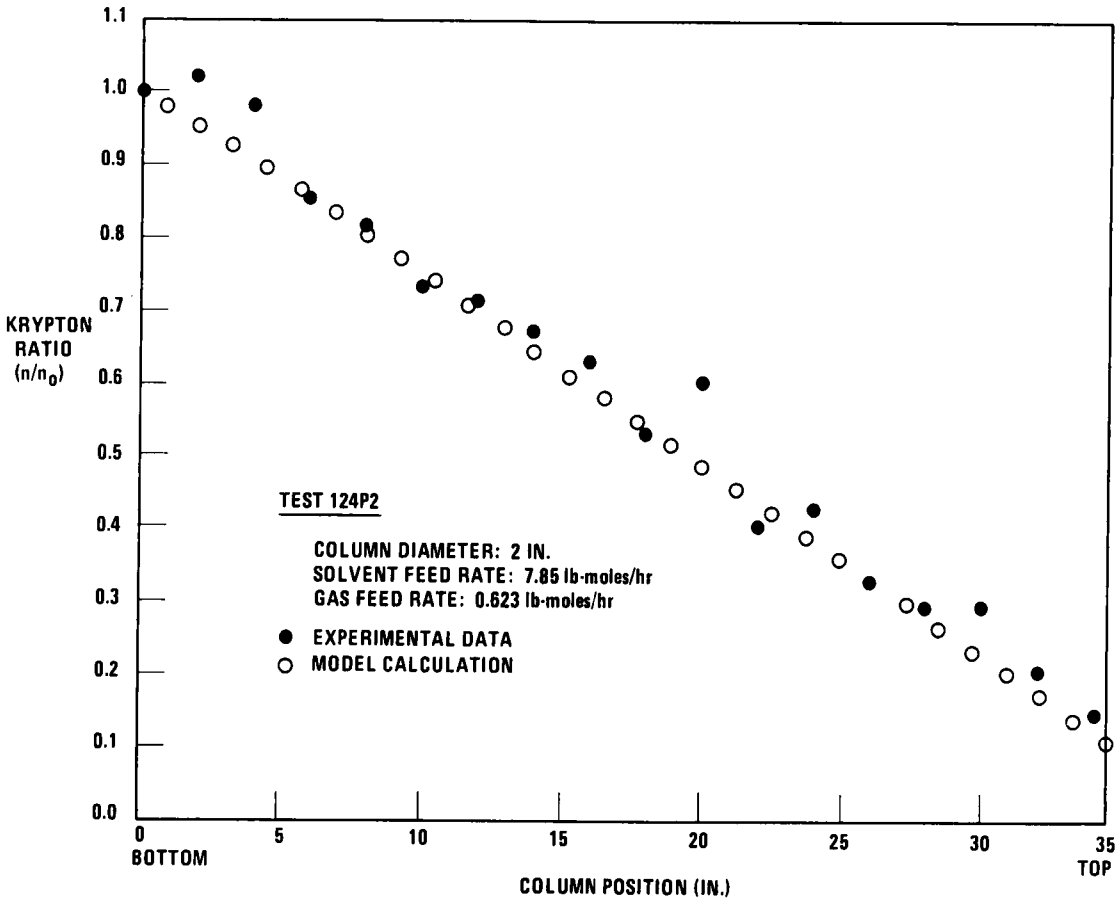

Figure V-8

EXPERIMENTAL AND CALCULATED KRYPTON PROFILES
FOR TEST 124P2

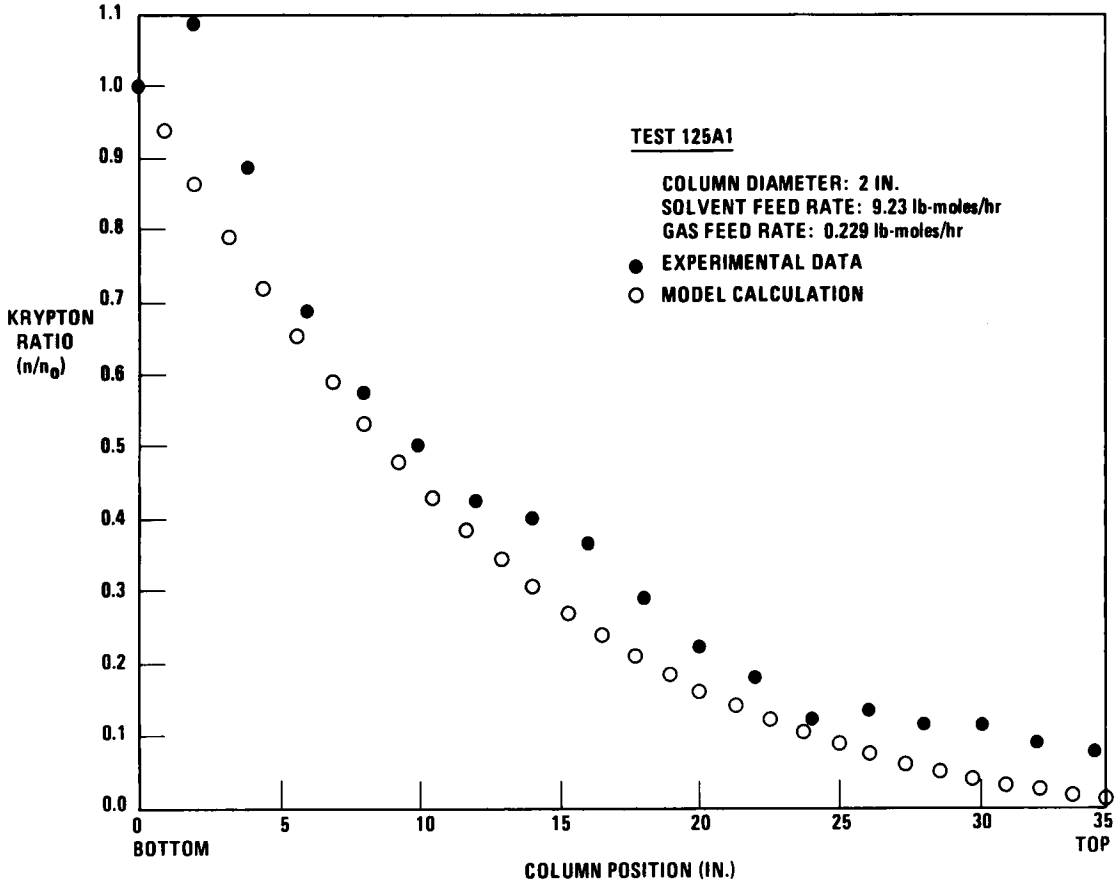

Figure V-9

EXPERIMENTAL AND CALCULATED KRYPTON PROFILES
FOR TEST 125A1

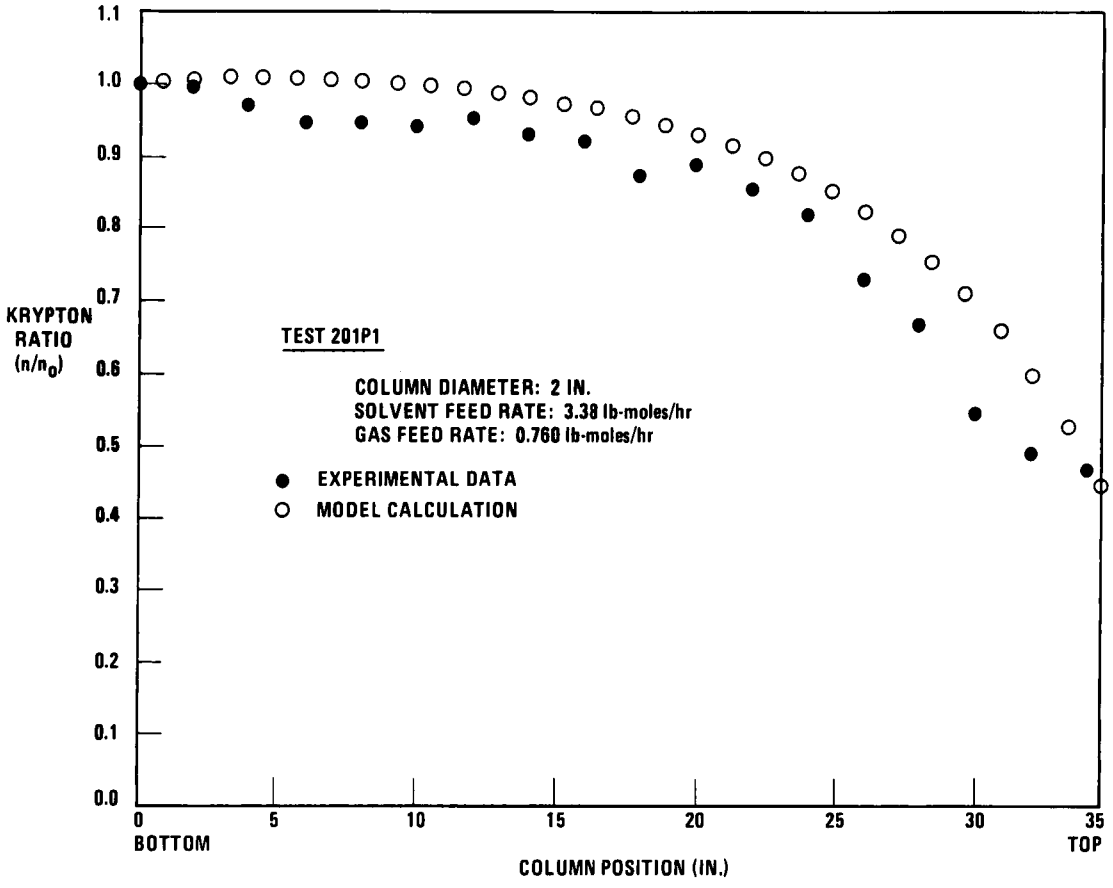

Figure V-10

EXPERIMENTAL AND CALCULATED KRYPTON PROFILES
FOR TEST 201P1

for the next, any errors will accumulate at the bottom of the column. It is useful, therefore, to compare the calculated and experimental values of the feed gas compositions and flow rates. These are presented in Table V-3 along with the operating conditions for the nine sets of data used. As krypton is present in only trace quantities, the feed gas is essentially a binary mixture and only the concentration of R-12 is listed. Here, also, the agreement is quite good.

C. COMPARISON OF EXPERIMENTAL DATA AND MODEL CALCULATIONS

The model and the data closely agree for the nine sets of data used to formulate the mass transfer correlations. However, a more valid test is a comparison of the model's calculations with experimental data not used in the development of the model. The remaining 46 sets of the data are compared to the calculations of the model in Appendix B. The agreement in these cases is similar to that obtained in the nine sets discussed previously. An overall comparison is provided in Figure V-11 where the experimentally determined feed gas flow rates are plotted versus the calculated values for every set of experimental data collected. As can be seen, these values agree within 5%. With the solvent feed rate between 3.3 and 9.3 lb mole/hr and the gas feed rate between 0.23 and 1.6 lb moles/hr, the calculations of the model accurately match the performance of each of the three test absorbers.

TABLE V-3

OPERATING CONDITIONS AND MODEL COMPARISONS FOR DATA USED IN CORRELATIONS

Test Number	Column Diameter (in.)	Temperature (°F)	Pressure (atm)	Solvent Feed Rate (lb-moles/hr)	Off-Gas Flow Rate (lb-moles/hr)	Off-Gas R-12 Content (%)	Feed Gas Flow Rate (lb-moles/hr)		Feed Gas R-12 Content (%)	
							Measured	Calculated	Measured	Calculated
1026A1	4	- 7.53	8.31	9.30	0.400	16.4	0.512	0.515	8.2	7.6
1117A1	4	-15.61	8.30	4.79	1.420	13.7	1.419	1.409	8.0	7.4
1118P1	4	-13.14	8.29	3.34	0.608	14.5	0.620	0.621	6.9	7.5
1207A1	3	-13.18	8.24	6.24	0.985	14.6	1.008	1.015	8.4	7.2
1212P1	3	-10.65	8.18	3.34	1.000	15.6	0.996	0.962	7.6	6.4
1214P2	3	- 6.94	8.24	9.20	0.435	16.8	0.520	0.543	8.2	7.1
124P2	2	-10.89	8.26	7.85	0.540	15.3	0.623	0.629	7.5	7.2
125A1	2	- 4.28	8.24	9.23	0.132	17.8	0.229	0.262	8.4	8.4
201P1	2	-10.72	8.31	3.38	0.764	15.3	0.760	0.750	7.2	6.5

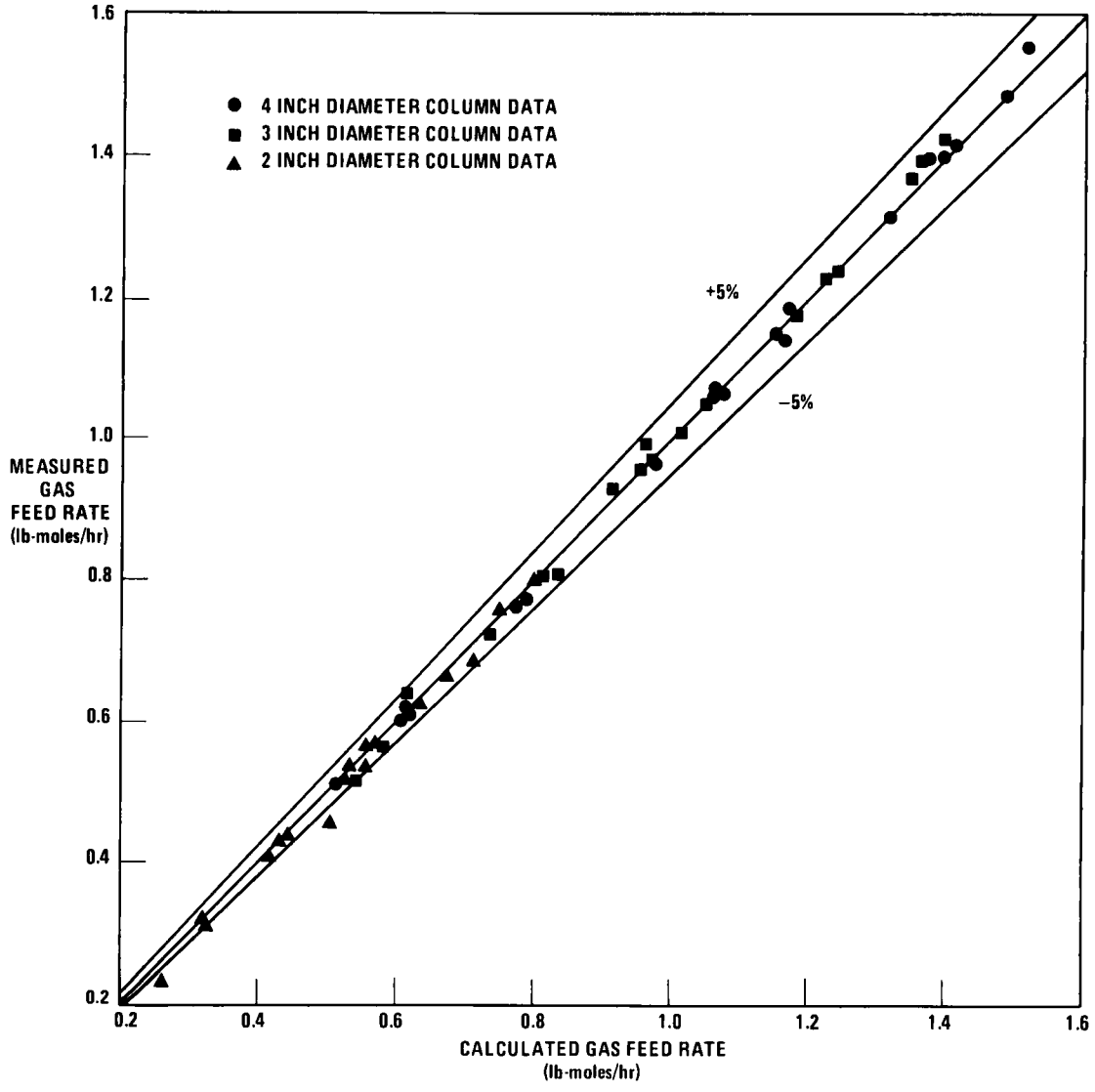

Figure V-11

COMPARISON OF EXPERIMENTAL AND CALCULATED FEED GAS FLOW RATES

CHAPTER VI

DISCUSSION OF RESULTS

A. COLUMN DIAMETER

The main purpose of this work is to examine the effect of column diameter on the performance of the fluorocarbon process absorber. The performance of packed columns in which the ratio of the column diameter to the diameter of a particle of the packing material is less than eight, can be significantly influenced by wall effects.[4] As the particle diameter for Goodloe packing is not clearly defined, it is necessary to determine the extent to which wall effects influence the performance of the ORGDP pilot plant absorber so that pilot plant data can be extrapolated for the design of a larger column.

The calculations of the model described in the last chapter are based on the flow rates per unit cross-sectional area. Other than this, no allowances are made for column diameter. The same mass transfer correlations are employed for each of the three test absorbers. Yet, as can be seen from the experimental and calculated krypton profiles in Appendix B and from Figure V-11, where the experimental and calculated values of the gas feed rate are compared, the model matches the performance of the three columns equally well. Therefore, when operated at the same conditions, with the flow rates expressed per unit cross-sectional area, there is no significant difference between the performance of the three columns. These columns are then large enough that their performance is not influenced by wall effects. Furthermore, in this system, the mass

transfer efficiency of a column large enough to avoid significant wall effects, is in no other way effected by column diameter. This is the same conclusion Groenhof reached in his work with Raschig rings.[16, 17] For the fluorocarbon process, with the solvent feed rate between 40 and 400 lb moles/hr-ft^2 and the feed gas flow rate between 6 and 36 lb moles/hr-ft^2, pilot plant absorption data obtained from columns with diameters of 2 inches or greater can, in fact, be directly extrapolated for the design of a larger facility, as claimed by the manufacturer of Goodloe packing.[28] The model developed in this work will adequately describe the performance of a larger column, provided the column is properly designed. Particular attention was given to the design of the test absorbers to ensure good distribution of both phases. In large diameter columns, uniform distribution may be difficult to achieve and should be an important design consideration.

B. CARRIER GAS COABSORPTION

The effect, identified by Merriman,[26] that carrier gas coabsorption has on the performance of the fluorocarbon process absorber was examined through use of the model developed in this work. Three cases were calculated which varied only in the amount of nitrogen absorbed. Since more nitrogen is absorbed in cases with large solvent feed to gas feed rate ratios, the three cases were calculated at the temperature, pressure, and feed flow rates of test 1026A1, in which this ratio is relatively large. In order to isolate the effect of carrier gas coabsorption, in each case, the feed gas was saturated with R-12, thereby essentially eliminating any driving force for the flux of nitrogen or R-12 across the gas phase. The three cases differ in the nitrogen

content of the solvent feed. The solvent is saturated with nitrogen in case I, contains one-half the equilibrium amount in case II, and is pure R-12 in case III. The krypton profiles for these three cases are shown in Figure VI-1.

If the solvent feed is not saturated with nitrogen, a driving force exists for the transfer of nitrogen across the liquid phase. However, as the gas phase is saturated with R-12, it will not transfer just nitrogen to the liquid phase, but rather both nitrogen and R-12 in a ratio equal to that of the gas phase concentrations. Figure VI-2 shows the sum of nitrogen and R-12 flux profiles and the krypton flux profile for each case. In case I, as the solvent feed is saturated with nitrogen, no driving force for the transfer of R-12 or nitrogen exists and hence none occurs. The flux of krypton, therefore, arises solely from its own concentration gradient. In case II, there is a driving force and interphase transfer of nitrogen and R-12 does occur. At the top of the column where the solvent is the purest, the largest driving force exists, resulting in the greatest flux. The interaction between the fluxes of nitrogen, R-12, and krypton, as described by equations II-9 and II-10, page 12, causes the flux of krypton to be greater than that caused by its concentration gradient alone. This increase in the flux of krypton, due to coabsorption of the carrier gas, is reflected in the increased removal shown in Figure VI-1. Case III shows the same effect as case II; but as a greater driving force exists for the transfer of nitrogen, the R-12-nitrogen flux is greater, causing a corresponding increase in the flux of krypton and even better column performance.

Figure VI-3 shows the dramatic change in the gas flow rate along the column due to absorption of the carrier gas. Obviously, a method of

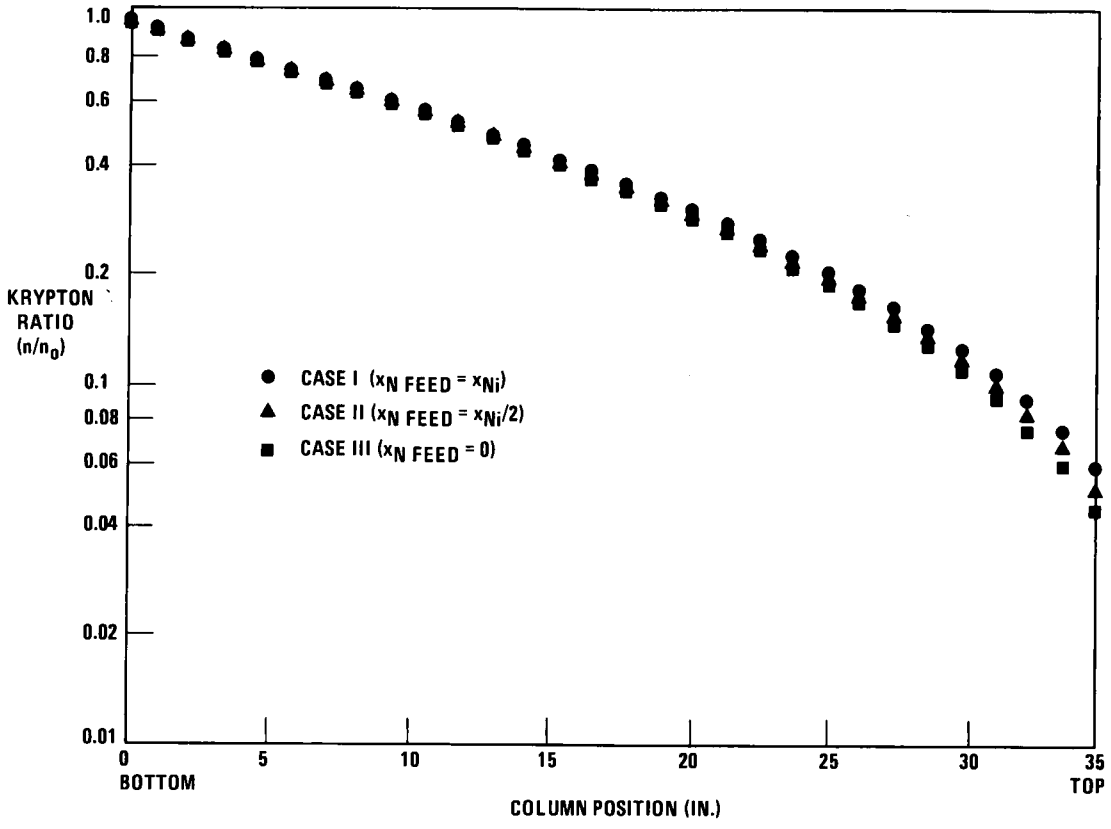

Figure VI-1

EFFECT OF CARRIER GAS COABSORPTION ON ABSORBER KRYPTON PROFILE

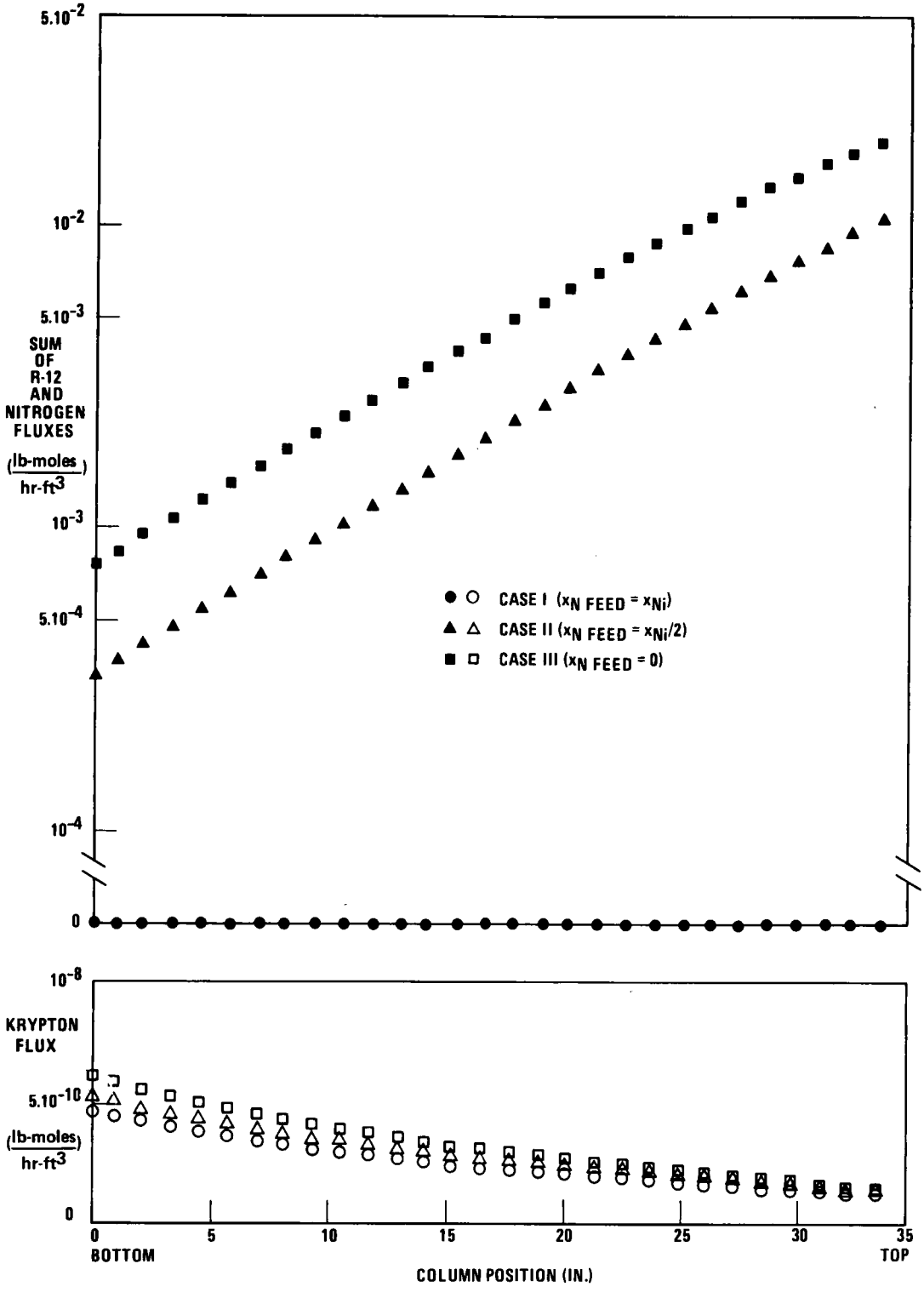

Figure VI-2
EFFECT OF CARRIER GAS COABSORPTION ON FLUX PROFILES

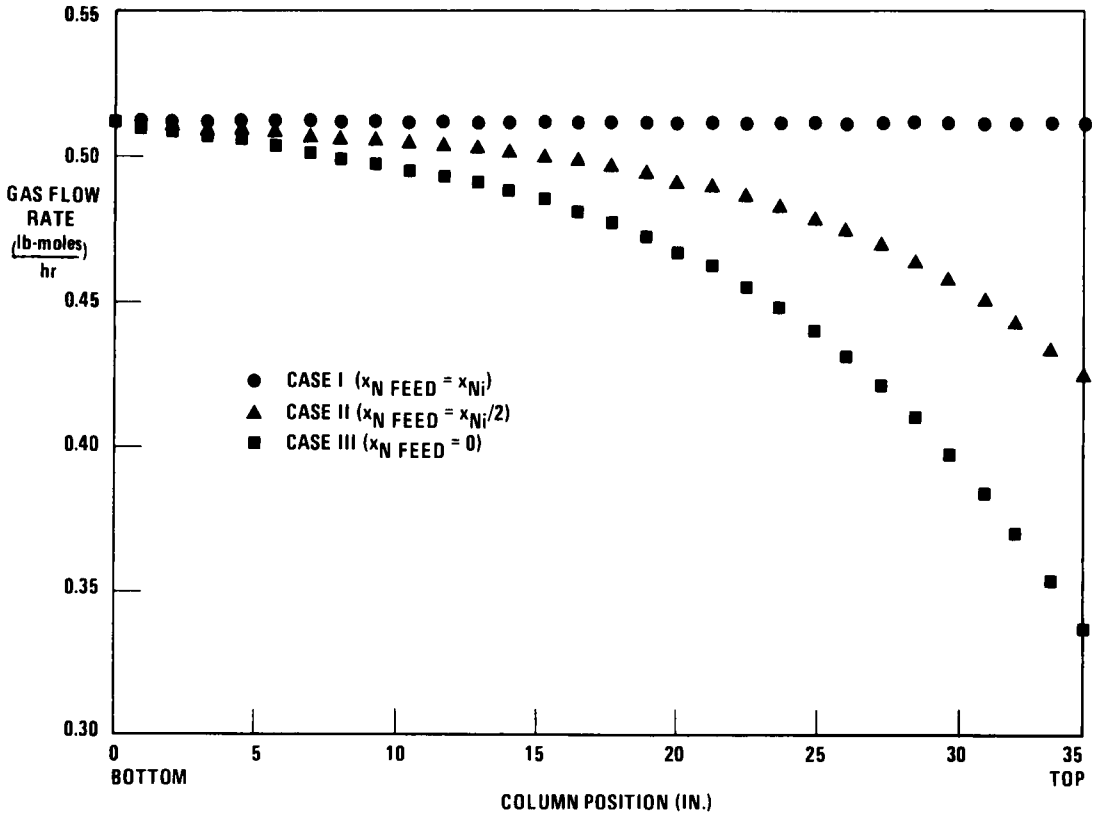

Figure VI-3

EFFECT OF CARRIER GAS COABSORPTION ON GAS FLOW RATE

analysis which assumes that only one component transfers phases or that the gas flow rate is constant, such as Colburn's equation, equation II-28, page 17, should not be applied to an absorber in which the carrier gas is absorbed to an appreciable extent as artifically high mass transfer correlations would result.

Although the effect due to carrier gas coabsorption can be increased by increasing the solubility of nitrogen either through reducing the temperature or increasing the pressure, these parameters are often fixed by other process considerations. However, for a given set of operating conditions, in the fluorocarbon process, full advantage is taken of the enhanced absorber performance caused by coabsorption of the carrier gas by providing the absorber with a solvent feed consisting of essentially pure R-12.

C. SOLVENT VAPORIZATION

Several of the experimental and calculated krypton profiles shown in Appendix B, those of test 1207P2, for example, contain a slight hump in which the molar krypton ratio exceeds unity. This indicates that the amount of krypton at this point is slightly greater than the amount present at the bottom of the column. During the development of the model, it became apparent that this effect was caused by vaporization of the solvent into the subsaturated gas feed. In essence, this is the inverse of carrier gas coabsorption.

In a manner very similar to that used for carrier gas coabsorption, the model was used to examine the effects due to vaporization of the solvent. Three cases were calculated in which varying amounts of solvent were allowed to vaporize. The calculations were made at the

temperature, pressure, and feed flow rates of test 1117A1. The low feed solvent to feed gas flow rate ratio of this test allows a significant amount of the solvent to vaporize. In order to avoid the effect of carrier gas coabsorption, the solvent feed was saturated with nitrogen in all three cases. The cases differ in the R-12 content of the feed gas. The feed gas consists of an equilibrium mixture of nitrogen and R-12 in case I, contains one-half the equilibrium amount of R-12 in case II, and is pure nitrogen in case III. The krypton profiles for these three cases are shown in Figure VI-4. The profiles for cases II and III clearly show a build-up in the amount of krypton within the column.

Figure VI-5 shows the sum of the nitrogen and R-12 flux profiles and the krypton flux profile for each of the three cases. In cases II and III, where the feed gas is not saturated with R-12, a driving force exists for the transfer of R-12 across the gas phase. However, similar to carrier gas coabsorption, as the liquid phase is at equilibrium, R-12 will not be transferred alone; but rather the flux from the liquid phase to the gas will consist of R-12 and nitrogen in a ratio equal to that of their liquid phase concentrations. In case I, as the bulk components of both phases are essentially at equilibrium, there is no flux of either nitrogen or R-12, and the flux of krypton arises solely from its own concentration gradients. The flux of krypton in this case is always positive, and the krypton profile steadily decreases up the column. A driving force for the transfer of R-12 does exist in cases II and III. The resultant flux of R-12 and nitrogen in these cases is largest at the bottom of the column where the gas phase contains the least R-12. This flux, however, is in the opposite direction that the krypton would move in deference to its own concentration

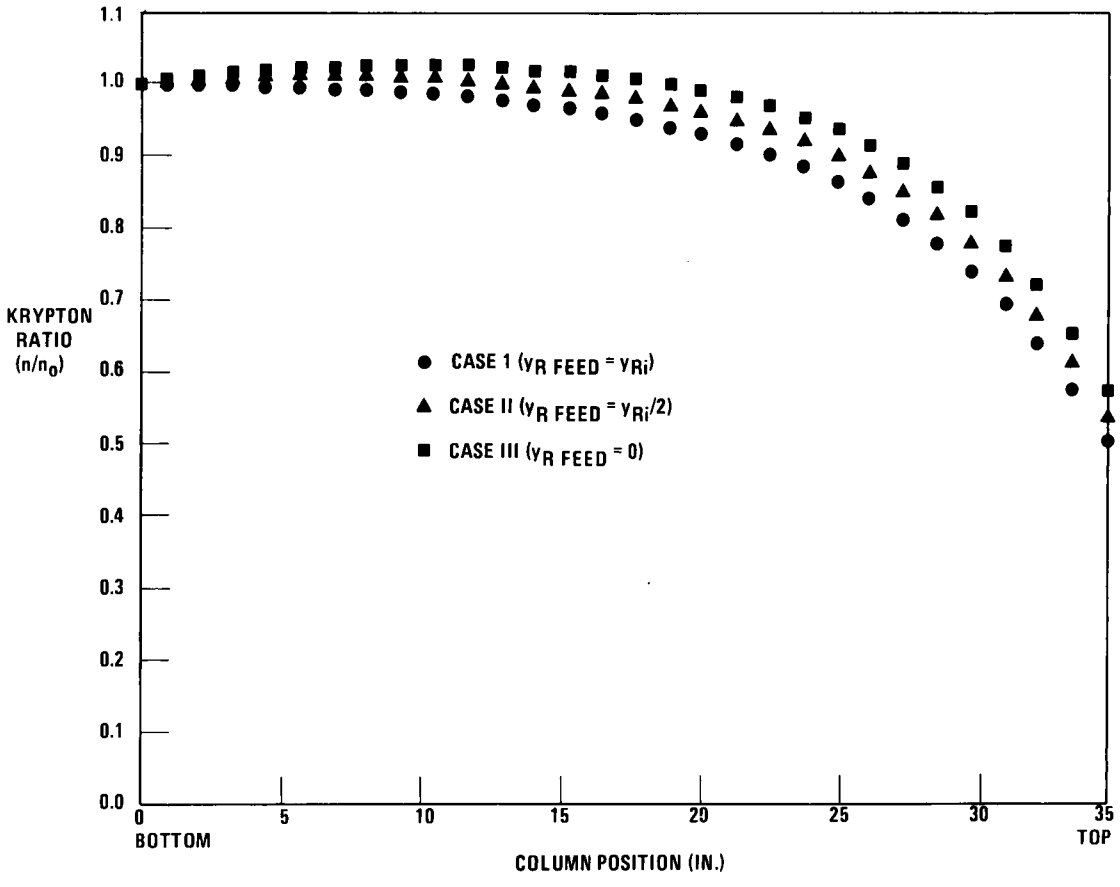

Figure VI-4

EFFECT OF SOLVENT VAPORIZATION ON ABSORBER KRYPTON PROFILE

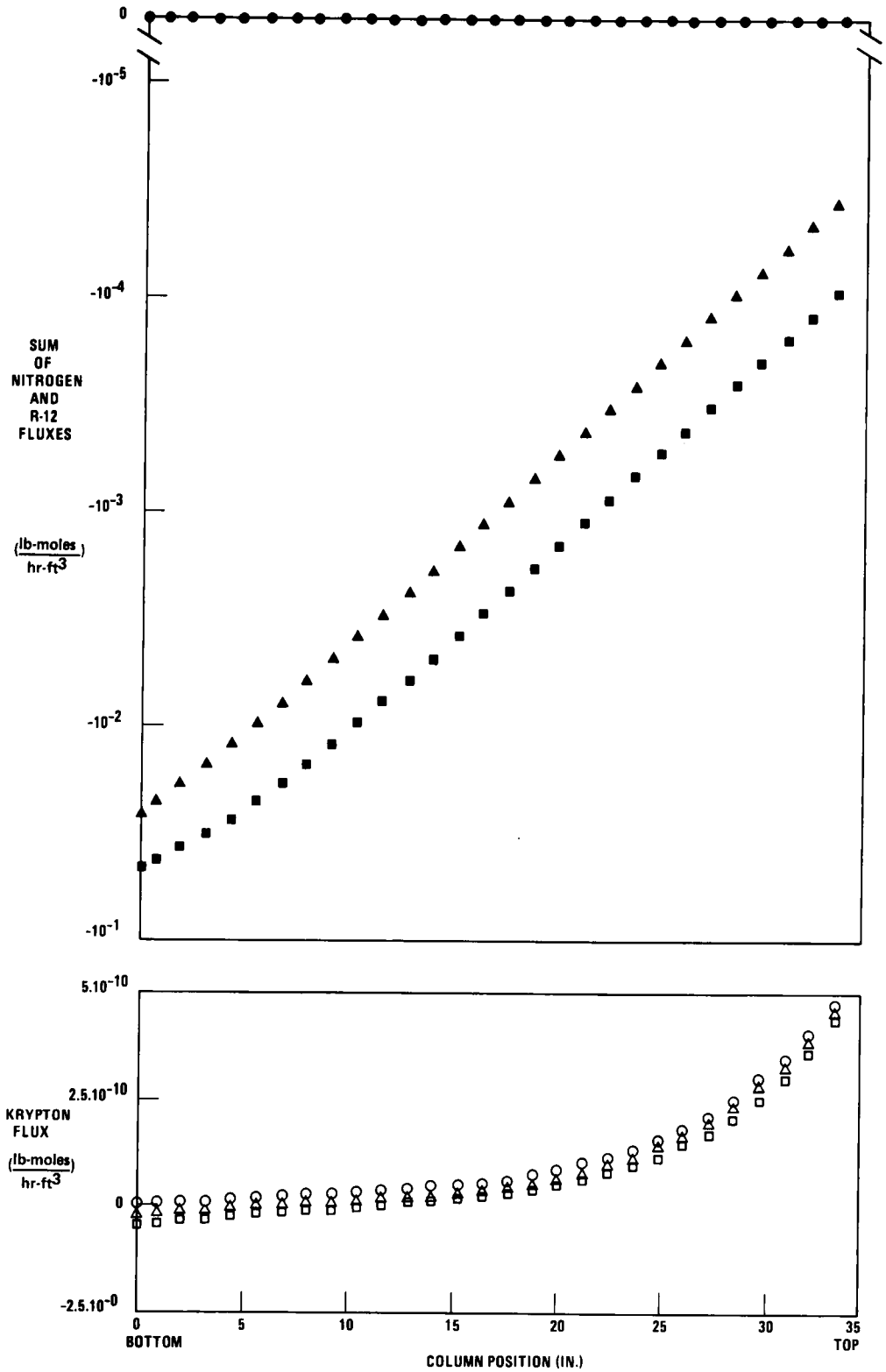

Figure VI-5
EFFECT OF SOLVENT VAPORIZATION ON FLUX PROFILES

gradients. The interaction between these opposing driving forces, as described by equations II-9 and II-10, page 12, causes the flux of krypton to be less than that in case I. Where the R-12-nitrogen flux is large enough, this interaction causes the krypton to move against its own concentration gradient. Consequently, in cases II and III, the bottom portion of the column is actually functioning as a stripper, which causes the hump in the krypton profiles and the deterioration of column performance. This is the "reverse diffusion" described by Toor and Sebulsky.[47]

Figure VI-6 shows the increase in the gas flow rate caused by vaporization of the solvent. As was the case for carrier gas coabsorption, analysis of a column in which solvent vaporization occurs should account for flow rate variations, allow all components to undergo interphase transfer, and account for the interaction between the various fluxes. The application of more simplified approaches would result in mass transfer correlations of lesser magnitude. In cases where both carrier gas absorption and solvent vaporization occur, as in the fluorocarbon process absorber, the flow rate of the column off-gas can be greater, smaller, or very close to the feed gas flow rate. The effects of carrier gas absorption and solvent vaporization probably go unnoticed or are ignored in many of the industrial systems which employ volatile solvents or soluble carrier gases. Analysis of these systems with the more commonly used simplified techniques would produce results which when extrapolated to other situations might lead to significant errors.

The feed to the fluorocarbon process from a nuclear fuel reprocessing plant will not contain any R-12, and therefore represents the worst possible case with respect to solvent vaporization. However,

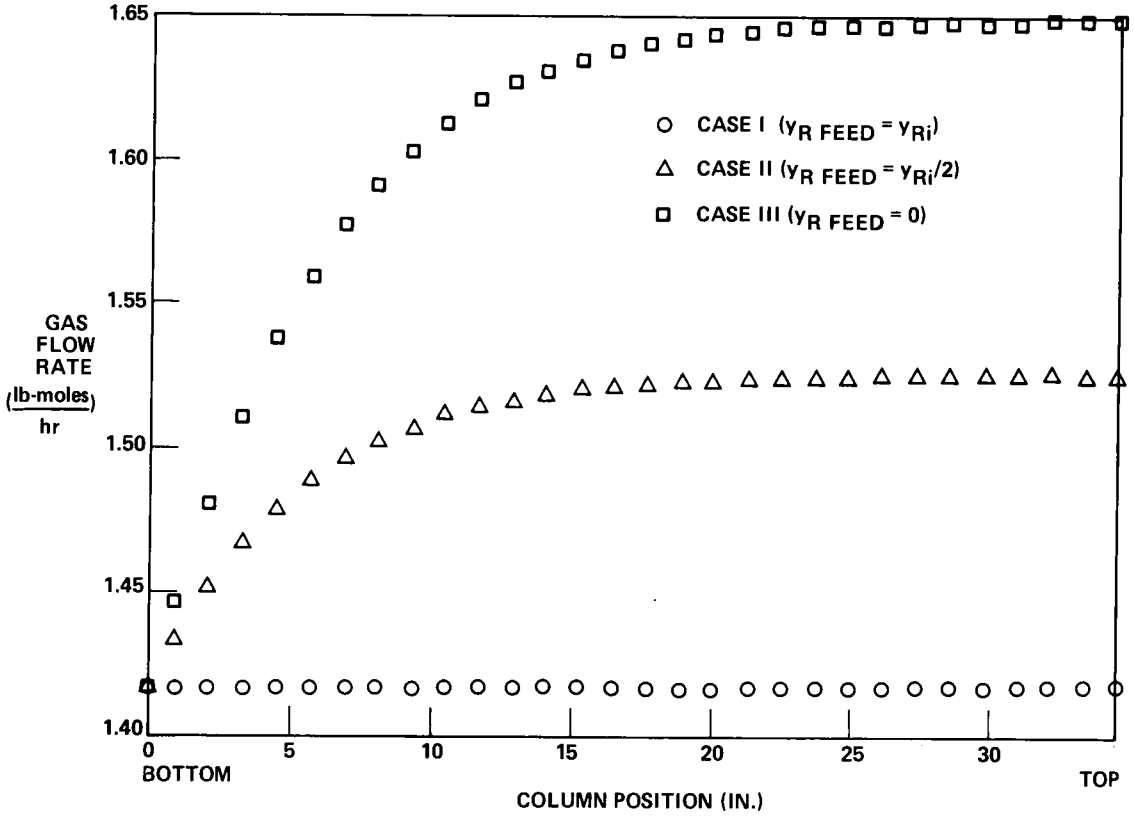

Figure VI-6

EFFECT OF SOLVENT VAPORIZATION
ON GAS FLOW RATE

if the feed stream could be saturated with R-12 prior to introduction into the absorber, the detrimental effect of solvent vaporization should be eliminated. Following this line of thought, an injector system, capable of adding gaseous R-12 to the process feed, has recently been fabricated and installed in the ORGDP pilot plant. Absorber tests have been conducted with a feed gas consisting of pure nitrogen and, through use of the injector, feed streams containing various amounts of R-12. Although a thorough analysis of these data has not yet been completed, the column did perform as anticipated. A hump appeared in the krypton profile when the feed gas was pure nitrogen. The size of the hump decreased, and the overall performance of the absorber was noticeably improved in tests in which the injector was in use. When the injector was used to saturate the feed stream with R-12, the hump disappeared completely as expected. Furthermore, the injector was used to create a feed stream that was supersaturated with R-12. In this case, the excess solvent should condense within the column and, as in the case of carrier gas coabsorption, cause the flux of krypton to increase. This in fact occurred, and the column performed better during this test than it had in any other case. Although further work is needed on the injector system, it appears very promising and, in principle, might be applied to improve the performance of other absorption systems.

CHAPTER VII

CONCLUSIONS AND RECOMMENDATIONS

A. CONCLUSIONS

Through the course of this work, the following conclusions were reached:

1. The mass transfer efficiency of the fluorocarbon process absorber is not significantly effected by column diameter when carried out in Goodloe packed columns with diameters greater than or equal to 2 inches.

2. Absorber performance data collected at the ORGDP pilot plant can confidently be extrapolated for the design of a larger facility.

3. The model developed in this work will adequately describe the performance of a properly designed pilot- or full-scale column.

4. As shown by Merriman,[26] the absorption of krypton is enhanced by coabsorption of the carrier gas.

5. Solvent vaporization can occur in the fluorocarbon process absorber and will adversely affect the absorption of krypton.

6. The detrimental effects of solvent vaporization can be eliminated by saturating the feed gas with R-12.

7. Supersaturating the feed gas with the process solvent will improve the performance of the absorber.

B. RECOMMENDATIONS

The following recommendations are made for future work in this area:

1. The effects of carrier gas coabsorption and solvent vaporization should be included in the analysis of any absorption system employing either a soluble carrier gas or a volatile solvent.

2. The solvent injector system should be thoroughly evaluated for application to both the fluorocarbon process absorber and gas absorption systems in general.

3. The absorber model should be expanded to include species other than krypton that might be present in the feed to the fluorocarbon process.

4. As more accurate solubility data become available, it should be incorporated into the model.

5. If the test absorbers fabricated in this effort are used in any future program, a method for accurately reproducing the bottommost position for the gamma scanner should be provided to avoid the shift in the krypton profiles encountered in this work.

LIST OF REFERENCES

LIST OF REFERENCES

1. Ackley, R. D., and Notz, K. J., *The Distribution of Xenon Between Gaseous and Liquid CO_2*, USDOE Report ORNL-5122, Oak Ridge, Tennessee (1976).

2. Aziz, R. A., "Comment on the Paper 'Second Virial Coefficients and Force Constants, E_o and r_o, of Six Halogen-Substituted Methanes'," *J. Chem. Phys., 58*, 4711 (1973).

3. Aziz, R. A., and Poole, G. R., "Sound Velocity in Liquid CCl_2F_2 and the Law of Corresponding States," *A.I.Ch.E.J., 18*, 430 (1972).

4. Baker, T., Chilton, T. H., and Vernon, H. C., "The Course of Liquid Flow in Packed Towers," *Trans. Am. Inst. Chem. Eng., 31*, 296 (1935).

5. Bird, R. B., Stewart, W. E., and Lightfoot, E. N., *Transport Phenomena*, John Wiley & Sons, New York (1966).

6. Bragg, L. B., "Goodloe Column Packing," *Ind. Engr. Chem., 49*, 1062 (1957).

7. Chase, R. L., *Nuclear Pulse Spectrometry*, McGraw-Hill, New York (1961).

8. Choi, W. M., Michel, R. C., and Varlet, J. P., *Flooding Characteristics of Packed Columns with High Efficiency Packings*, USDOE Report ORNL/MIT-223, Oak Ridge, Tennessee (1976).

9. Colburn, A. P., "Simplified Calculation of Diffusional Processes," *Ind. Engr. Chem., 33*, 459 (1941).

10. Colburn, A. P., and Drew, T. B., "The Condensation of Mixed Vapors," *Trans. Am. Inst. Chem. Engr., 33*, 197 (1937).

11. E. I. duPont de Nemours and Company, Inc., *Thermodynamic Properties of Freon-12 Refrigerant*, Technical Bulletin T-12, Wilmington, Delaware (1956).

12. Environmental Protection Agency, *Environmental Analysis of the Uranium Fuel Cycle. Part II, Nuclear Power Reactors*, USEPA Report EPA-520/9-73-003-C, Washington, D. C. (1974).

13. Environmental Protection Agency [40 CFR Part 190], *Federal Register*, Vol. *40*, No. 104, 23420 (May 29, 1975).

14. Fulham, M. J., and Hulbert, V. B., "Gamma Scanning of Large Towers," *Chem. Engr. Progress, 71*, 6 (1975).

15. Gardner, R. P., and Ely, R. L., *Radioisotope Measurement Applications in Engineering*, Reinhold Publishing Corporation, New York (1967).

16. Groenhof, H. C., "Scaling-up of Packed Columns, Part I," *Chem. Engr. J., 14*, 181 (1977).

17. Groenhof, H. C., "Scaling-up of Packed Columns, Part II," *Chem. Engr. J., 14*, 193 (1977).

18. Hildebrand, J. H., "Thermodynamic Parameters for Dissolved Gases," *Proc. Nat. Acadam. Sci. U.S., 64*, 1331 (1969).

19. Hirschfelder, Curtis, and Bird, *Molecular Theory of Gases and Liquids*, John Wiley & Sons, New York (1954).

20. Jones, D. W., and Jones, J. B., "Tray Performance Evaluation," *Chem. Engr. Progress, 71*, 6 (1975).

21. Kallen, B. J., Trevenow, L. E., and Steindler, M. J., *Tritium and Noble Gas Fission Products in the Nuclear Fuel Cycle. Part II, Fuel Reprocessing Plants*, USDOE Report ANL-8135, Argonne National Laboratory, Argonne, Illinois (1975).

22. Letter to B. E. Kanak from E. J. Bragg, Metex Corporation, April 12, 1977.

23. Markas, S. E., and Beckmann, R. B., "Radioisotope Technique for the Determination of Flow Characteristics in Liquid-Liquid Extraction Columns," *A.I.Ch.E.J., 3*, 223 (1957).

24. McCaw, D. D., Hulbert, V. G., and Smith, A. E., *Gamma Scanning of Large Sieve Tray Towers*, Atomic Energy of Canada Limited Report AECL-5283, Chalk River, Ontario, Canada (1976).

25. McHarness, R. C., Eiseman, B. J., and Martin, J. J., "Freon-12," *Refrigeration Engineering*, 32 (September 1955).

26. Merriman, J. R., *Analysis of a Multicomponent Gas Absorption System with Carrier Gas Coabsorption*, PhD Thesis, The University of Tennessee, Knoxville, Tennessee (1975).

27. Merriman, J. R., *The Solubility of Gases in CCl_2F_2: A Critical Review*, USDOE Report KY-G-400, Paducah, Kentucky (1977).

28. Metex Corporation, Process Equipment Division, *How to Design a Goodloe Column*, Technical Bulletin, Edison, New Jersey (1975).

29. Metex Corporation, Process Equipment Division, *Instructions for the Installation of Goodloe Packing*, Technical Bulletin, Edison, New Jersey (1978).

30. Miller, J. W., Schorr, G. R., and Yaws, C. L., "Viscosity of Gas," *Chem. Engr., 83* (25), 155 (1976).

31. Neufeld, P. D., Janzen, A. R., Aziz, R. A., "Empirical Equations to Calculate 16 of the Transport Collision Integrals for the Lennard-Jones (12-6) Potential," *J. Chem. Phys., 57*, 1100 (1972).

32. Notz, K. J., and Meservey, A. B., *The Solubility of Krypton in Liquid CO_2*, USDOE Report ORNL-5121, Oak Ridge, Tennessee (1976).

33. Perry, R. H., and Chilton, C. H., Editors, *Chemical Engineer's Handbook*, 5th Edition, McGraw-Hill Book Company, New York (1973).

34. Private communication with M. J. Stephenson, Union Carbide Corporation, Nuclear Division, Oak Ridge, Tennessee, September 18, 1978.

35. Ramm, V. M., *Absorption of Gases*, Israel Program for Scientific Translation, Jerusalem (1968).

36. Reid, R. C., Prausnitz, J. M., and Sherwood, T. K., *The Properties of Gases and Liquids*, 3rd Edition, McGraw-Hill Book Company, New York (1977).

37. Shaffer, J. H., Shockley, W. E., and Greene, C. E., *The Solubility of Krypton and Xenon at Infinite Dilution in Dichlorodifluoromethane*, USDOE Report ORNL/TM-6652, Oak Ridge, Tennessee (1978).

38. Shulman, H. L., Ullrich, C. F., Proulx, A. Z., and Zimmerman, J. O., "Performance of Packed Columns II. Wetted and Effective-Interfacial Areas, Gas- and Liquid-Phase Mass Transfer Rates," *A.I.Ch.E.J., 1*, 253 (1955).

39. Shulman, H. L., Ullrich, C. F., and Wells, N., "Performance of Packed Columns I. Total, Static, and Operating Holdups," *A.I.Ch.E.J., 1*, 247 (1955).

40. Shulman, H. L., Ullrich, C. F., Wells, N., and Proulx, A. Z., "Performance of Packed Columns III. Holdup for Aqueous and Nonaqueous Systems," *A.I.Ch.E.J., 1*, 259 (1955).

41. Steinberg, M., *The Recovery of Fission Product Xe and Kr by Absorption Processes*, USDOE Report BNL-542, Brookhaven National Laboratory, Long Island, New York (1959).

42. Steinberg, M., and Manowitz, B., "Recovery of Fission Product Noble Gases," *Ind. Engr. Chem., 51*, 1 (1959).

43. Stephenson, M. J., *Analysis of a Fractional Gas Stripper*, USDOE Report K-1895, Oak Ridge, Tennessee (1978).

44. Stephenson, M. J., Dunthorn, D. I., Reed, W. D., and Pashley, J. H., *Absorption Process for Removing Krypton from the Off-Gas of an LMFBR Fuel Reprocessing Plant*, USDOE Report K-L-6338, Oak Ridge, Tennessee (1974).

45. Stephenson, M. J., Eby, R. S., and Huffstetler, V. C., *ORGDP Selective Absorption PIlot Plant for Decontamination of Fuel Reprocessing Plant Off-Gas*, USDOE Report K-1876, Oak Ridge, Tennessee (1977).

46. Stephenson, M. J., Merriman, J. R., and Dunthorn, D. I., *Experimental Investigation of the Removal of Kr and Xe from Contaminated Gas Streams by Selective Absorption in Fluorocarbon Solvents: Phase I Completion Report*, USDOE Report K-1780, Oak Ridge, Tennessee (1970).

47. Toor, H. L., and Sebulsky, R. T., "Multicomponent Mass Transfer," *A.I.Ch.E.J.*, *7*, 558 (1961).

48. Treybal, R. E., *Mass-Transfer Operations*, 2nd Edition, McGraw-Hill Book Company, New York (1968).

49. Whitman, W. G., "The Two-Film Theory of Gas Absorption," *Chem. Met. Engr.*, *29*, 146 (1923).

50. Yamamoto, Y., and Takeda, H., "Solubility of ^{85}Kr in Some Organic Solvents," *J. Fac. Engr. U. Tokyo, A-7*, 44 (1970).

APPENDIXES

APPENDIX A

PHYSICAL PROPERTIES

A. KRYPTON

Distribution Coefficient

The equilibrium gas-liquid distribution of krypton can be expressed in the form of Henry's law,

$$y = mx, \qquad \text{A-1}$$

where m = Henry's law constant, D/P, and

D = distribution coefficient, atm.

Values of the distribution coefficient for krypton in R-12 have been determined by several investigators. Steinberg[41] performed the initial work at Brookhaven National Laboratory. Yamamoto and Takeda[50] obtained some data at the University of Tokyo. More recently, some values have been determined at Oak Ridge National Laboratory by Shaffer.[37] Merriman[27] has estimated values of D_K through use of Hildebrand's regular solution theory. This experimental data, Merriman's prediction, and a least squares fit of Shaffer's data are presented for the region of interest to this work in Figure A-1. As the experimental details of Shaffer's work are better known than those of the other authors and his data adequately cover the desired temperature range, the correlation of his data,

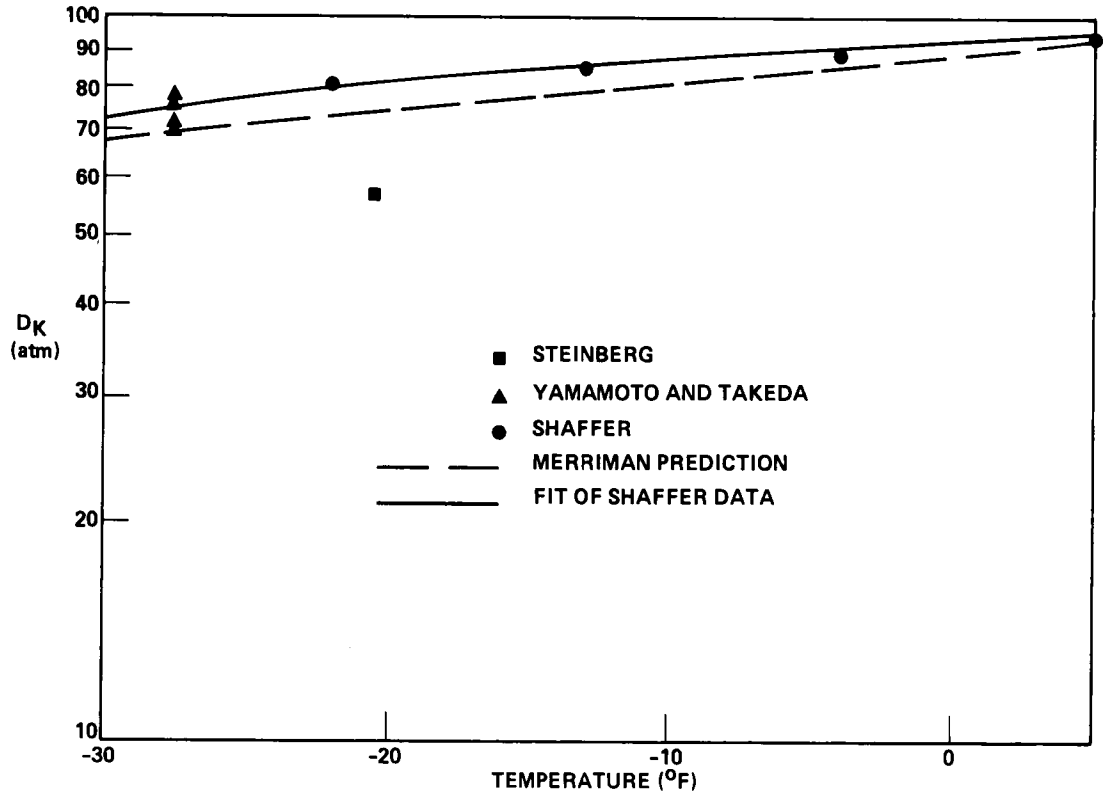

Figure A-1

KRYPTON DISTRIBUTION COEFFICIENTS

$$D_K = e^{\left(5.156 - \frac{65.317}{T + 104.93}\right)}, \text{ atm}, \qquad \text{A-2}$$

is used in this work.

Molar Volume and Lennard-Jones Parameters

The molar volume of krypton at its normal boiling point, V_{bK}, is required to determine the liquid phase diffusivity. This quantity is estimated with

$$V_b/V_c = 0.38,^{(18)} \qquad \text{A-3}$$

where V_c = critical volume, 92.2 cm^3/g-mole for krypton.[5]

The Lennard-Jones force parameters used in the calculation of the gas phase diffusivity are

$$\varepsilon_K = 190°K, \qquad \text{A-4}$$

and

$$\sigma_K = 3.61 \text{ Å}.^{(5)} \qquad \text{A-5}$$

B. NITROGEN

Distribution Coefficient

The published data on the equilibrium distribution of nitrogen in R-12 is limited and exhibits considerable scatter. Steinberg[41] and Yamamoto and Takeda[50] have provided a few points in the range of interest. Stephenson[34] has calculated some additional values from data collected on the flash chamber of the ORGDP pilot plant.

Merriman[27] has developed an expression for estimating values of D_N based on regular solution theory as he did for krypton. Stephenson has proposed using the expression

$$D_N = e^{6.097 + 0.00166T}, \qquad \text{A-6}$$

which represents an average of the experimental data, assuming the temperature dependency of Merriman's prediction. Figure A-2 shows these data, Merriman's estimate, and Stephenson's average. In this work, Stephenson's correlation is used in equation A-1 to determine the equilibrium distribution of nitrogen.

Viscosity of Gaseous Nitrogen

The viscosity of nitrogen is required to determine the viscosity of the gas mixture for use in the Reynolds and Schmidt numbers. This quantity is determined from the expression suggested by Miller,[30]

$$\mu_{GN} = 30.43 + 0.4989T - 1.093 \cdot 10^{-4} T^2, \text{ micropoise}, \qquad \text{A-7}$$

where T = temperature, °K.

Molar Volume and Lennard-Jones Parameters

The value of the molar volume used to determine the liquid phase diffusivity is

$$V_b = 31.2 \text{ cm}^3/\text{g-mole}.^{(33)} \qquad \text{A-8}$$

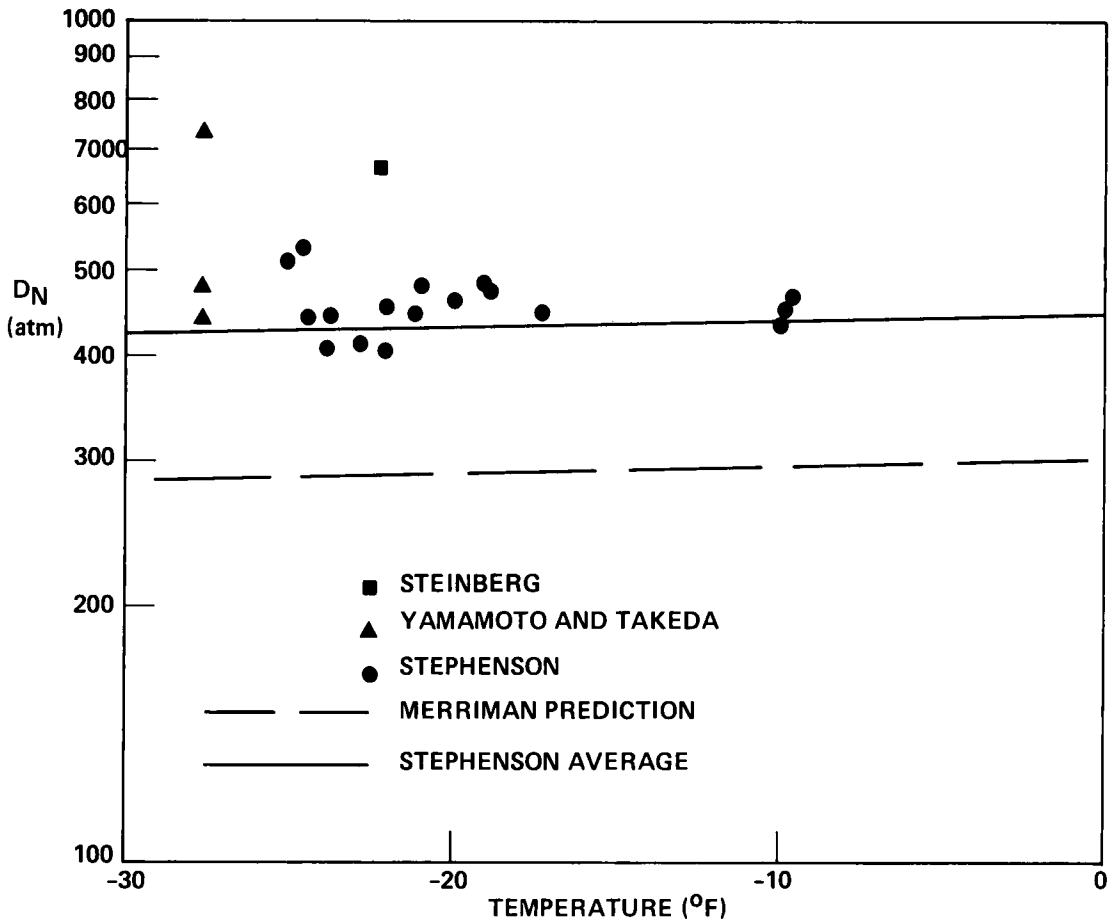

Figure A-2

NITROGEN DISTRIBUTION COEFFICIENTS

The Lennard-Jones force constants,

$$\varepsilon_N = 91.5 \text{ K} \qquad \text{A-9}$$

and

$$\sigma_N = 3.681 \text{ Å}, \text{(5)} \qquad \text{A-10}$$

are used to estimate the gas phase diffusivity.

C. DICHLORODIFLUOROMETHANE

Distribution Coefficient

The equilibrium distribution of R-12 is determined with Raoult's law,

$$y = \frac{P_R^o}{P} x, \qquad \text{A-11}$$

where P_R^o = vapor pressure of pure R-12, atm.

The expression used to determine P_R^o is that presented by McHarness,(25)

$$\log_{10} P_R^o = A + \frac{B}{T} + C \log_{10} T + DT, \qquad \text{A-12}$$

where A = 39.88381727,

B = -3436.632228,

C = -12.47152228,

D = 0.00473044244, and

T = temperature, °R.

Viscosities

The viscosities μ_{GR} and μ_{LR} are required to determine the Reynolds and Schmidt numbers for each phase. The expressions used,

$$\mu_{GR} = 0.00372 + 0.164 \cdot 10^{-4} T \qquad \text{A-13}$$

and

$$\mu_{LR} = e^{\left(-3.099 + \frac{933}{T}\right)}, \qquad \text{A-14}$$

where μ is in centipoise and T in °R, were both developed by Stephenson[43] to fit data provided by DuPont.[11]

Densities

The gas phase density is determined from the R-12 equation of state as given by McHarness,[25]

$$P = \frac{RT}{(V-b)} + \frac{A + BT \quad Ce^{-JT_r}}{(V-b)^2} + \frac{D + ET + Fe^{-JT_r}}{(V-b)^3}$$

$$+ \frac{G}{(V-b)^4} + \frac{HT + Ie^{-JT_r}}{(V-b)^5}, \qquad \text{A-15}$$

where P = pressure, psia,

R = gas constant, 0.088734 (lb/in.^{2}) ft^3/lb-°R,

T = temperature, °R,

V = volume, ft^3/lb,

T_r = reduced temperature, T/T_c,

T_c = critical temperature, 693.6°R,

b = 0.0065093886,

A = -3.409727134,

B = $1.59434848 \cdot 10^{-3}$,

C = -56.7627671,

D = 0.06023944654,

E = $-1.879618431 \cdot 10^{-5}$,

F = 1.311399084,

G = $-5.48737007 \cdot 10^{-4}$,

H = $3.468834 \cdot 10^{-9}$,

I = $-2.54390678 \cdot 10^{-5}$, and

J = 5.475.

McHarness also provided the correlation used for the density of liquid R-12,

$$\rho_{LR} = A + B\,(T_c - T) - C\,(T_c - T)^{1/2} + D\,(T_c - T)^{1/3} + E\,(T_c - T)^2, \qquad \text{A-16}$$

where A = 34.84,

B = 0.02696,

C = 0.834921,

D = 6.02683, and

E = $-6.55549 \cdot 10^{-6}$.

Surface Tension

The surface tension of R-12, σ_s, is needed to determine the operation void fraction, ε_o. The expression used,

$$\sigma_s = 11.8 \left(\frac{T_c - T}{193.6}\right)^{1.25}, \text{ dynes/cm,} \qquad \text{A-17}$$

was developed by Stephenson[43] from data given by DuPont.[11]

Lennard-Jones Parameters

The Lennard-Jones force parameters used for R-12,

$$\varepsilon_R = 302°K \qquad \text{A-18}$$

and

$$\sigma_R = 4.95 \text{ Å}, \qquad \text{A-19}$$

were obtained by averaging the values given by Hirschfelder, Curtis, and Bird,[19] Aziz,[2] and Aziz and Poole.[3]

APPENDIX B

PILOT PLANT DATA AND MODEL COMPARISONS

The operating parameters of the tests conducted and the calculated values of the feed gas flow rates and compositions are listed in Tables B-1, B-2, and B-3 for the 4-, 3-, and 2-inch-diameter columns, respectively. Since the gas streams are essentially binary mixtures of nitrogen and R-12, as was done earlier, only the R-12 percentages are listed. The experimental and calculated krypton profiles for the tests conducted on the 4-, 3-, and 2-inch-diameter columns are shown respectively in Figures B-1 through B-17, B-18 through B-32, and B-33 through B-46. The tests used in the formulation of the mass transfer correlations are tabulated in Chapter V and are not included here.

TABLE B-1

FOUR-INCH-DIAMETER COLUMN OPERATING CONDITIONS AND MODEL COMPARISONS

Test Number	Temperature (°F)	Pressure (atm)	Solvent Feed Rate (lb-moles/hr)	Off-Gas Flow Rate (lb-moles/hr)	Off-Gas R-12 Content (%)	Feed Gas Flow Rate (lb-moles/hr)		Feed Gas R-12 Content (%)	
						Measured	Calculated	Measured	Calculated
1028A1	-14.8	8.29	6.32	0.725	14.0	0.776	0.789	7.3	7.7
1102A1	-15.3	8.31	7.75	1.001	13.8	1.067	1.076	7.8	7.7
1102P1	-15.3	8.31	7.76	1.347	13.8	1.403	1.396	8.5	7.6
1103A1	-15.1	8.30	7.76	1.480	13.9	1.560	1.516	7.9	7.4
1104A1	- 7.5	8.28	9.25	1.371	16.5	1.400	1.374	9.4	6.1
1104P1	- 6.5	8.20	9.24	1.159	17.0	1.185	1.173	7.8	5.8
1108A1	- 6.1	8.30	9.22	0.930	17.0	0.967	0.977	8.2	6.1
1108P1	- 6.1	8.30	9.20	0.696	17.0	0.763	0.773	7.2	6.5
1109A1	-16.0	8.30	6.29	1.123	13.6	1.144	1.164	6.7	7.6
1109P1	-15.9	8.30	6.30	1.290	13.6	1.316	1.319	8.1	7.6
1110A1	-17.0	8.27	6.30	1.461	13.4	1.492	1.483	8.4	7.5
1110P1	-15.6	8.30	6.30	0.528	13.7	0.601	0.609	7.2	8.0
1111A1	-14.3	8.24	4.85	0.575	14.2	0.612	0.620	7.0	7.7
1111P1	-15.2	8.34	4.87	1.047	13.8	1.064	1.064	7.5	7.6
1115A1	- 9.0	8.28	9.19	1.102	16.0	1.152	1.152	8.9	6.8
1116A1	-14.2	8.26	4.79	0.570	14.2	0.623	0.615	7.3	7.6
1118A1	-14.6	8.32	3.35	1.080	14.0	1.074	1.062	7.6	7.3

TABLE B-2

THREE-INCH-DIAMETER COLUMN OPERATING CONDITIONS AND MODEL COMPARISONS

Test Number	Temperature (°F)	Pressure (atm)	Solvent Feed Rate (lb-moles/hr)	Off-Gas Flow Rate (lb-moles/hr)	Off-Gas R-12 Content (%)	Feed Gas Flow Rate (lb-moles/hr)		Feed Gas R-12 Content (%)	
						Measured	Calculated	Measured	Calculated
1207P1	-14.0	8.17	6.23	1.203	14.5	1.230	1.217	8.6	7.2
1207P2	-13.9	8.20	6.24	1.396	14.4	1.426	1.395	8.7	7.1
1208A1	-13.5	8.17	6.25	0.765	14.6	0.806	0.814	7.9	7.4
1208P1	-13.3	8.31	6.10	0.508	14.4	0.564	0.580	7.1	7.7
1208P2	-13.1	8.37	4.82	0.814	14.4	0.810	0.837	7.5	7.3
1209A1	-14.0	8.17	4.83	1.048	14.4	1.050	1.050	7.8	7.2
1209P1	-14.7	8.31	4.84	1.247	14.0	1.241	1.242	8.0	7.2
1213A1	-10.9	8.31	3.32	0.613	15.3	0.621	0.616	7.2	6.9
1213P1	-14.8	8.30	3.32	1.408	14.0	1.397	1.362	7.8	7.1
1214A1	- 7.7	8.24	9.15	0.900	16.5	0.959	0.956	8.8	6.3
1214P1	- 8.3	8.24	9.18	1.338	16.3	1.372	1.346	9.5	6.1
1215A1	-14.8	8.24	7.80	0.894	14.1	0.970	0.969	7.5	7.5
1215P1	-15.3	8.27	7.80	1.116	13.8	1.180	1.179	8.4	7.5
1216A1	-14.8	8.21	7.78	0.645	14.1	0.723	0.738	8.1	7.8
1216P1	-15.2	8.14	7.80	0.838	14.1	0.932	0.915	7.9	7.6

TABLE B-3

TWO-INCH-DIAMETER COLUMN OPERATING CONDITIONS AND MODEL COMPARISONS

Test Number	Temperature (°F)	Pressure (atm)	Solvent Feed Rate (lb-moles/hr)	Off-Gas Flow Rate (lb-moles/hr)	Off-Gas R-12 Content (%)	Feed Gas Flow Rate (lb-moles/hr)		Feed Gas R-12 Content (%)	
						Measured	Calculated	Measured	Calculated
119P1	-14.9	8.35	6.29	0.473	13.9	0.565	0.566	7.0	7.8
120A1	-15.1	8.28	6.30	0.352	13.9	0.437	0.442	7.1	8.0
120A2	-14.6	8.24	6.30	0.227	14.2	0.308	0.323	6.8	8.4
120P1	-15.8	8.24	6.30	0.604	13.8	0.665	0.677	6.8	7.7
120P2	-16.0	8.21	6.30	0.742	13.8	0.790	0.804	6.9	7.5
124A1	-10.7	8.28	7.84	0.426	15.4	0.515	0.526	7.8	7.5
124P1	-10.4	8.24	7.86	0.310	15.6	0.405	0.418	7.6	7.8
125P1	- 4.8	8.28	9.25	0.401	17.5	0.455	0.503	7.9	6.0
126A1	-16.8	8.31	4.88	0.642	13.3	0.686	0.691	6.4	7.6
126P1	-15.7	8.28	4.89	0.515	13.7	0.565	0.569	6.4	7.6
127P1	-15.3	8.31	4.88	0.365	13.8	0.427	0.429	6.7	7.8
131A1	-10.9	8.31	3.38	0.285	15.2	0.321	0.321	6.2	7.7
131P1	-12.3	8.31	3.38	0.516	14.8	0.537	0.532	6.7	7.0
202A1	-14.7	8.31	6.33	0.474	14.0	0.538	0.555	7.1	7.7

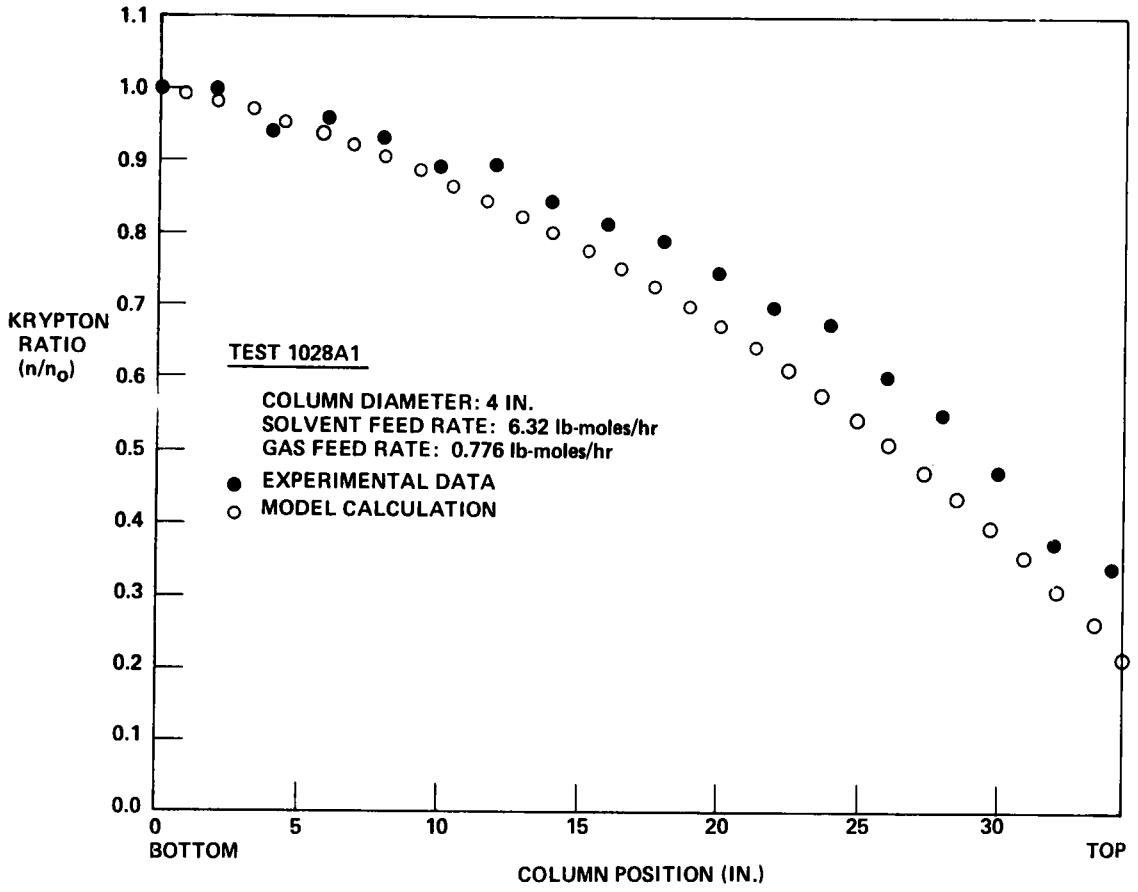

Figure B-1

EXPERIMENTAL AND CALCULATED KRYPTON PROFILES
FOR TEST 1028A1

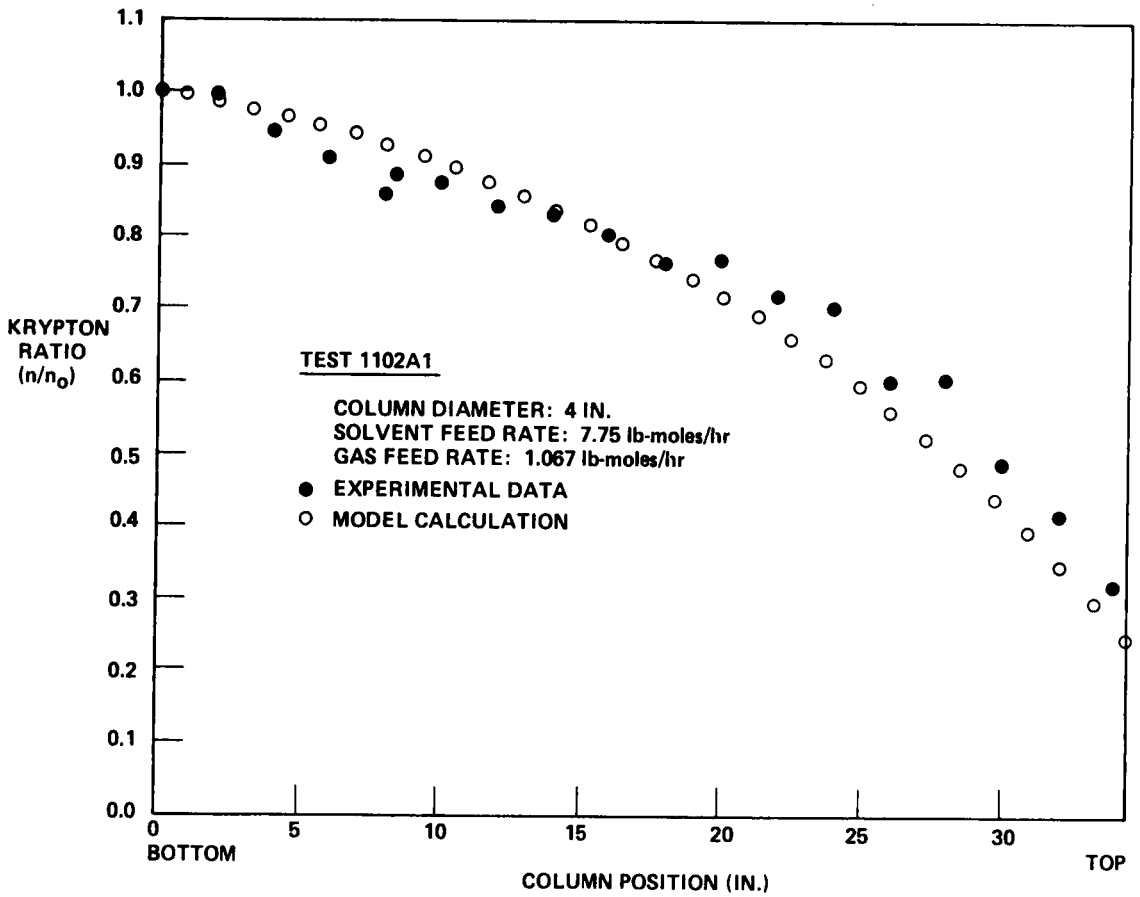

Figure B-2

EXPERIMENTAL AND CALCULATED KRYPTON PROFILES
FOR TEST 1102A1

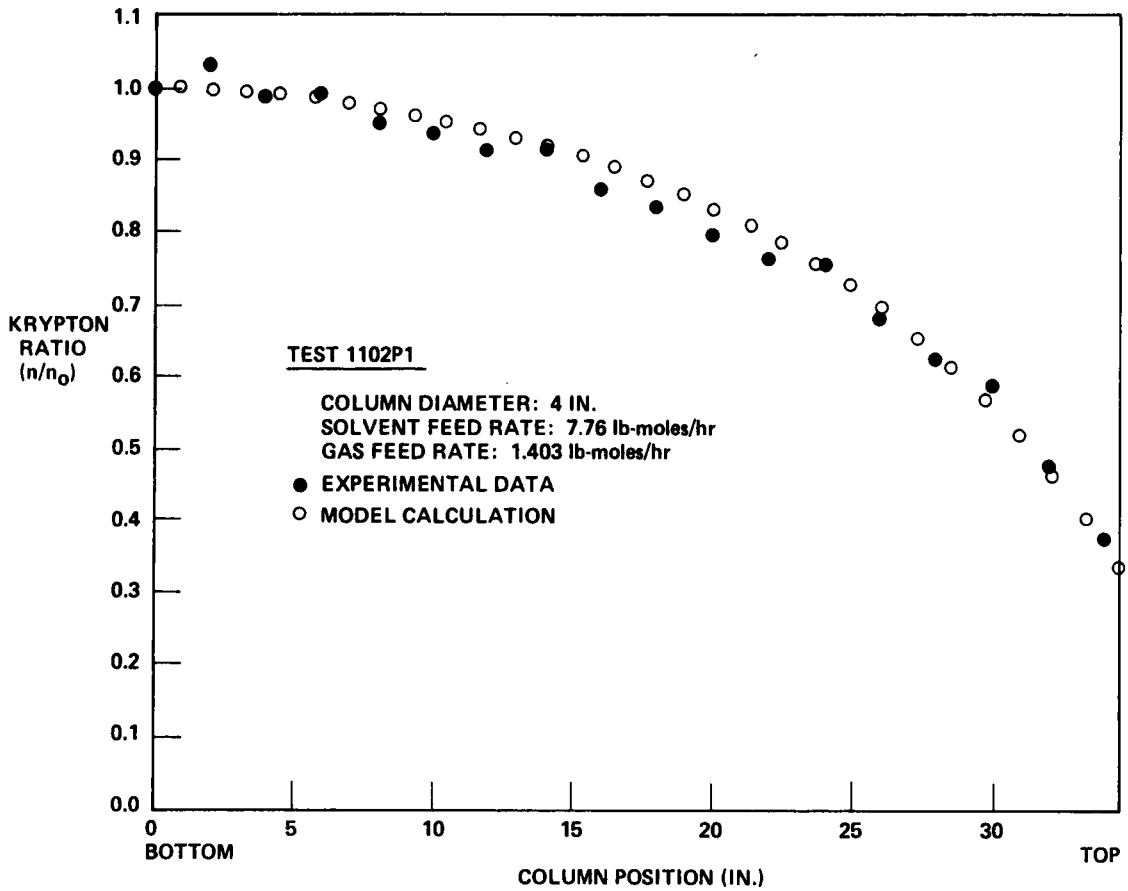

Figure B-3

EXPERIMENTAL AND CALCULATED KRYPTON PROFILES
FOR TEST 1102P1

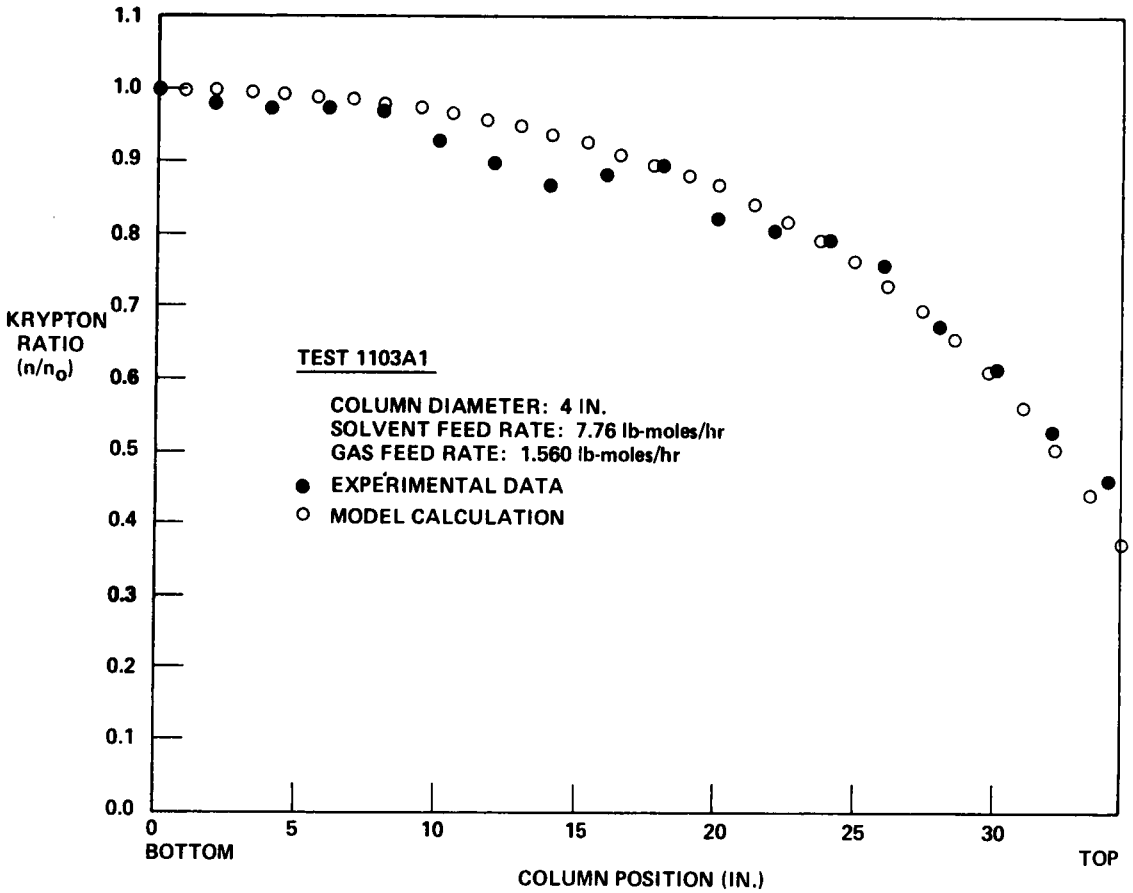

Figure B-4

EXPERIMENTAL AND CALCULATED KRYPTON PROFILES
FOR TEST 1103A1

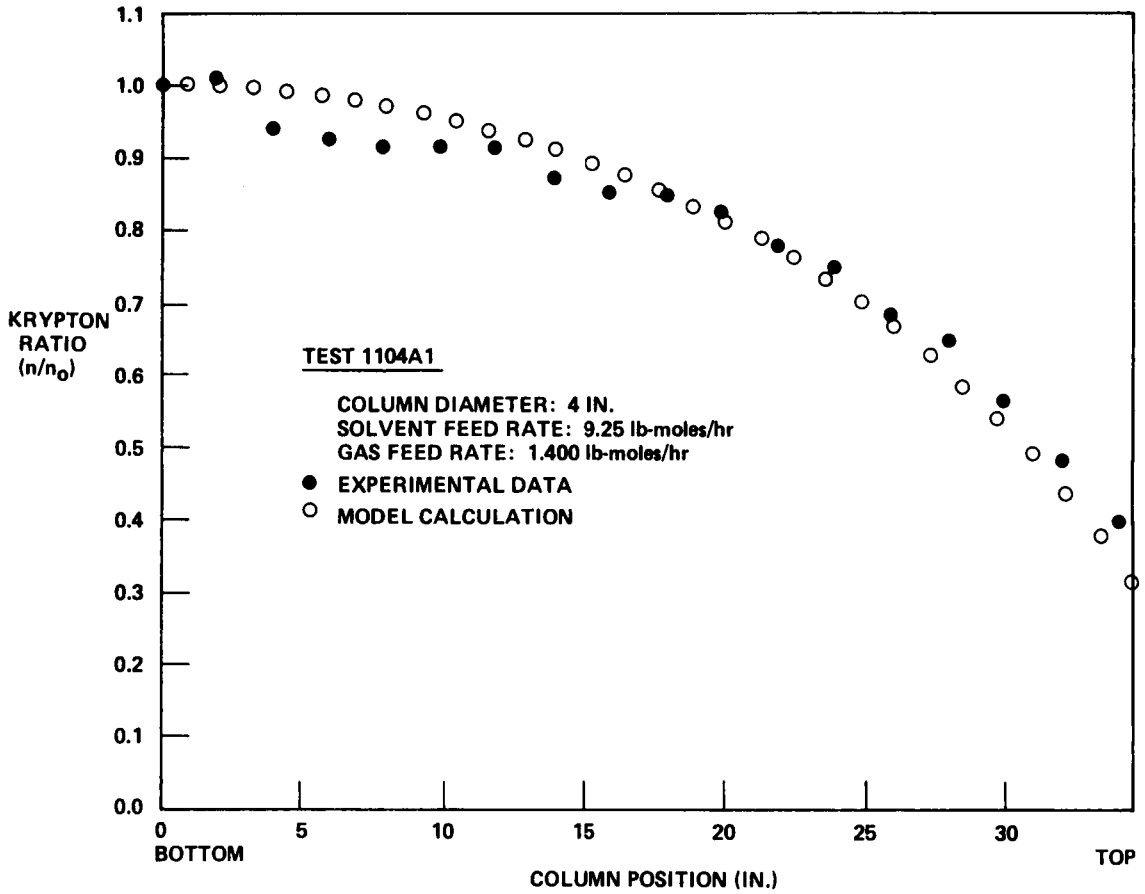

Figure B-5

EXPERIMENTAL AND CALCULATED KRYPTON PROFILES
FOR TEST 1104A1

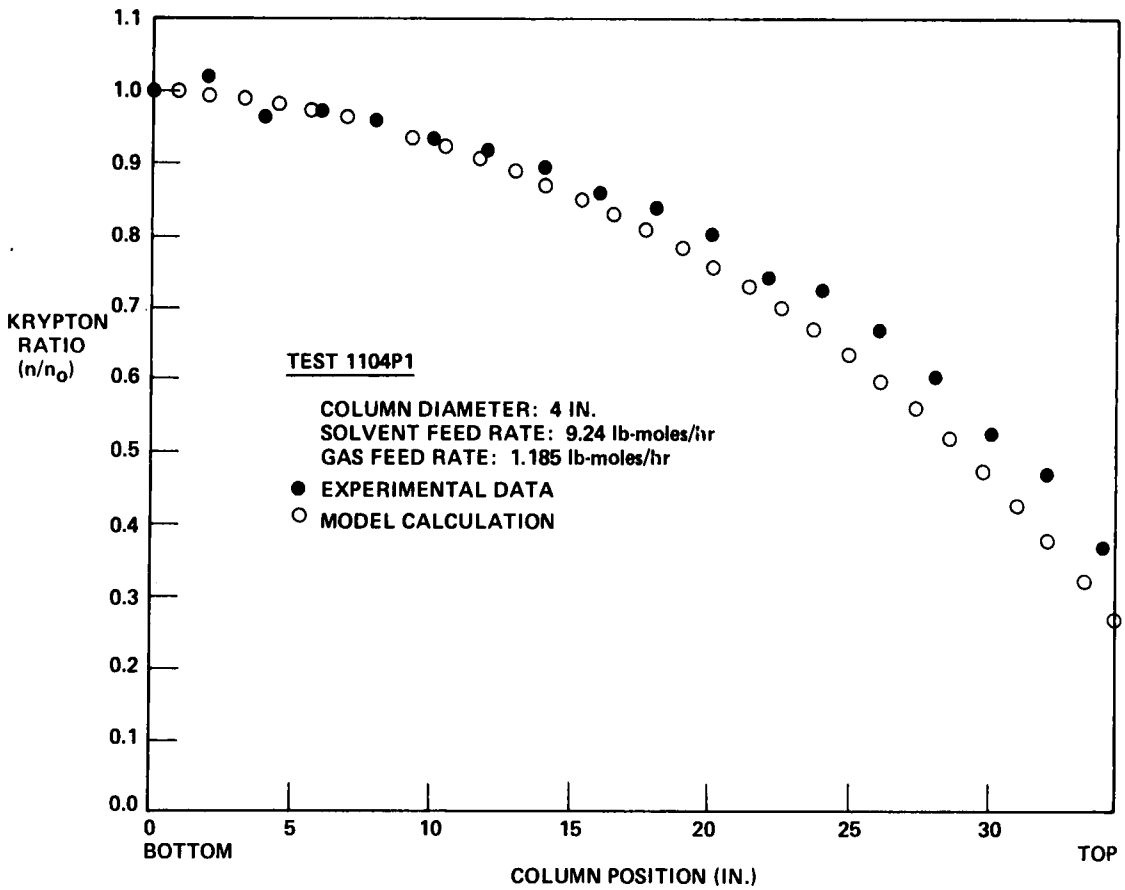

Figure B-6

EXPERIMENTAL AND CALCULATED KRYPTON PROFILES
FOR TEST 1104P1

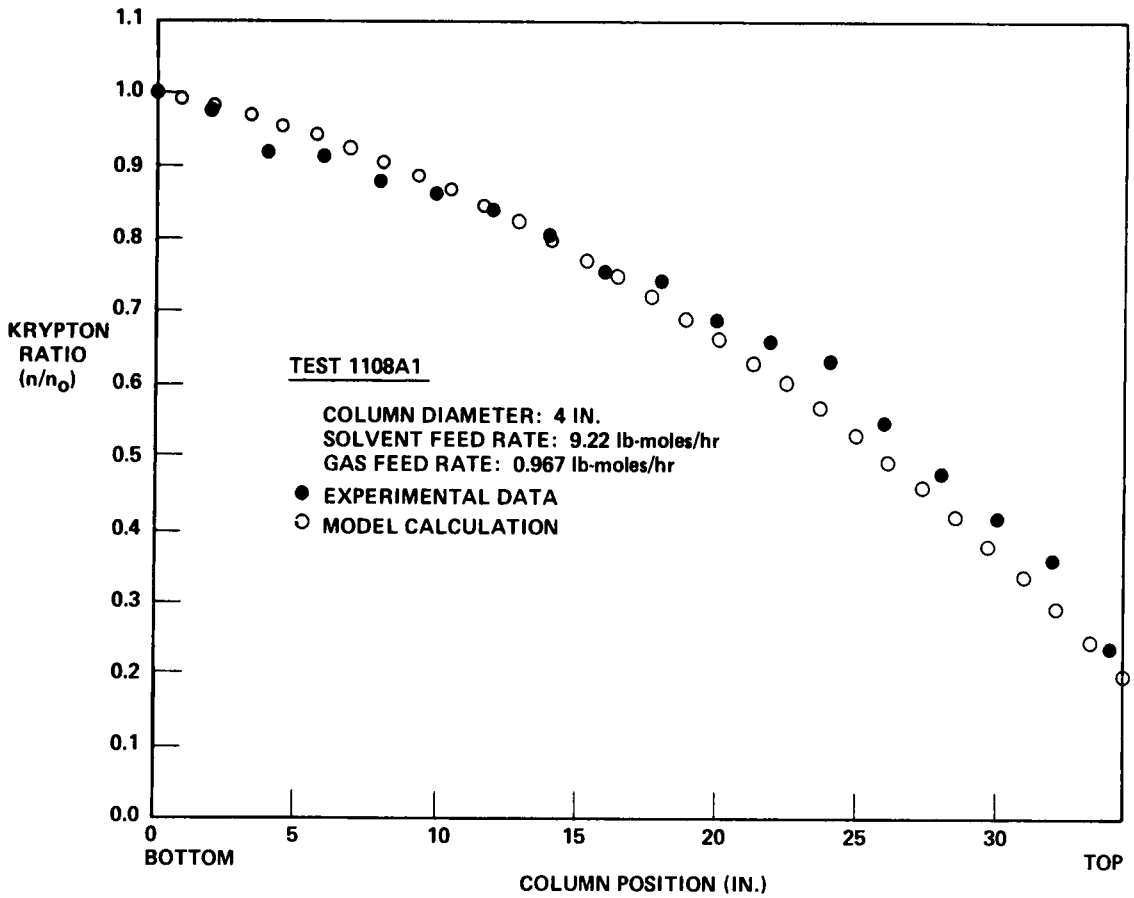

Figure B-7

EXPERIMENTAL AND CALCULATED KRYPTON PROFILES
FOR TEST 1108A1

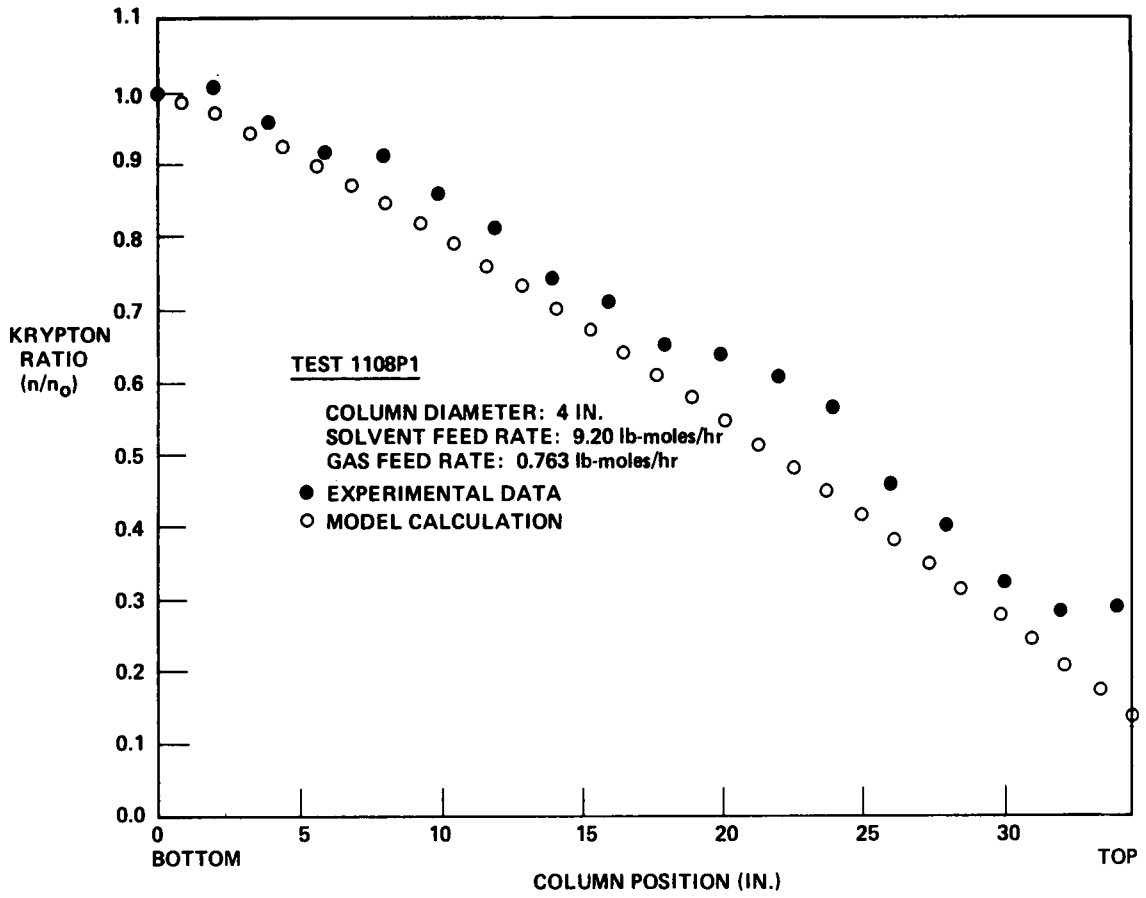

Figure B-8

EXPERIMENTAL AND CALCULATED KRYPTON PROFILES
FOR TEST 1108P1

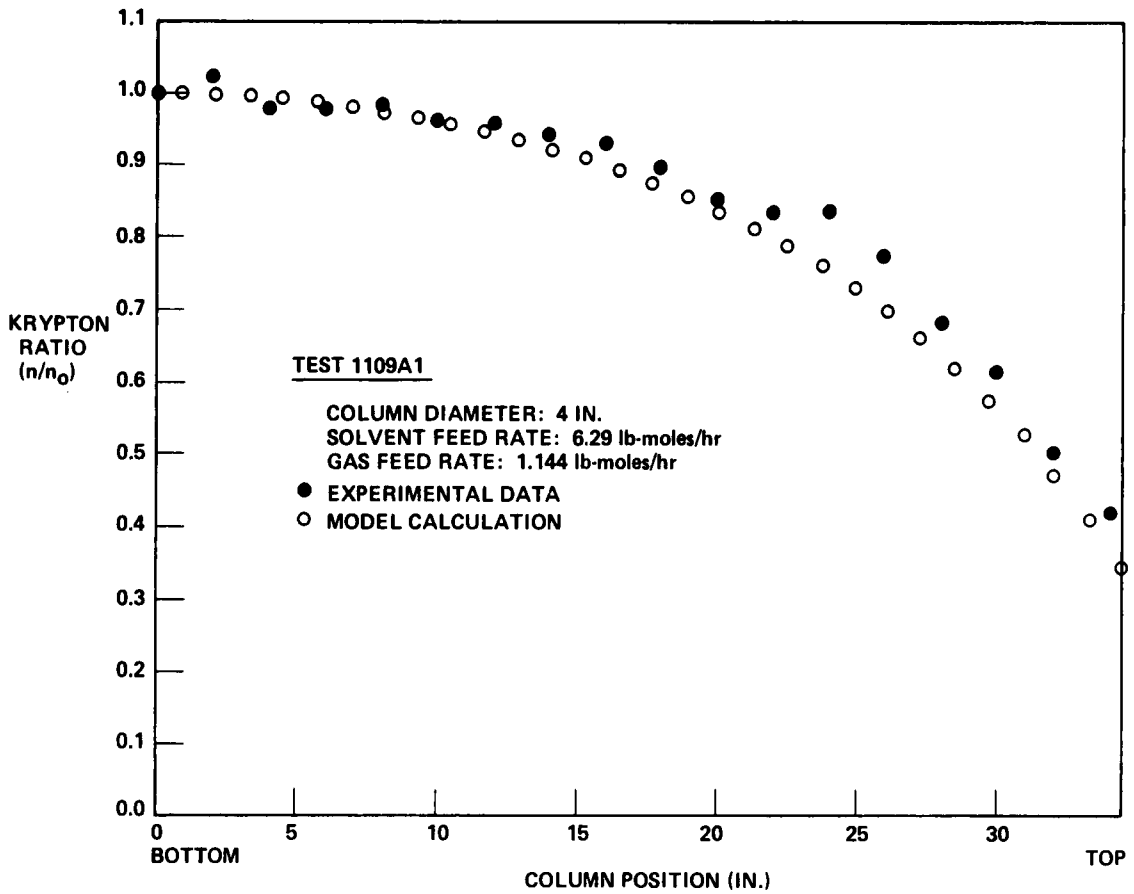

Figure B-9

EXPERIMENTAL AND CALCULATED KRYPTON PROFILES
FOR TEST 1109A1

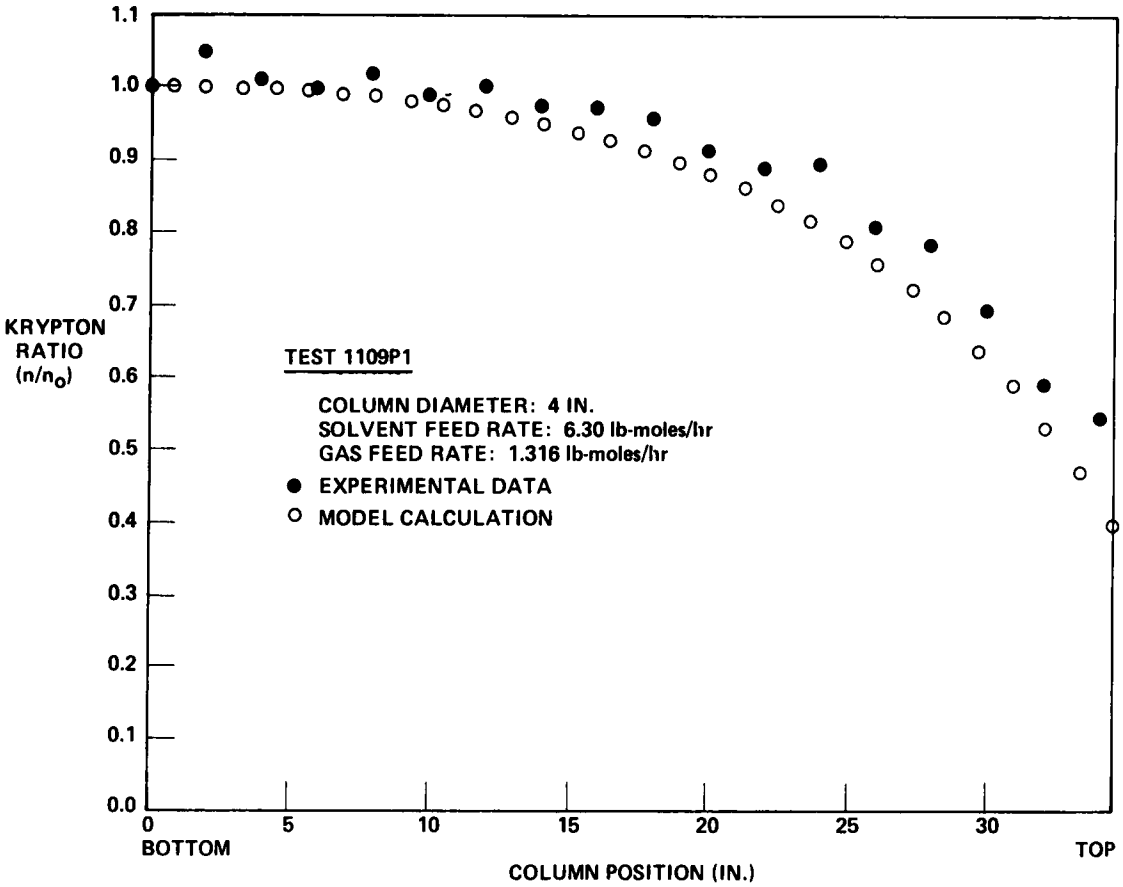

Figure B-10

EXPERIMENTAL AND CALCULATED KRYPTON PROFILES FOR TEST 1109P1

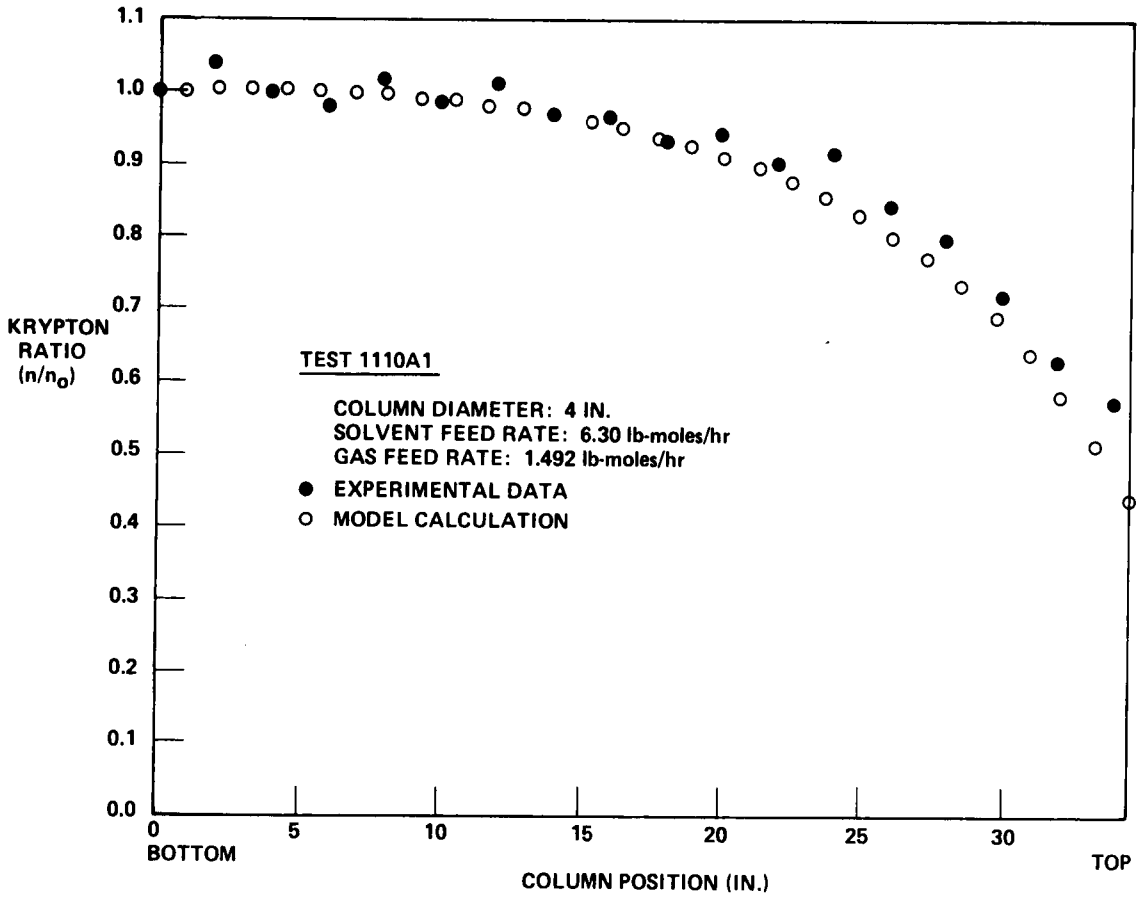

Figure B-11

EXPERIMENTAL AND CALCULATED KRYPTON PROFILES
FOR TEST 1110A1

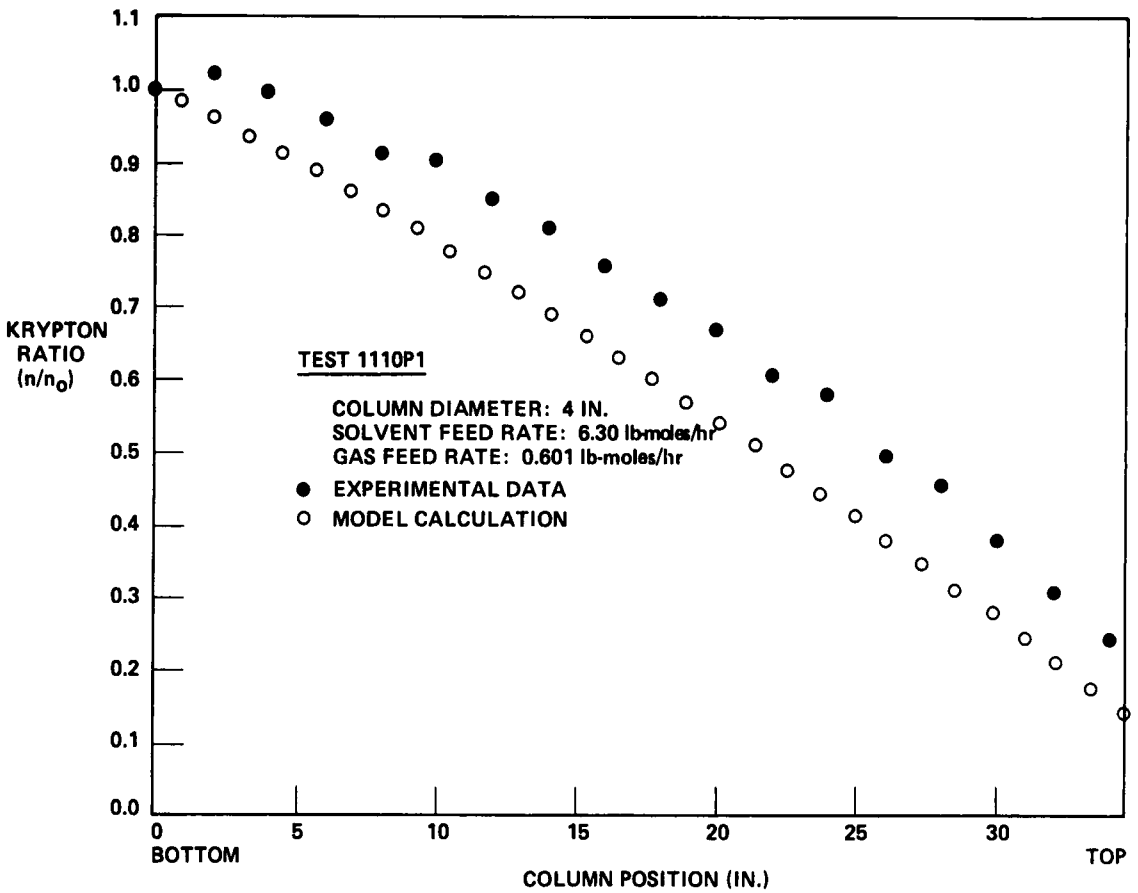

Figure B-12

EXPERIMENTAL AND CALCULATED KRYPTON PROFILES
FOR TEST 1110P1

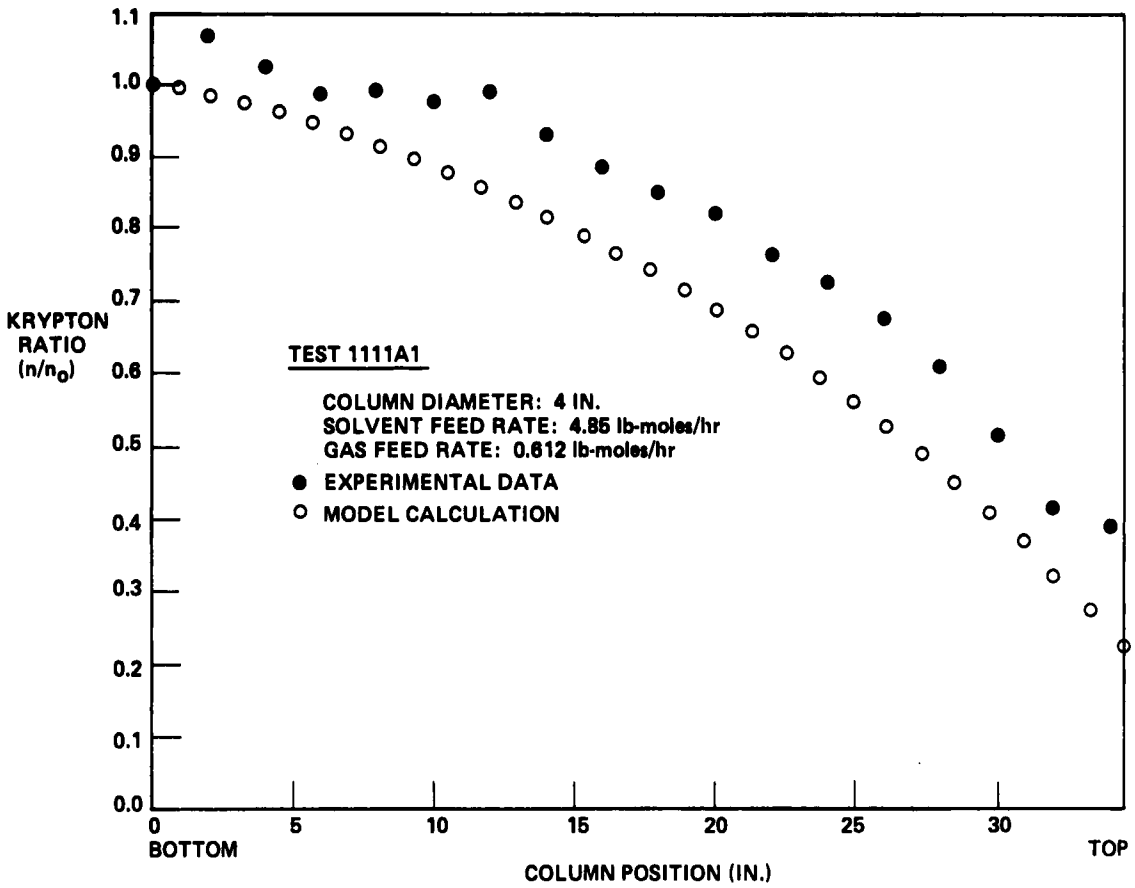

Figure B-13

EXPERIMENTAL AND CALCULATED KRYPTON PROFILES
FOR TEST 1111A1

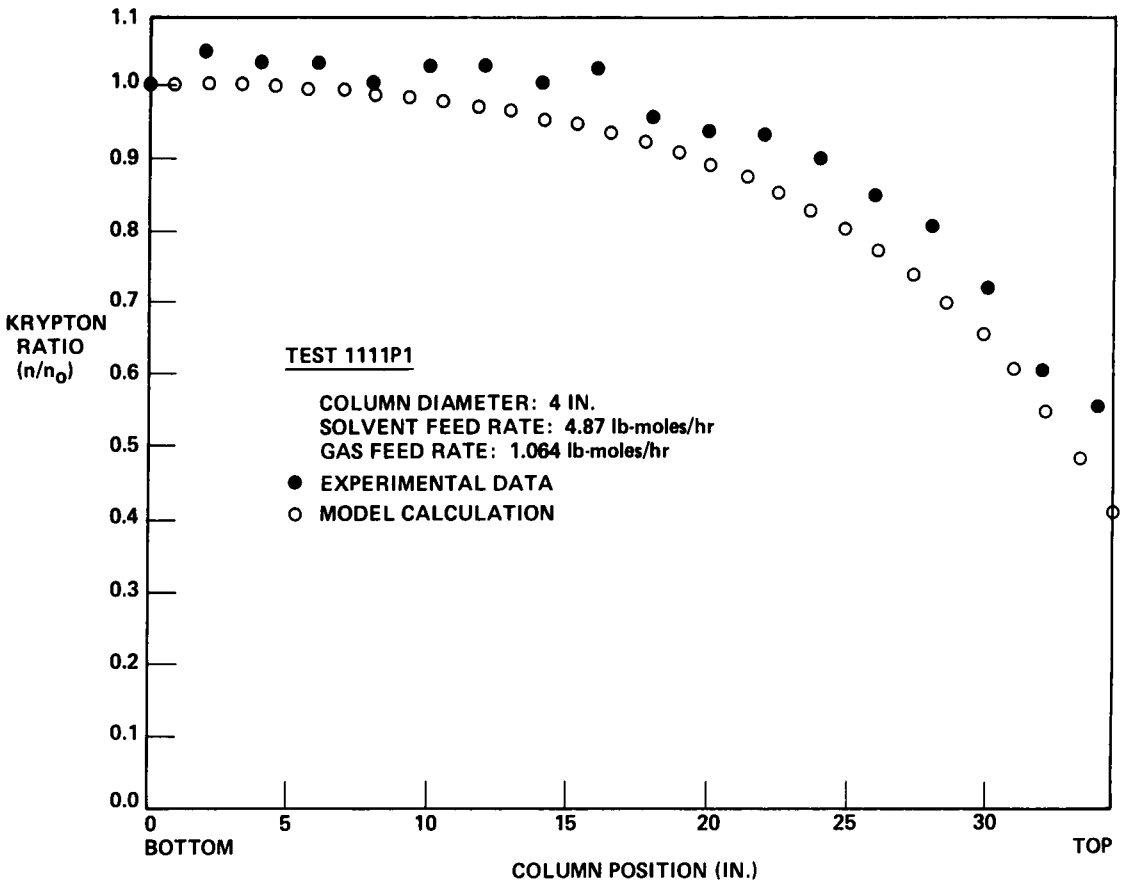

Figure B-14

EXPERIMENTAL AND CALCULATED KRYPTON PROFILES
FOR TEST 1111P1

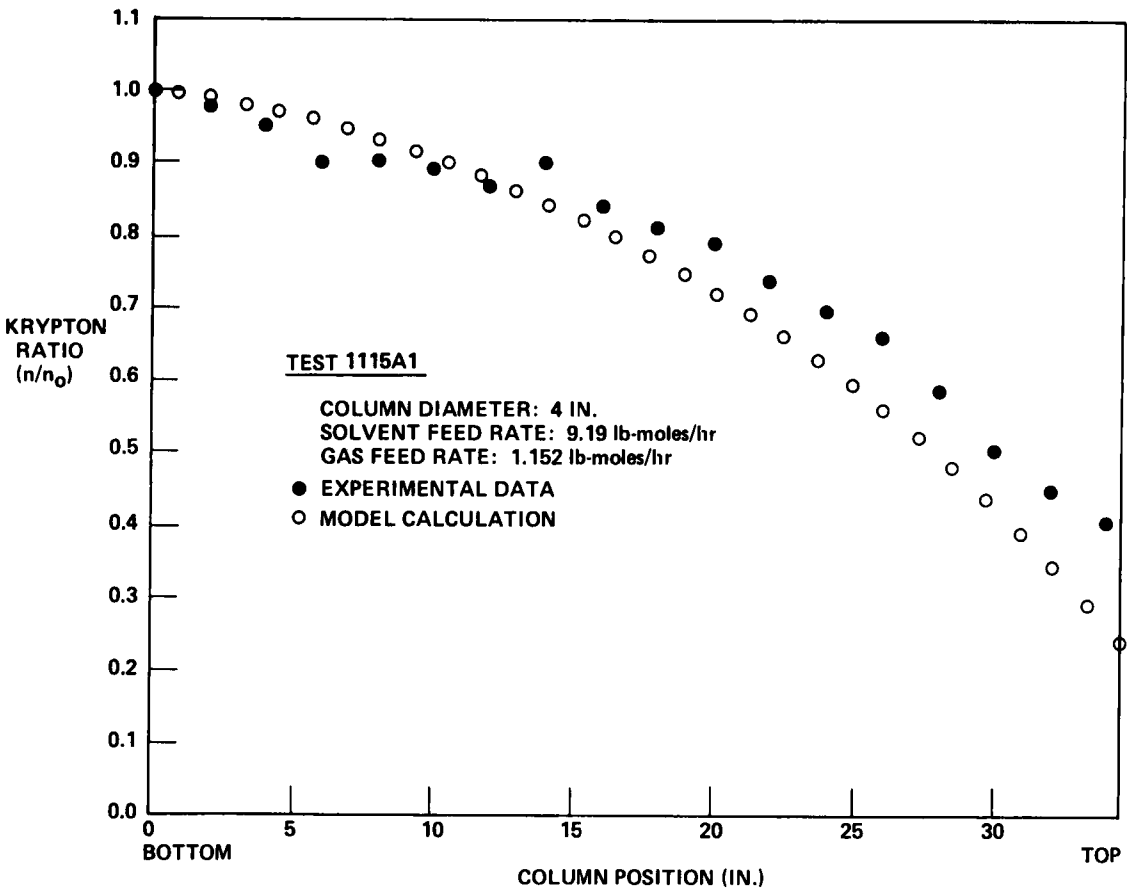

Figure B-15

EXPERIMENTAL AND CALCULATED KRYPTON PROFILES
FOR TEST 1115A1

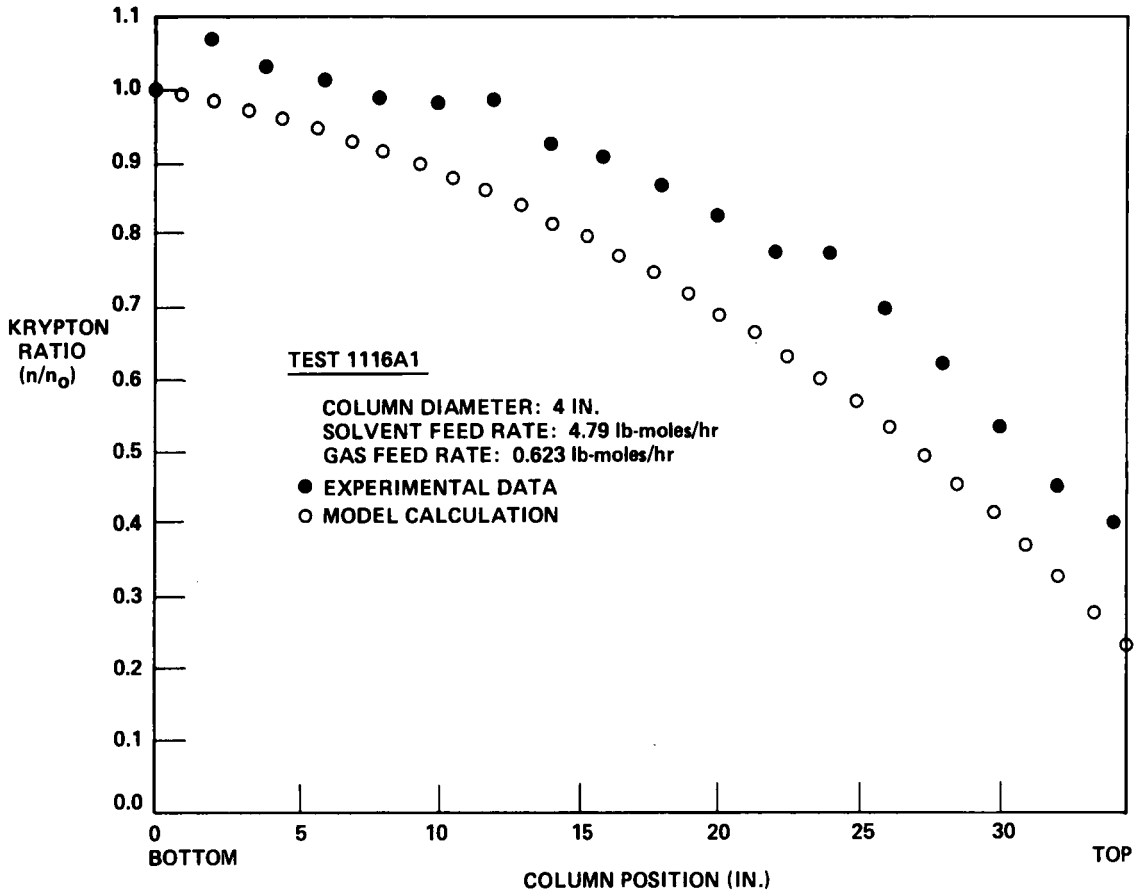

Figure B-16

EXPERIMENTAL AND CALCULATED KRYPTON PROFILES
FOR TEST 1116A1

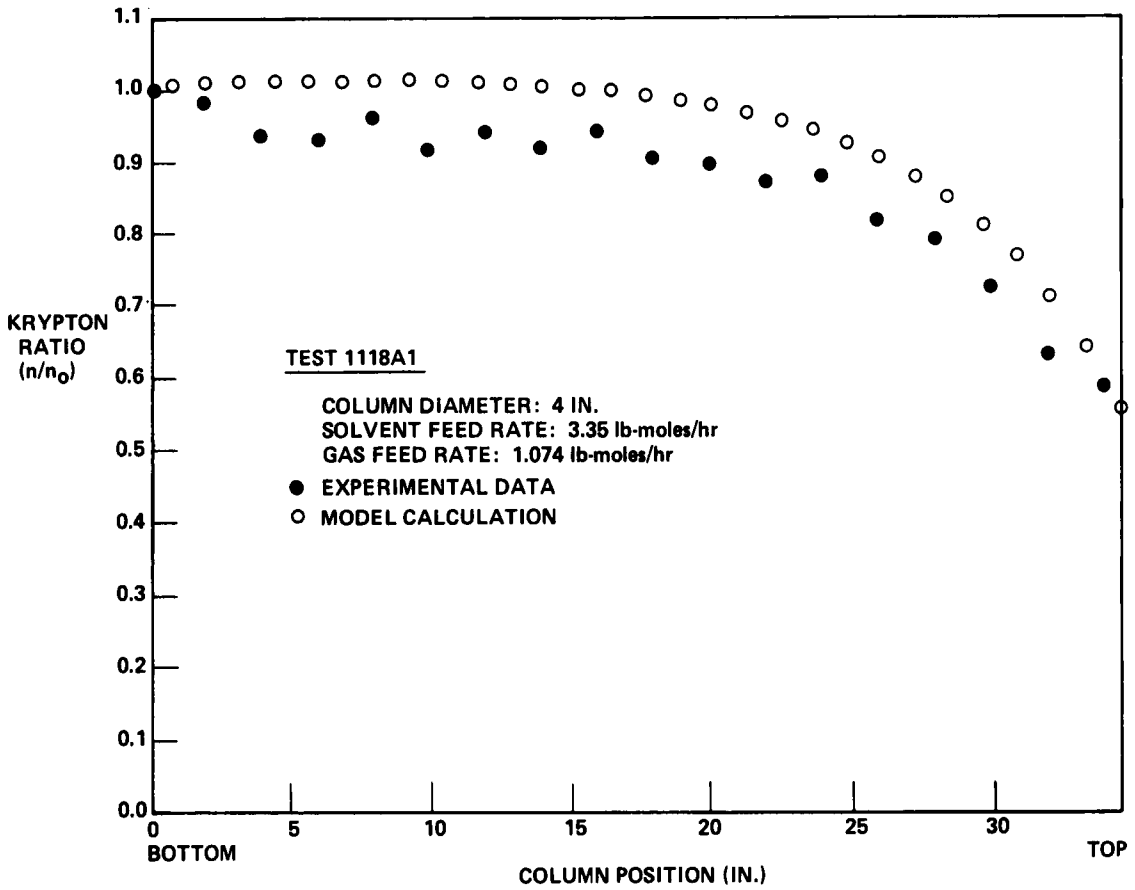

Figure B-17

EXPERIMENTAL AND CALCULATED KRYPTON PROFILES FOR TEST 1118A1

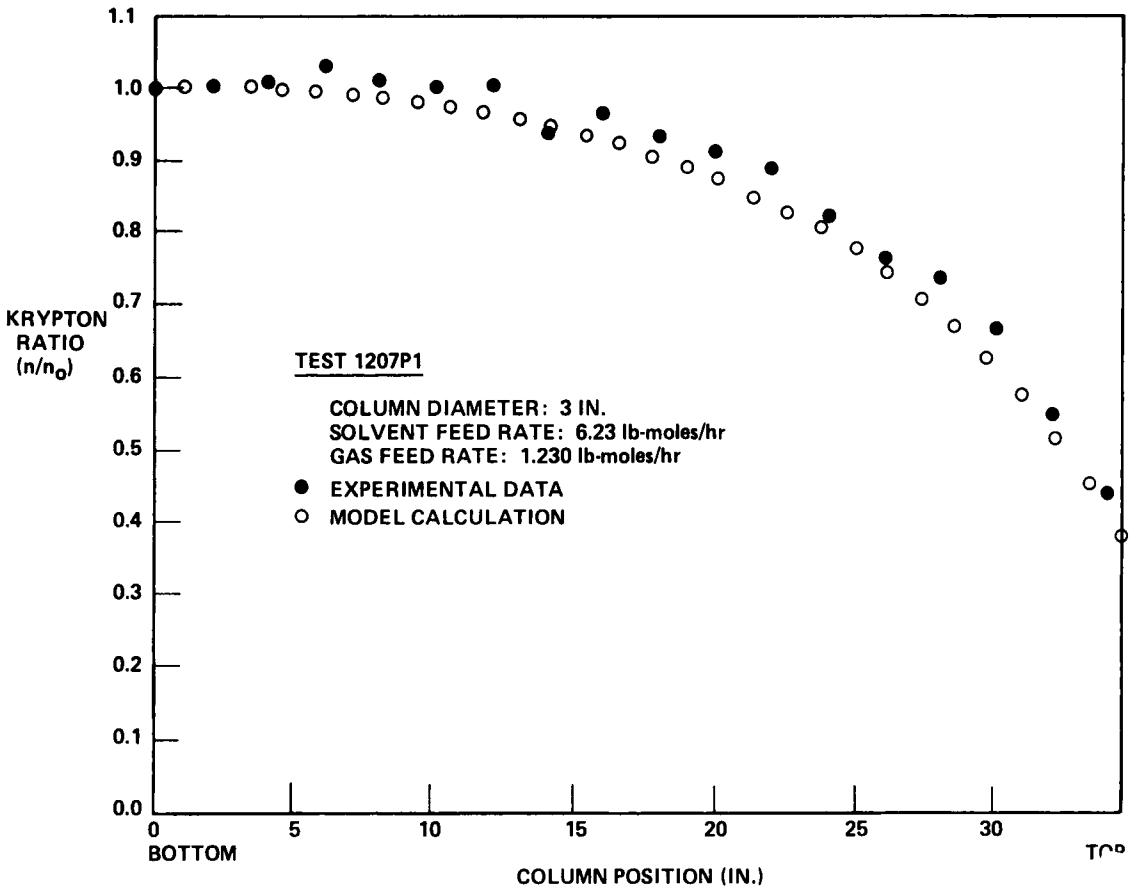

Figure B-18

EXPERIMENTAL AND CALCULATED KRYPTON PROFILES
FOR TEST 1207P1

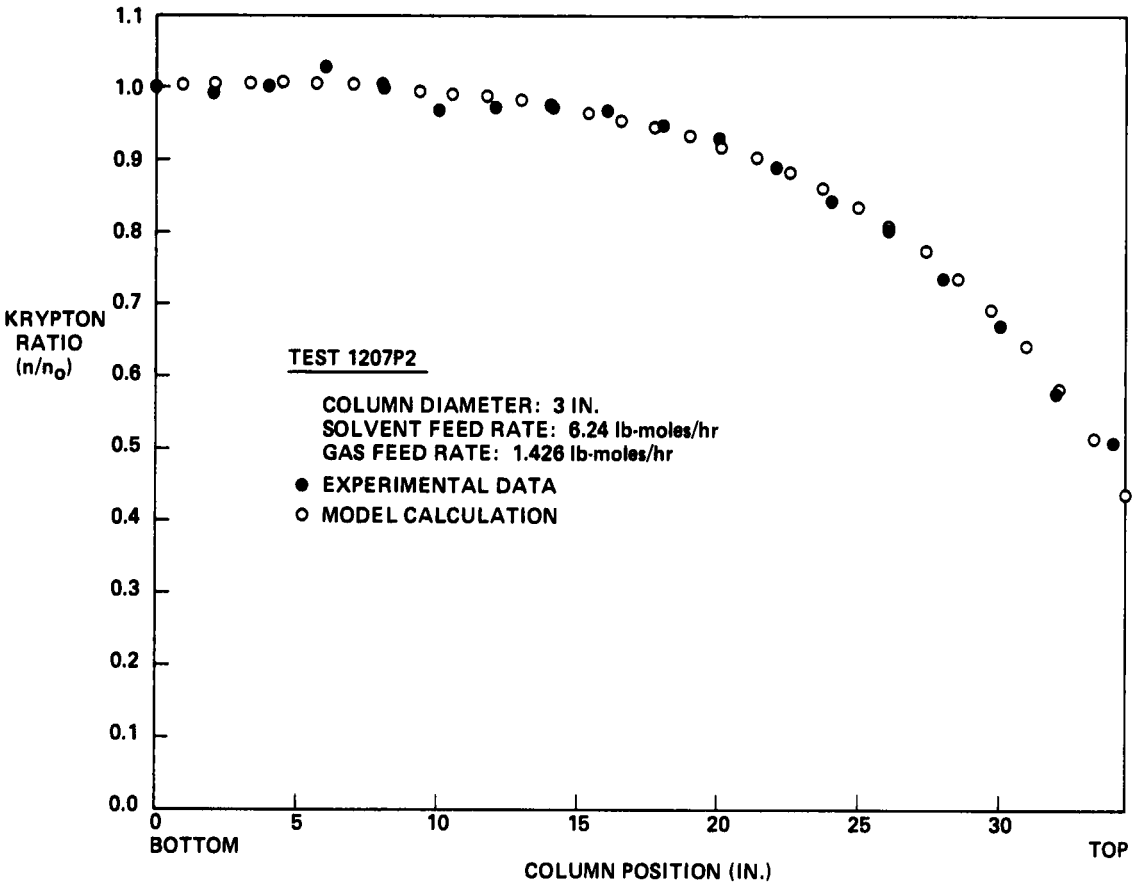

Figure B-19

EXPERIMENTAL AND CALCULATED KRYPTON PROFILES
FOR TEST 1207P2

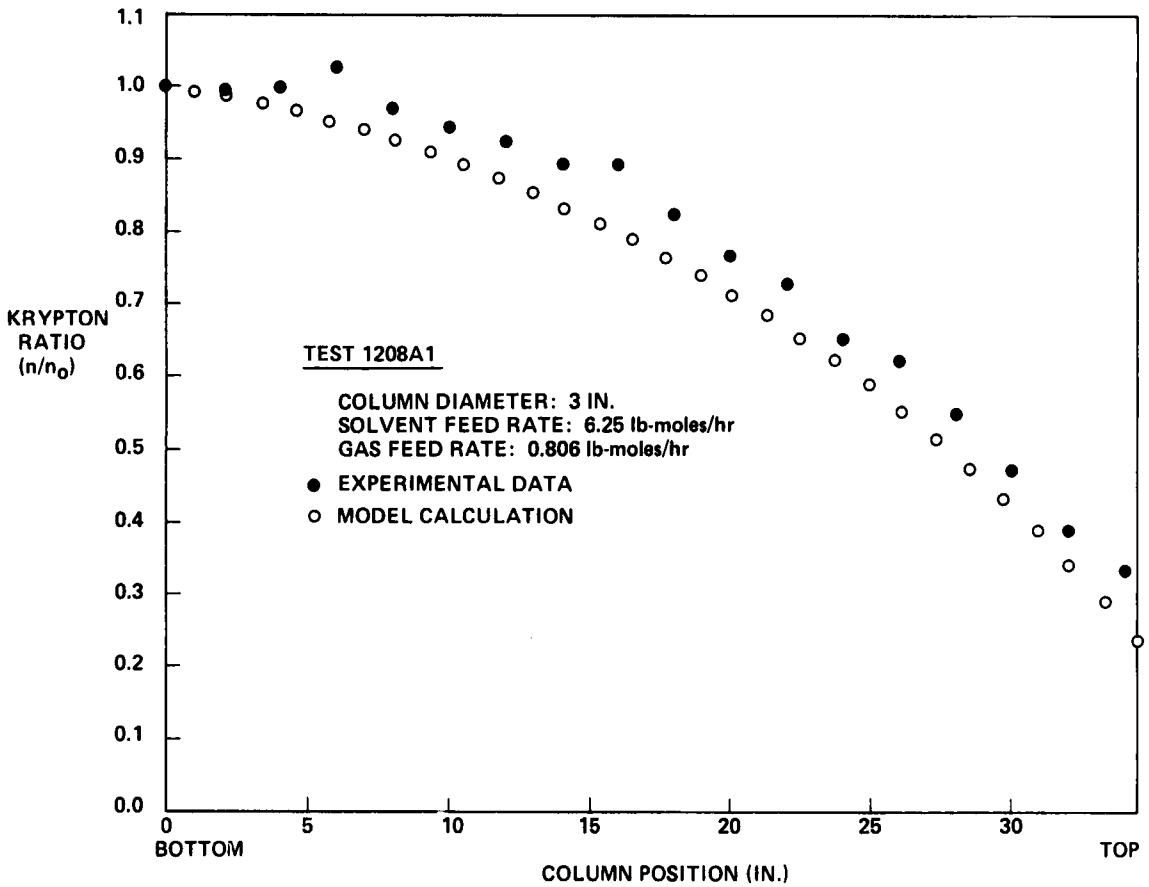

Figure B-20

EXPERIMENTAL AND CALCULATED KRYPTON PROFILES
FOR TEST 1208A1

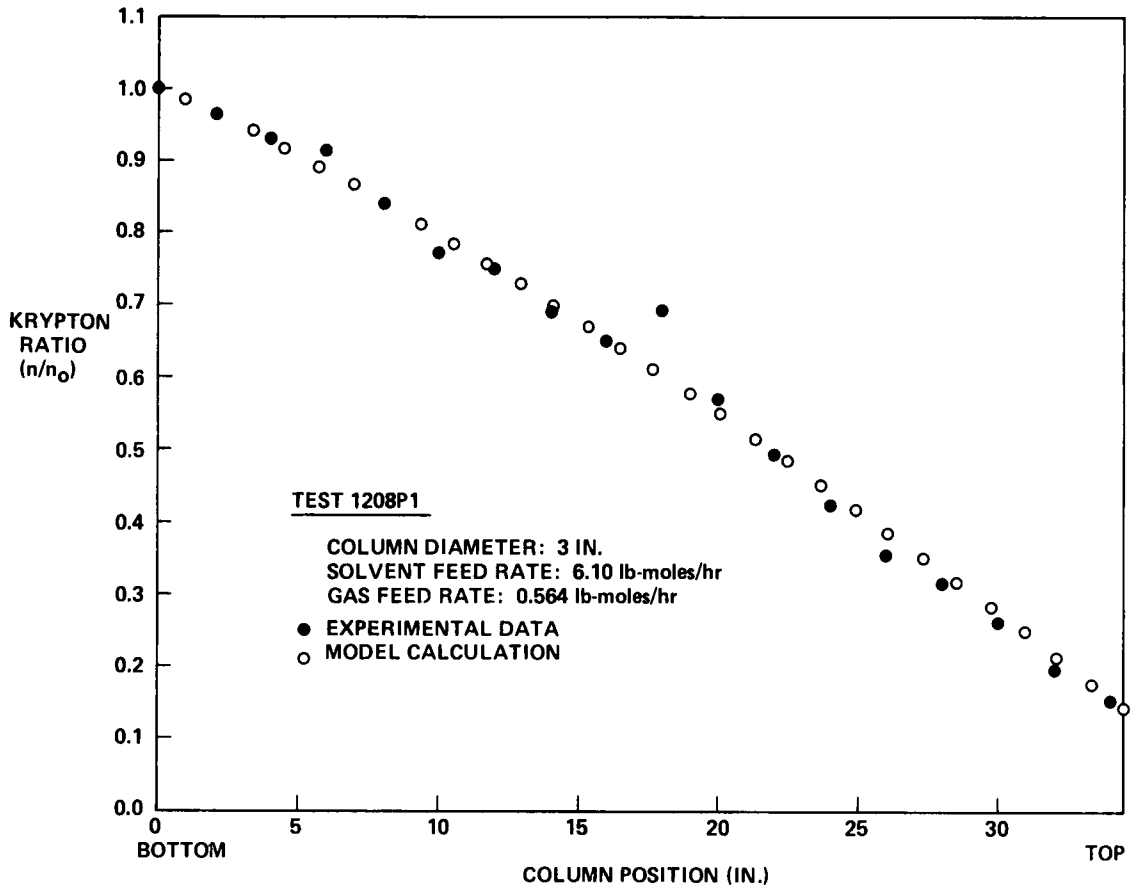

Figure B-21

EXPERIMENTAL AND CALCULATED KRYPTON PROFILES
FOR TEST 1208P1

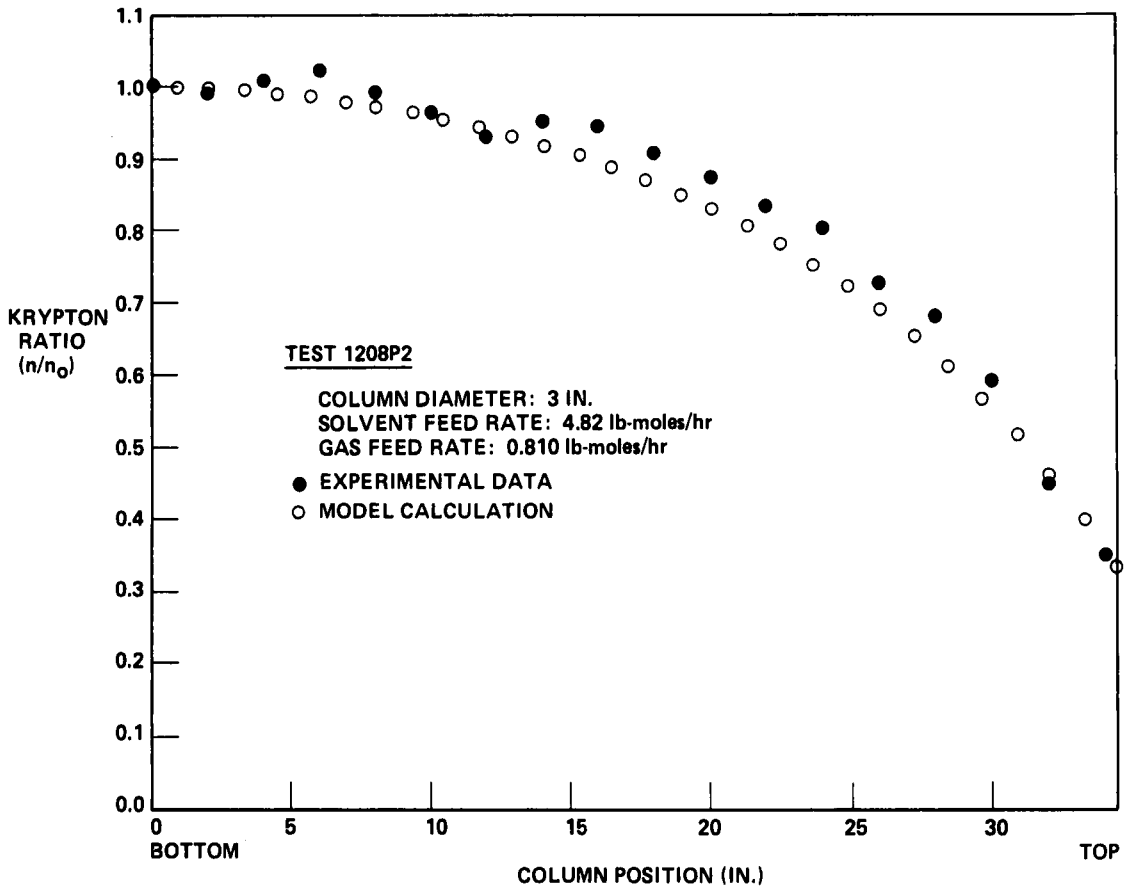

Figure B-22

EXPERIMENTAL AND CALCULATED KRYPTON PROFILES
FOR TEST 1208P2

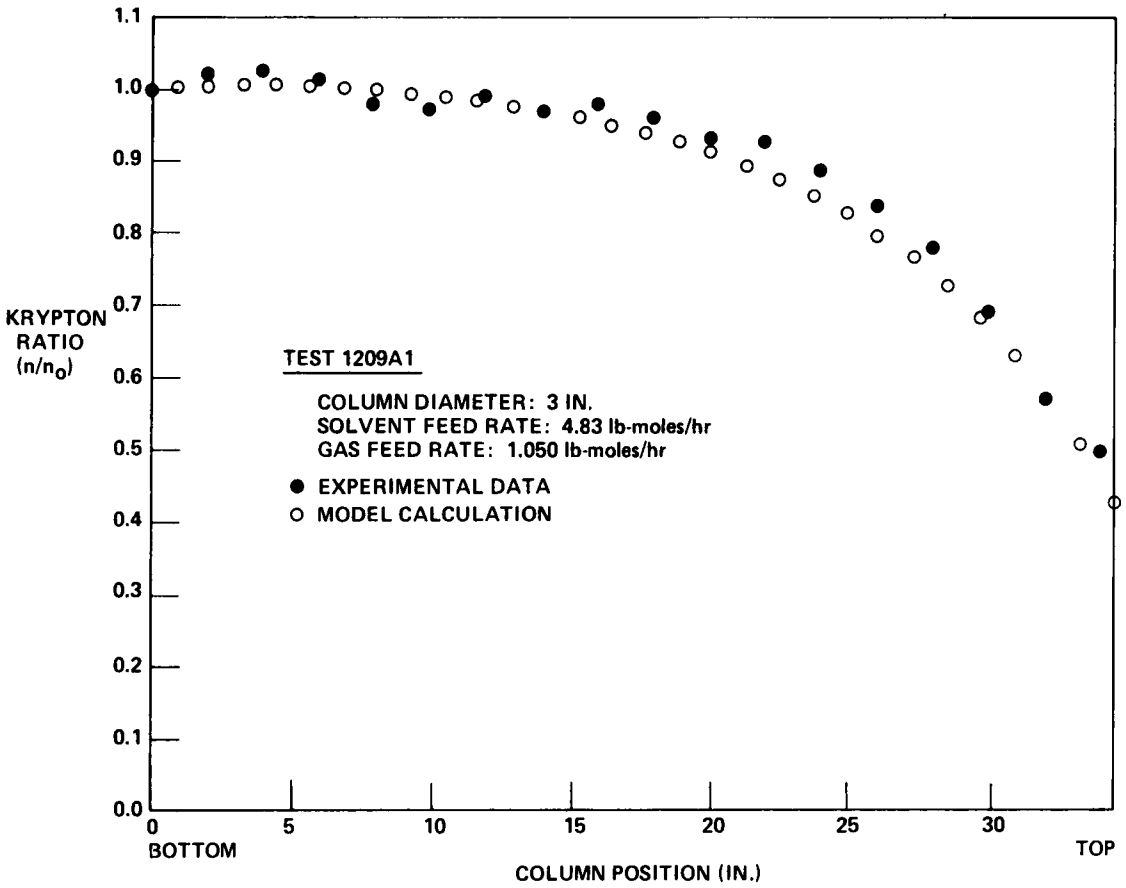

Figure B-23

EXPERIMENTAL AND CALCULATED KRYPTON PROFILES
FOR TEST 1209A1

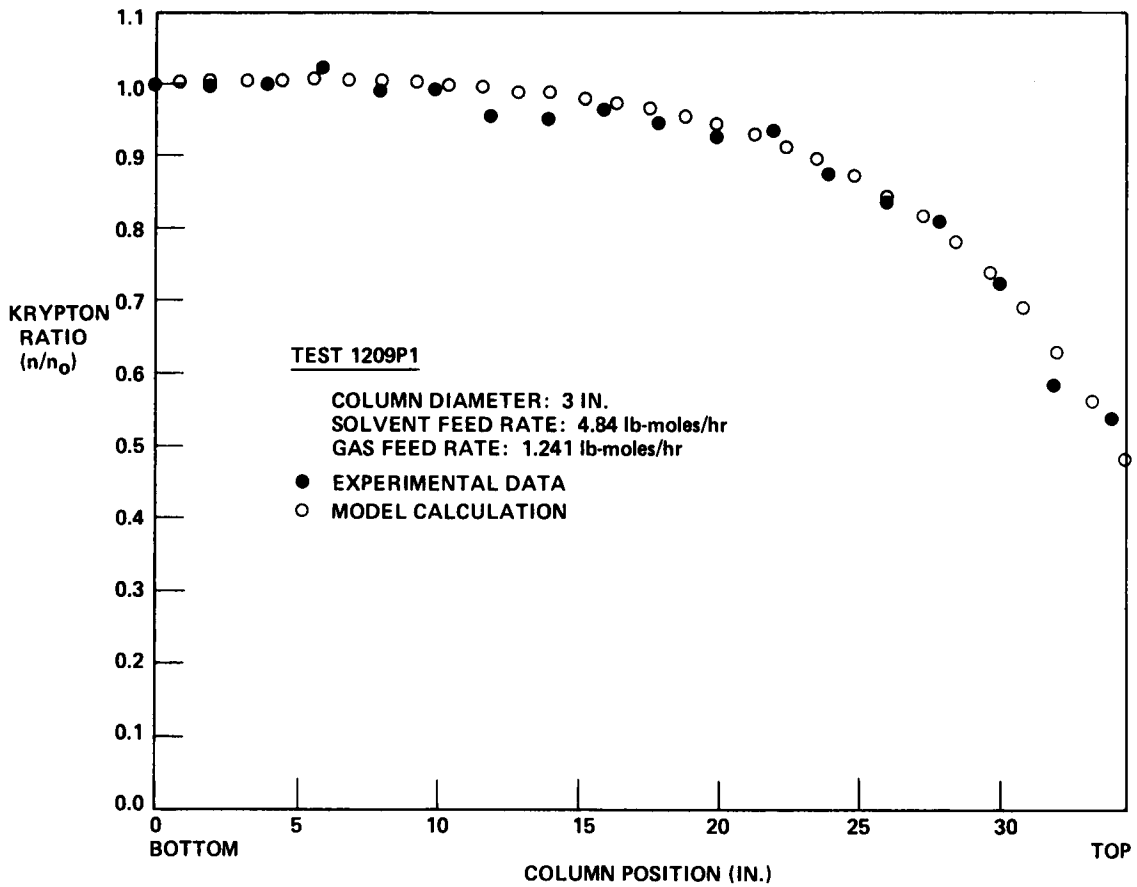

Figure B-24

EXPERIMENTAL AND CALCULATED KRYPTON PROFILES FOR TEST 1209P1

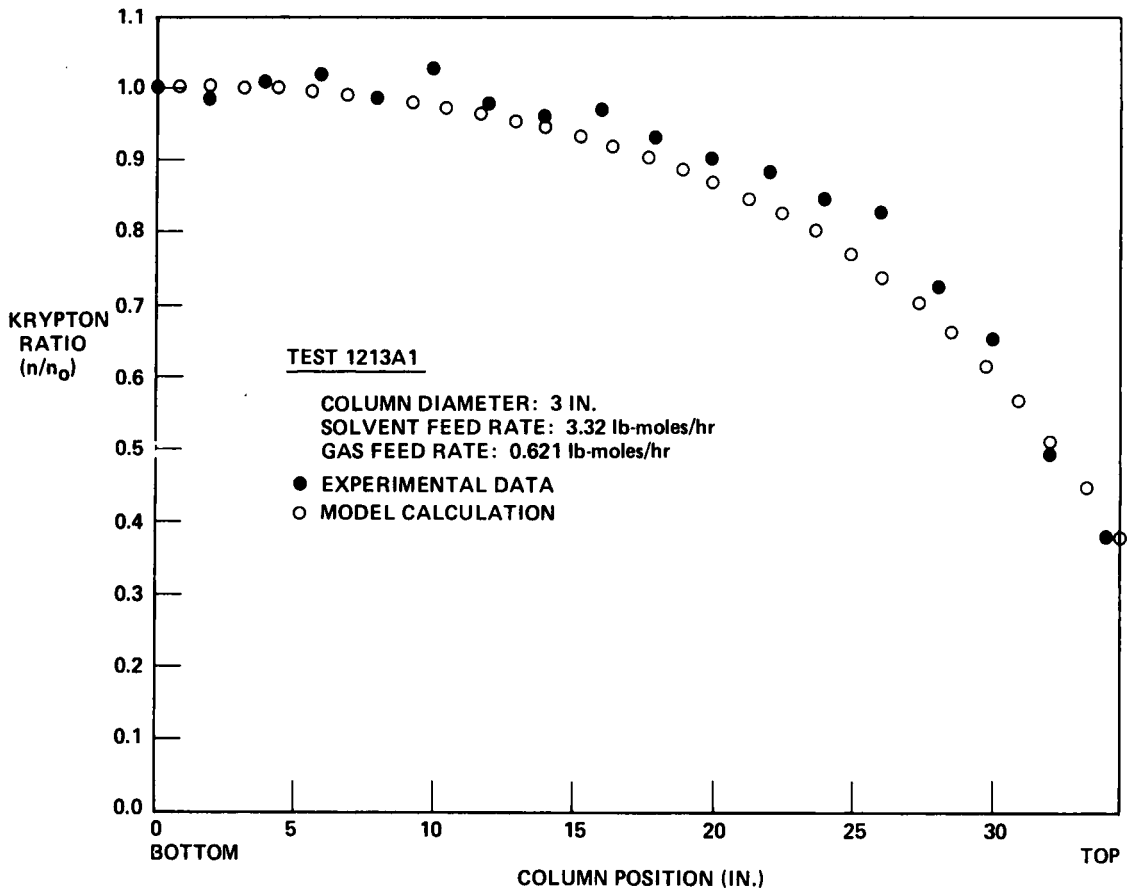

Figure B-25

EXPERIMENTAL AND CALCULATED KRYPTON PROFILES FOR TEST 1213A1

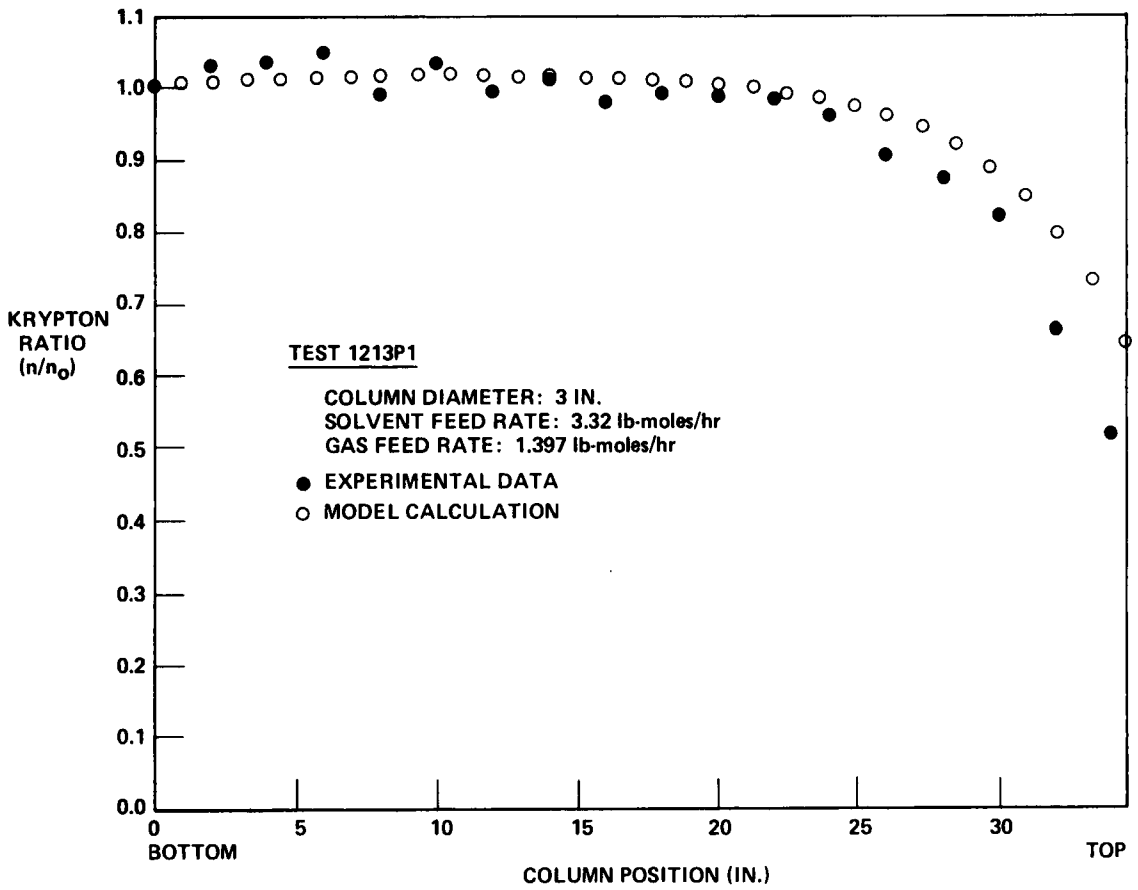

Figure B-26

EXPERIMENTAL AND CALCULATED KRYPTON PROFILES
FOR TEST 1213P1

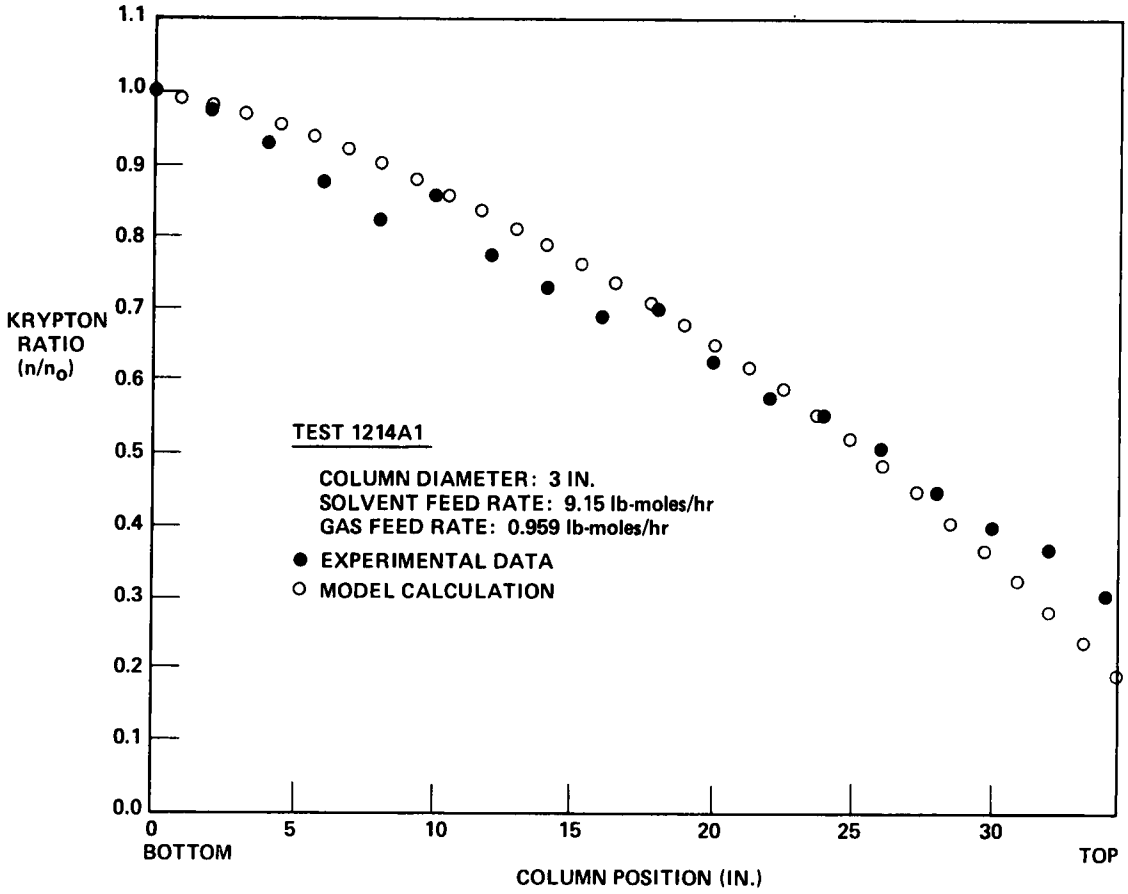

Figure B-27

EXPERIMENTAL AND CALCULATED KRYPTON PROFILES FOR TEST 1214A1

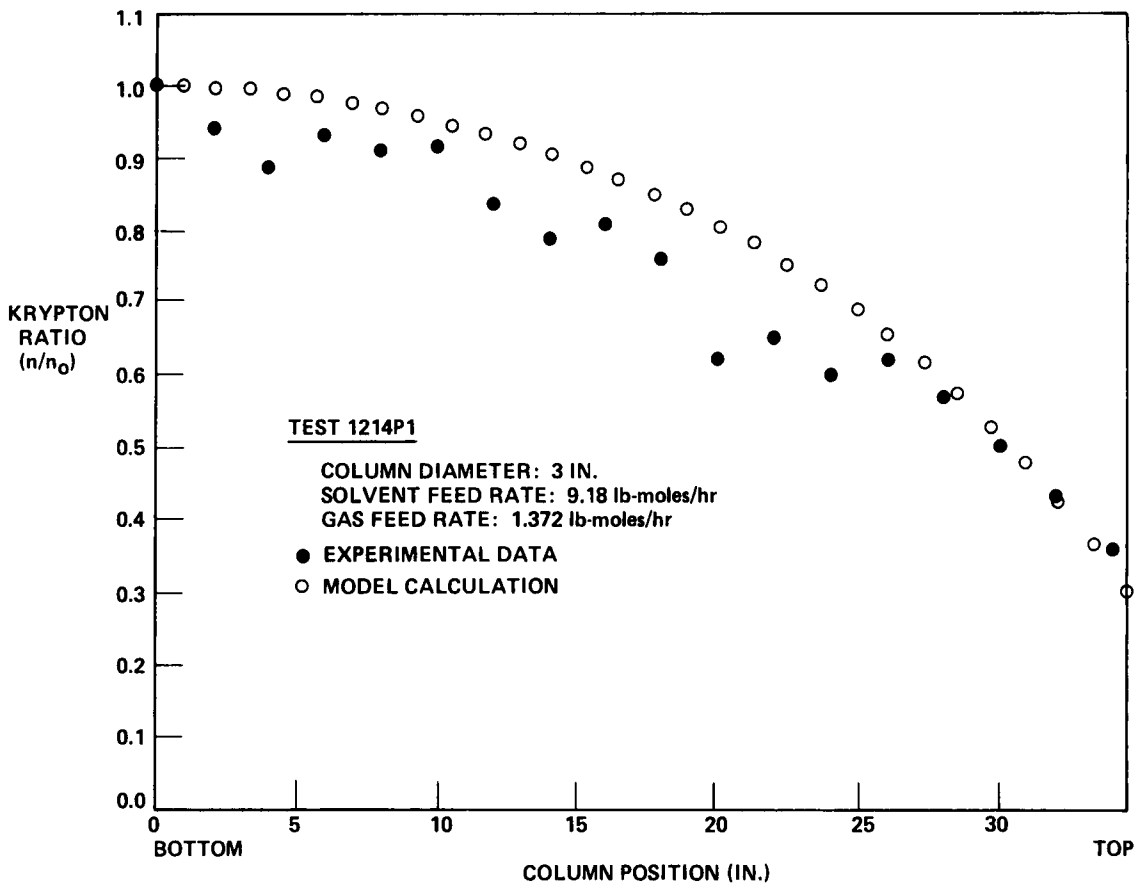

Figure B-28

EXPERIMENTAL AND CALCULATED KRYPTON PROFILES
FOR TEST 1214P1

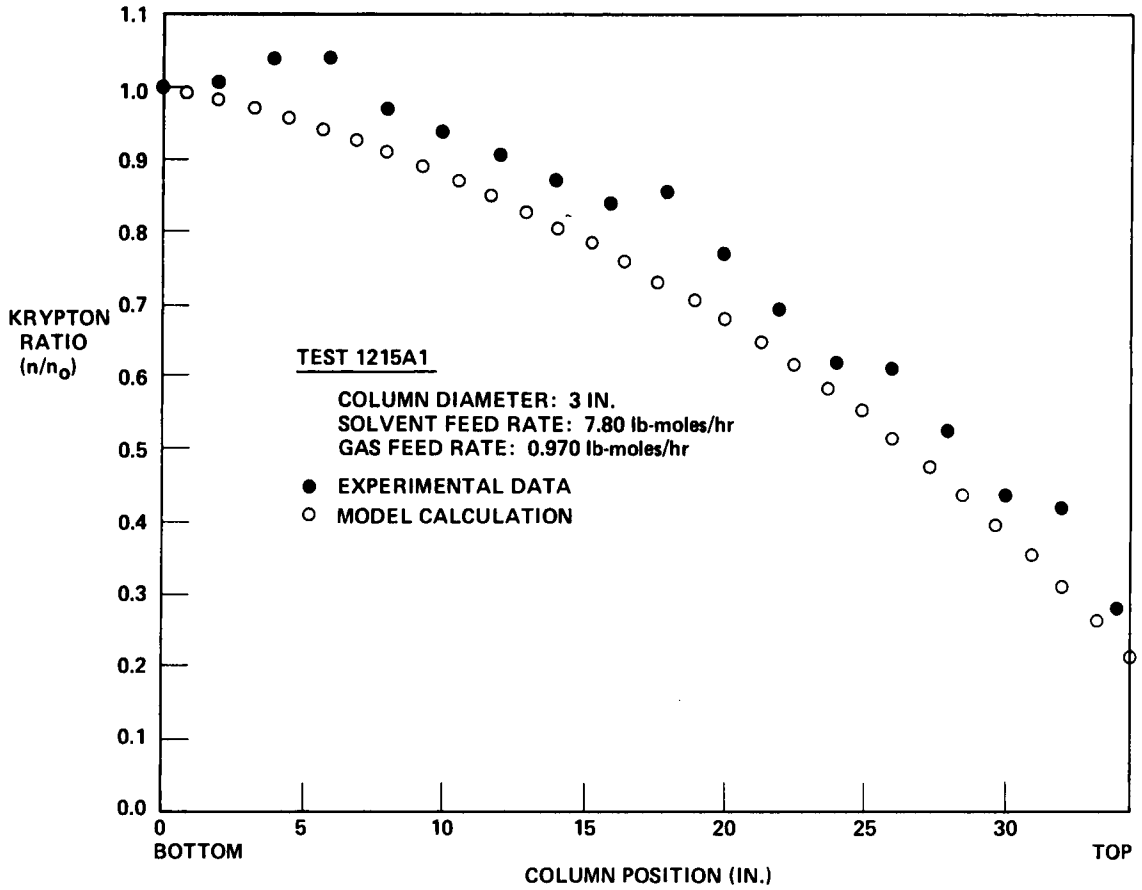

Figure B-29

EXPERIMENTAL AND CALCULATED KRYPTON PROFILES
FOR TEST 1215A1

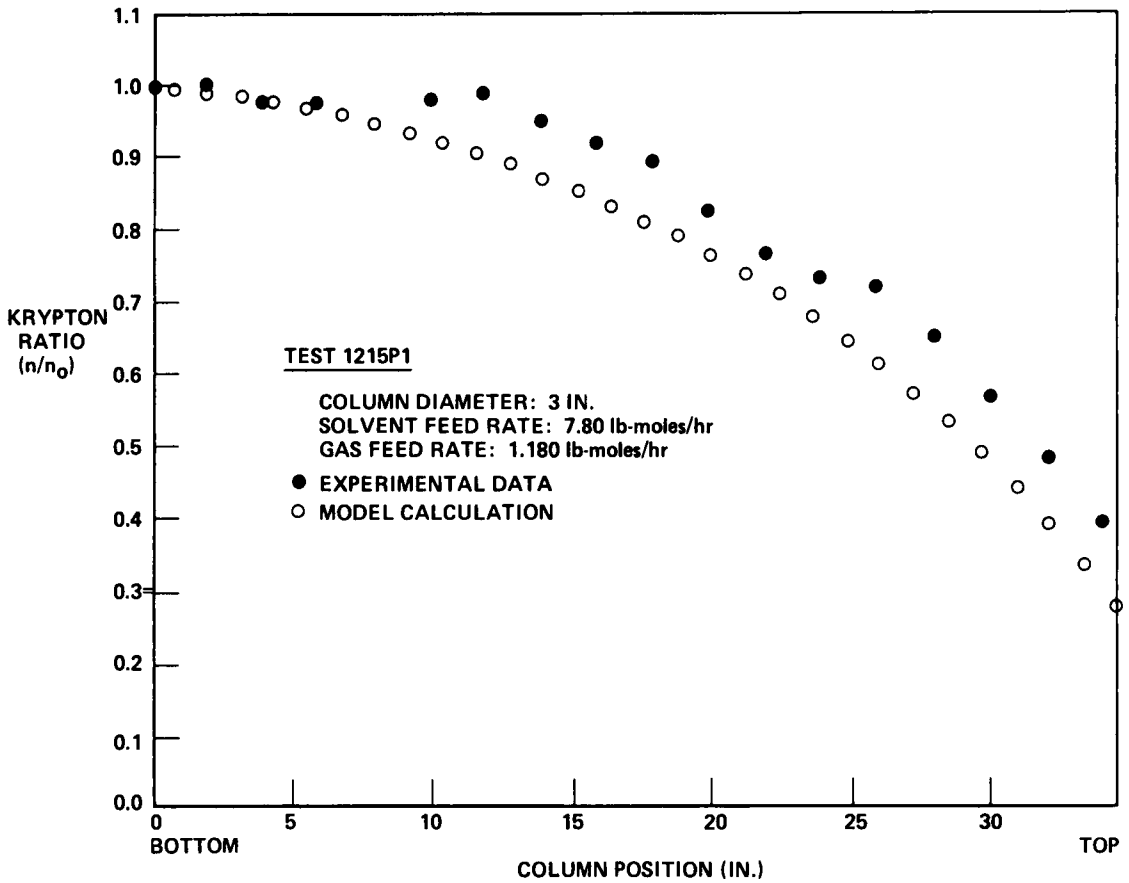

Figure B-30

EXPERIMENTAL AND CALCULATED KRYPTON PROFILES
FOR TEST 1215P1

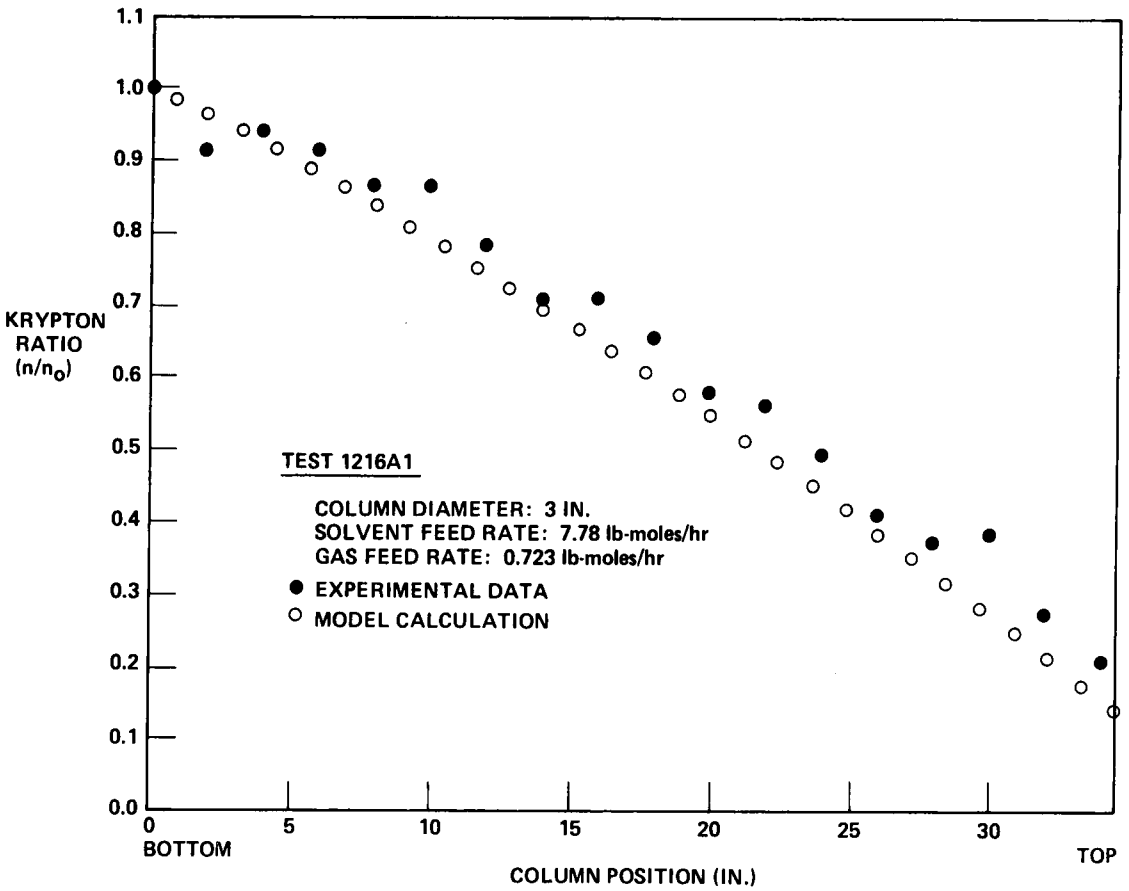

Figure B-31

EXPERIMENTAL AND CALCULATED KRYPTON PROFILES
FOR TEST 1216A1

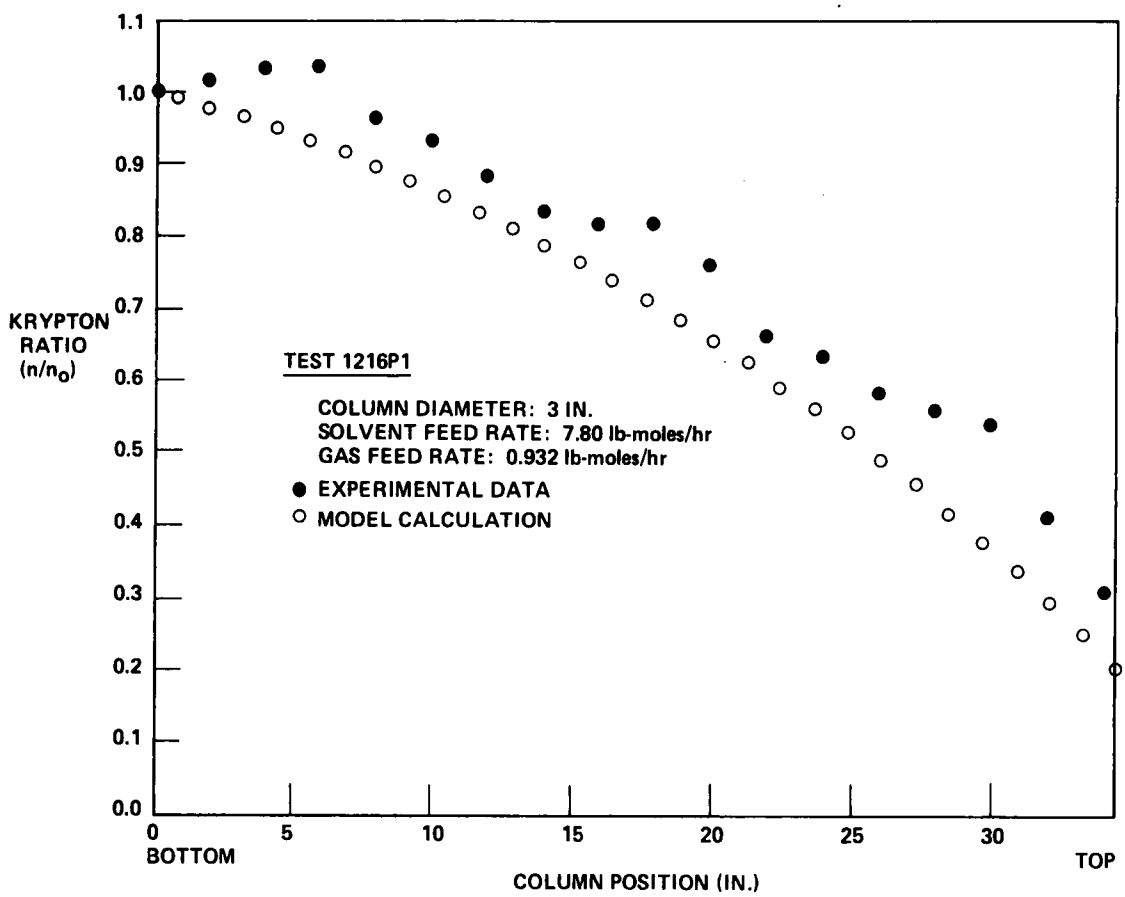

Figure B-32

EXPERIMENTAL AND CALCULATED KRYPTON PROFILES
FOR TEST 1216P1

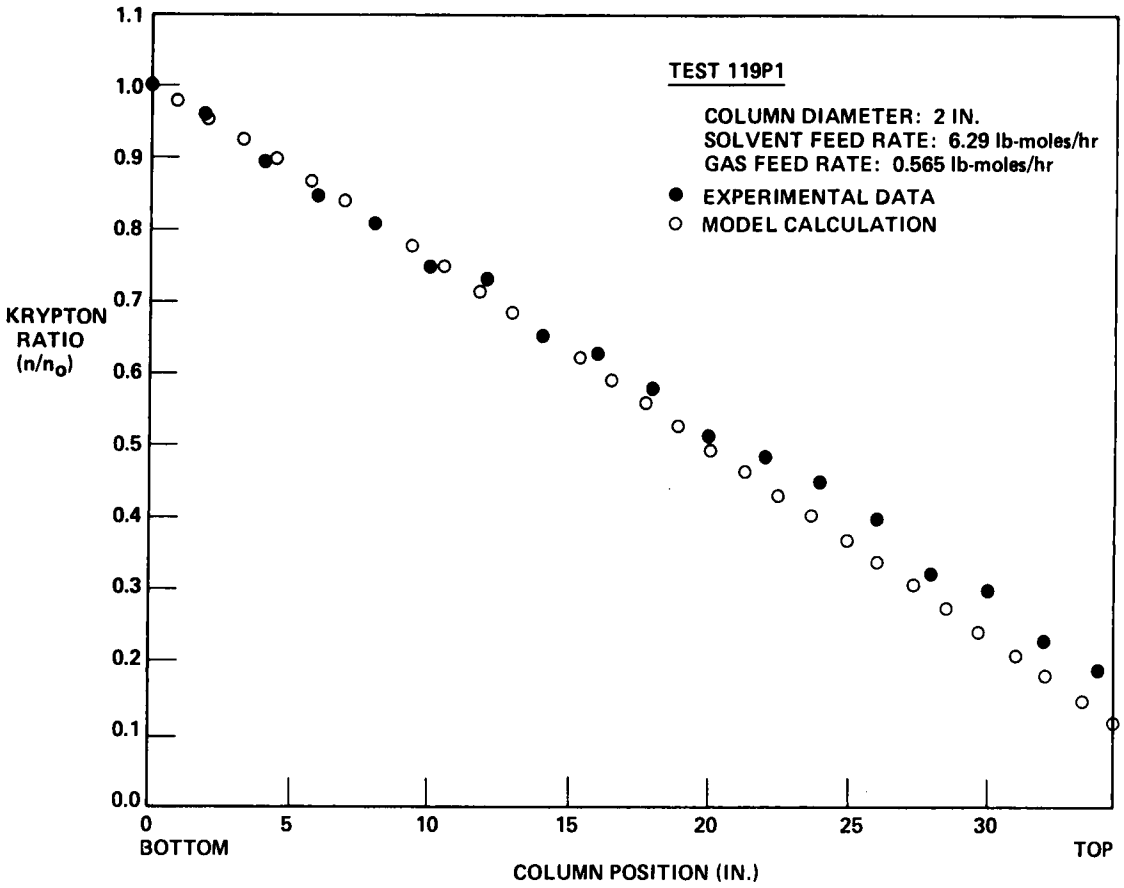

Figure B-33

EXPERIMENTAL AND CALCULATED KRYPTON PROFILES
FOR TEST 119P1

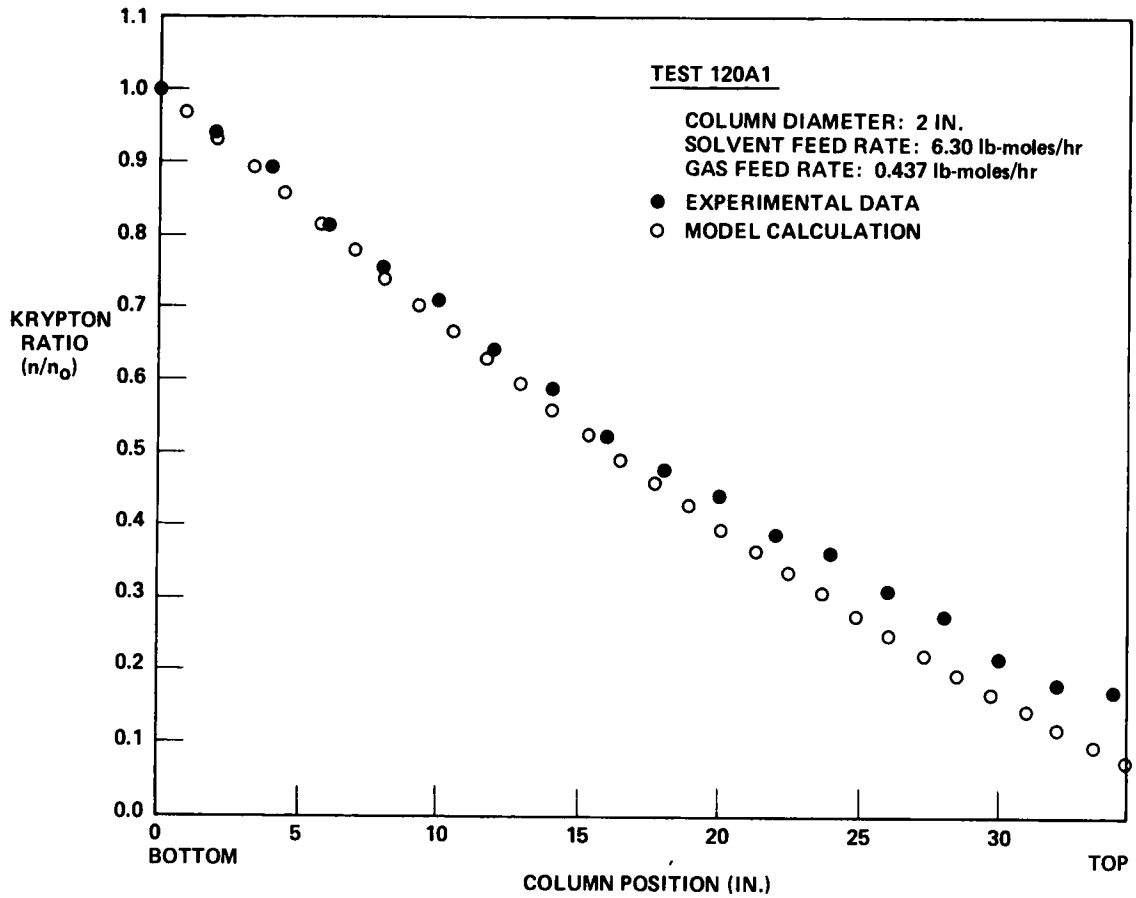

Figure B-34

EXPERIMENTAL AND CALCULATED KRYPTON PROFILES
FOR TEST 120A1

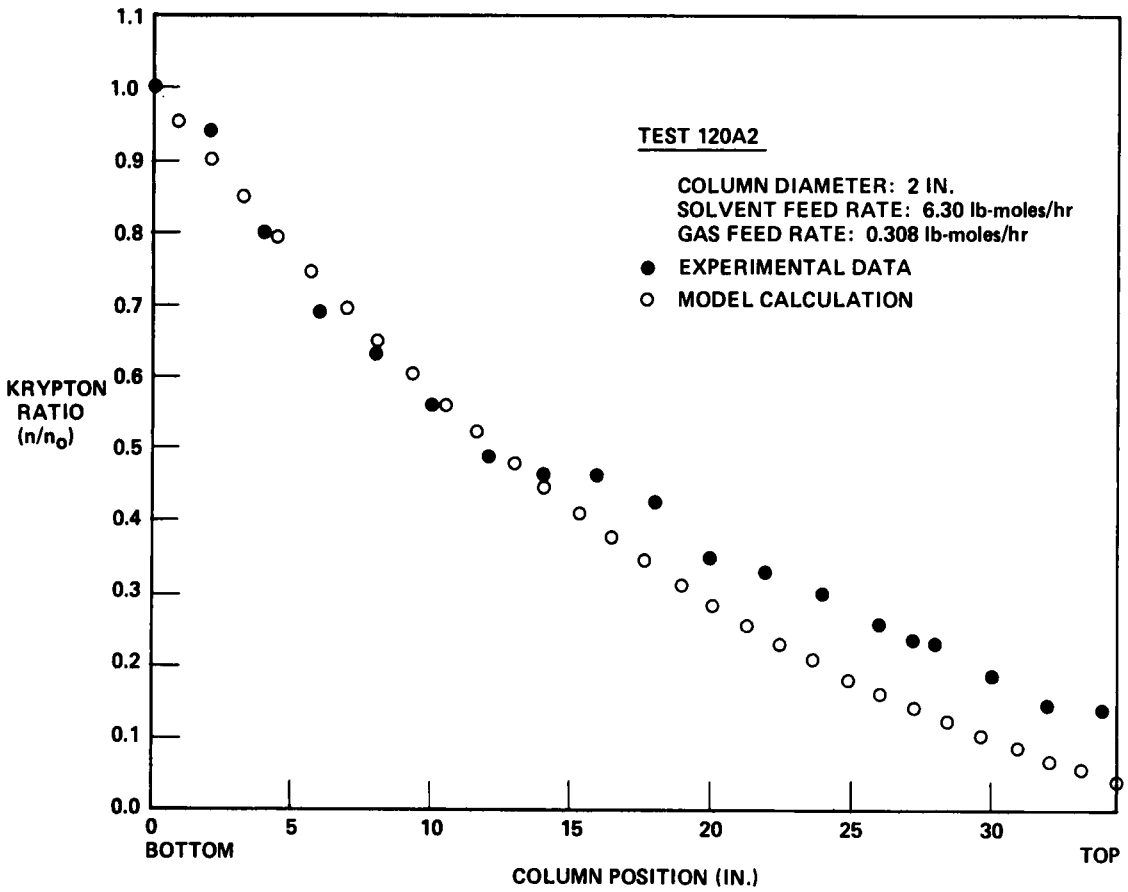

Figure B-35

EXPERIMENTAL AND CALCULATED KRYPTON PROFILES
FOR TEST 120A2

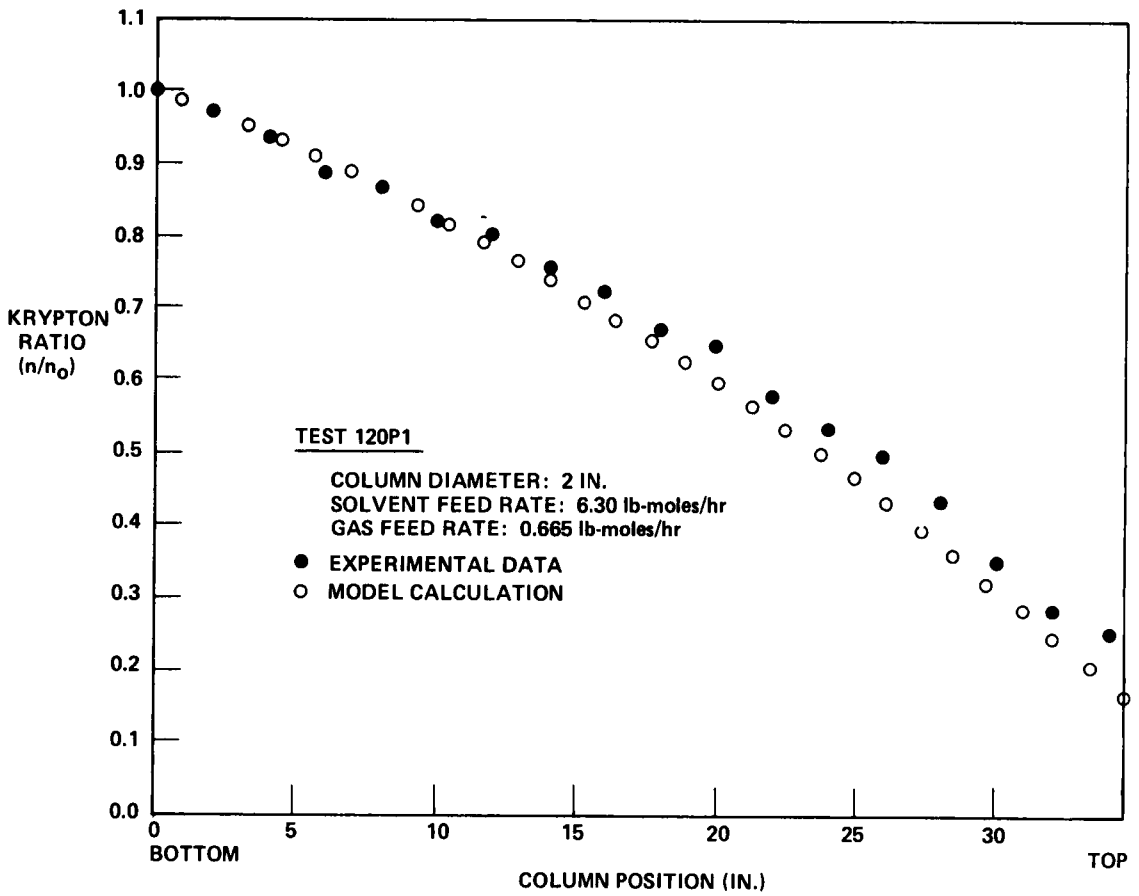

Figure B-36

EXPERIMENTAL AND CALCULATED KRYPTON PROFILES
FOR TEST 120P1

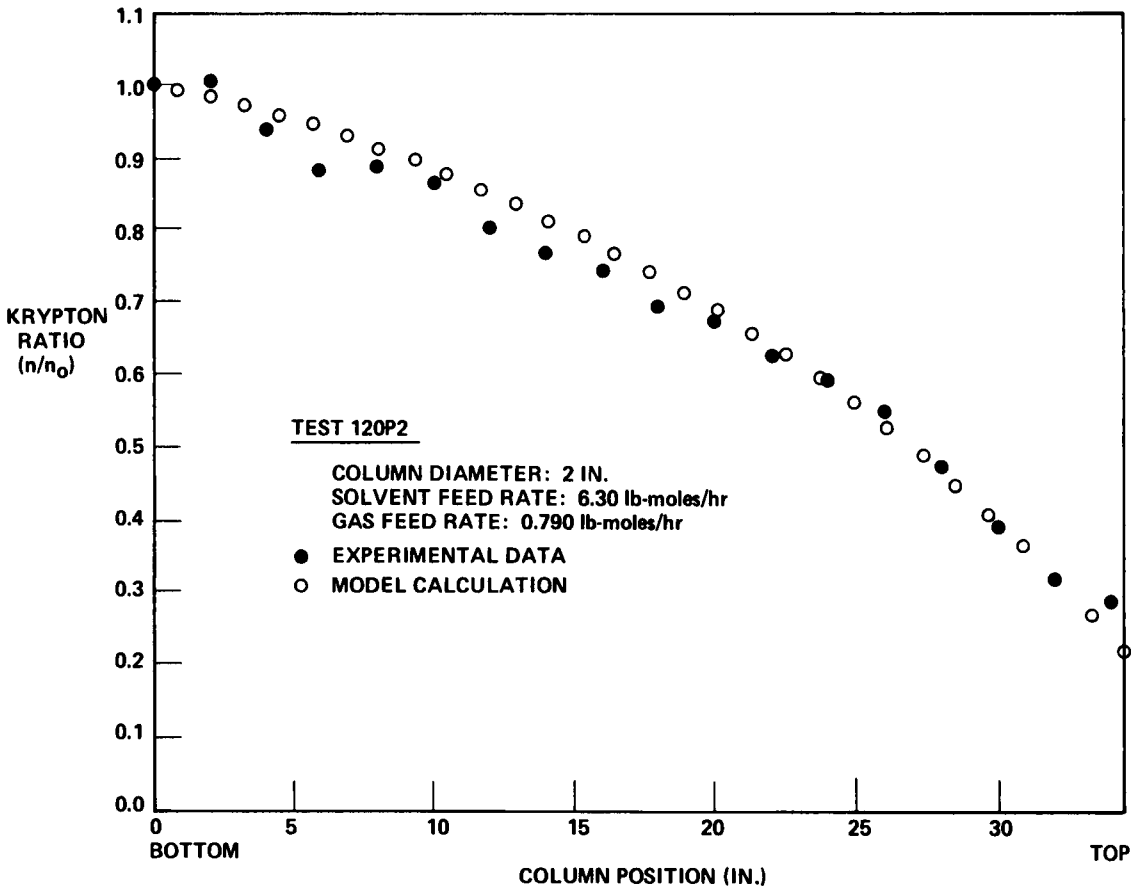

Figure B-37

EXPERIMENTAL AND CALCULATED KRYPTON PROFILES
FOR TEST 120P2

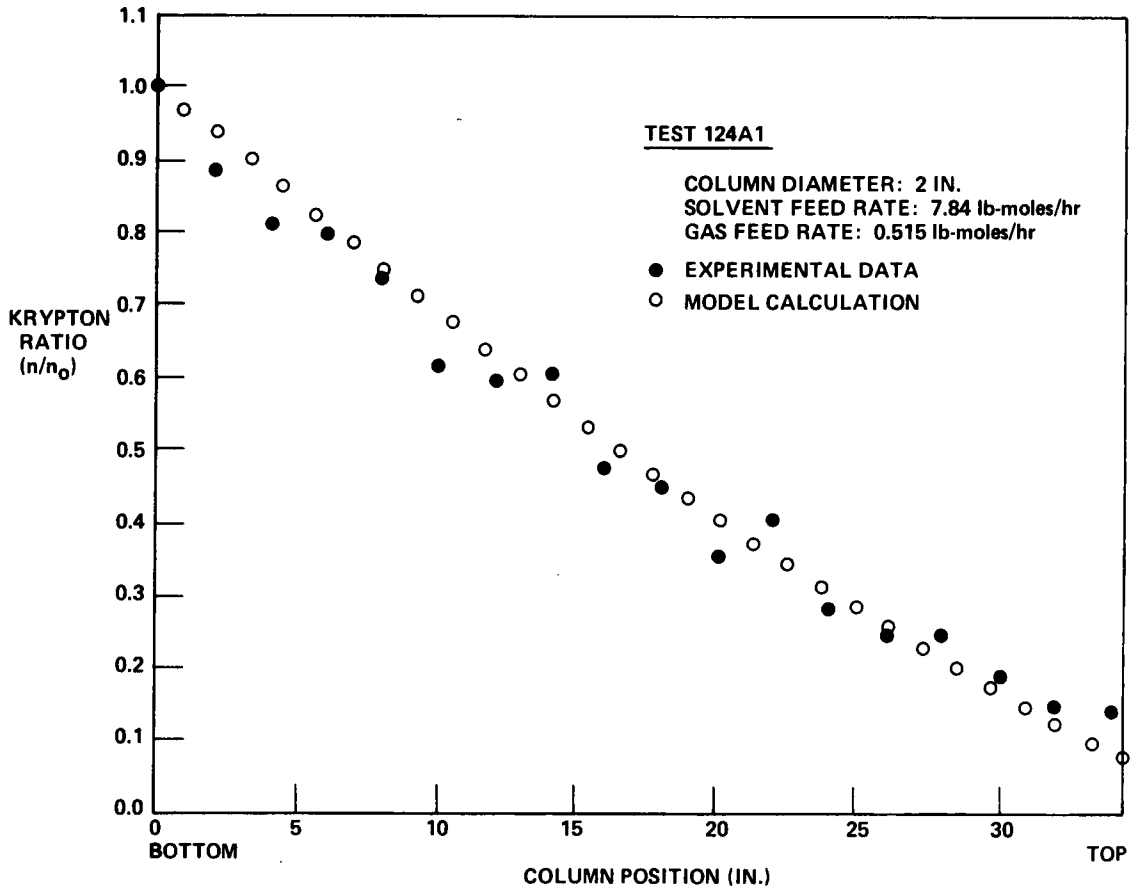

Figure B-38

EXPERIMENTAL AND CALCULATED KRYPTON PROFILES
FOR TEST 124A1

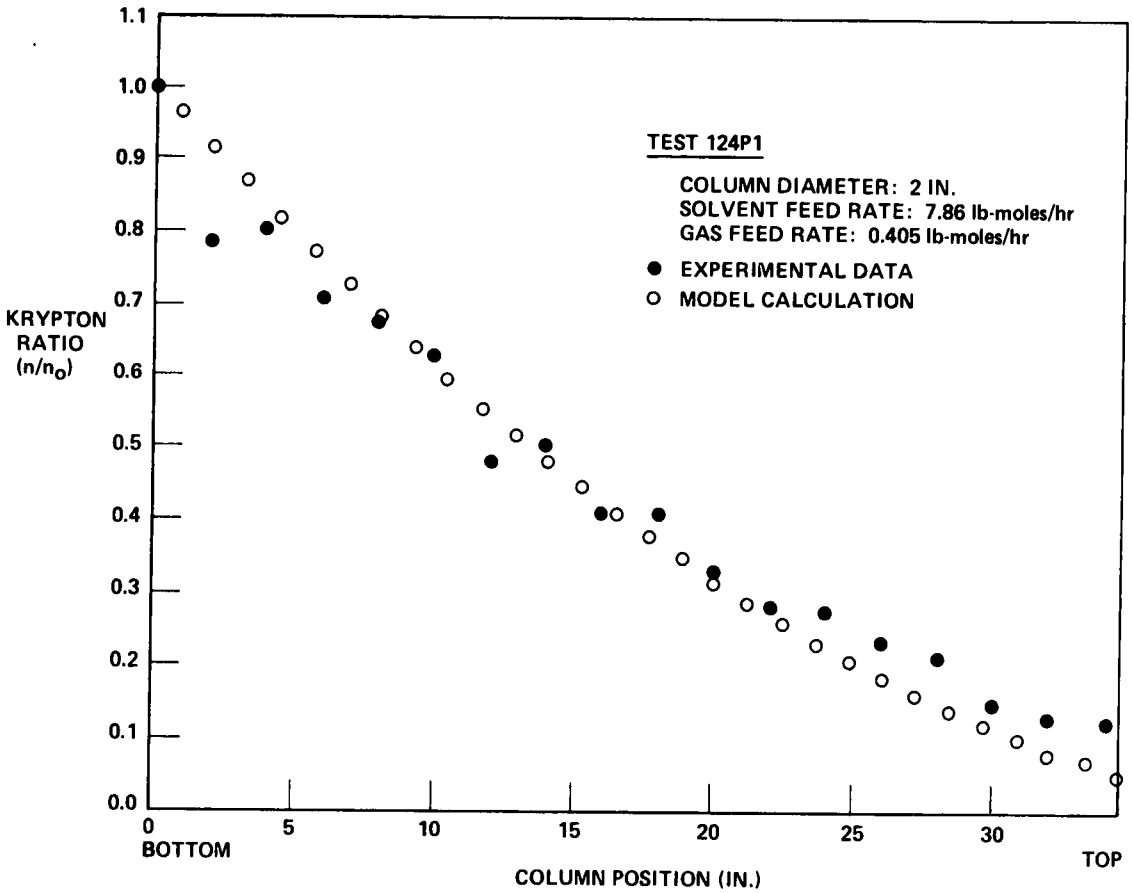

Figure B-39

EXPERIMENTAL AND CALCULATED KRYPTON PROFILES
FOR TEST 124P1

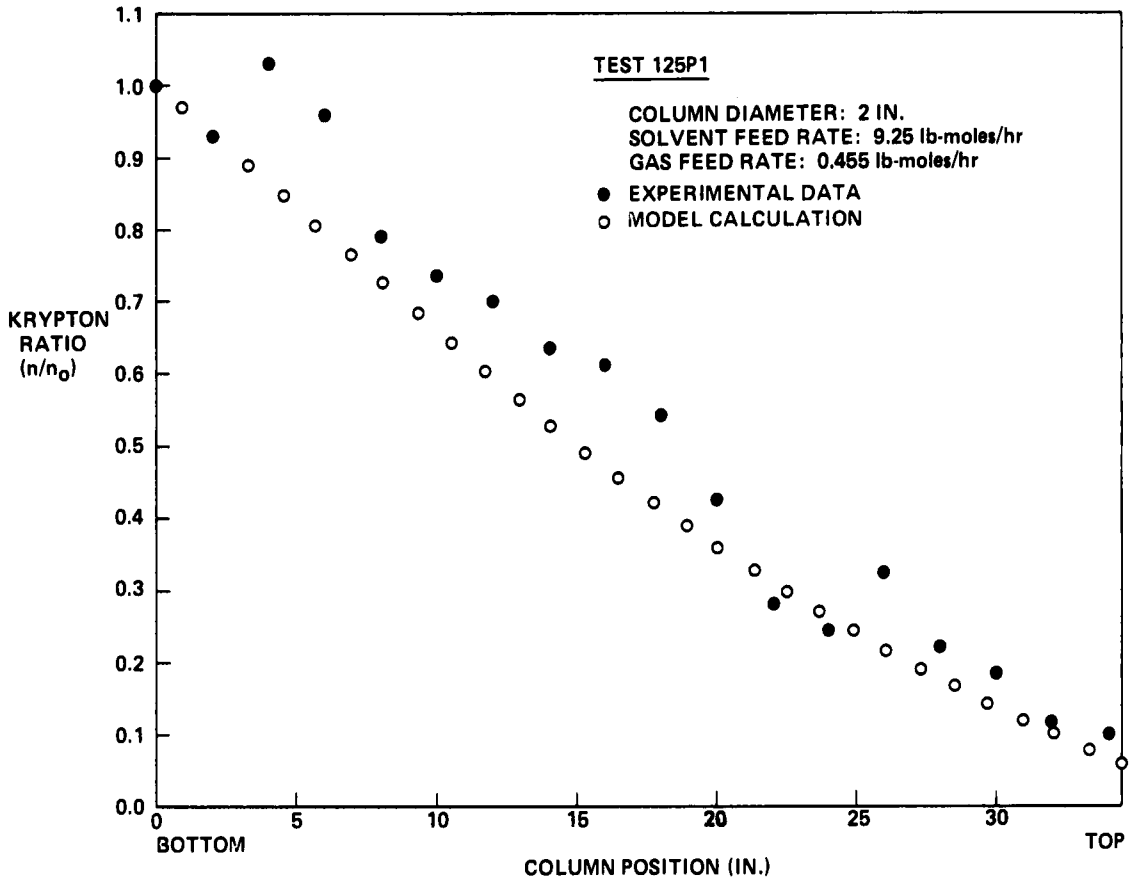

Figure B-40

EXPERIMENTAL AND CALCULATED KRYPTON PROFILES
FOR TEST 125P1

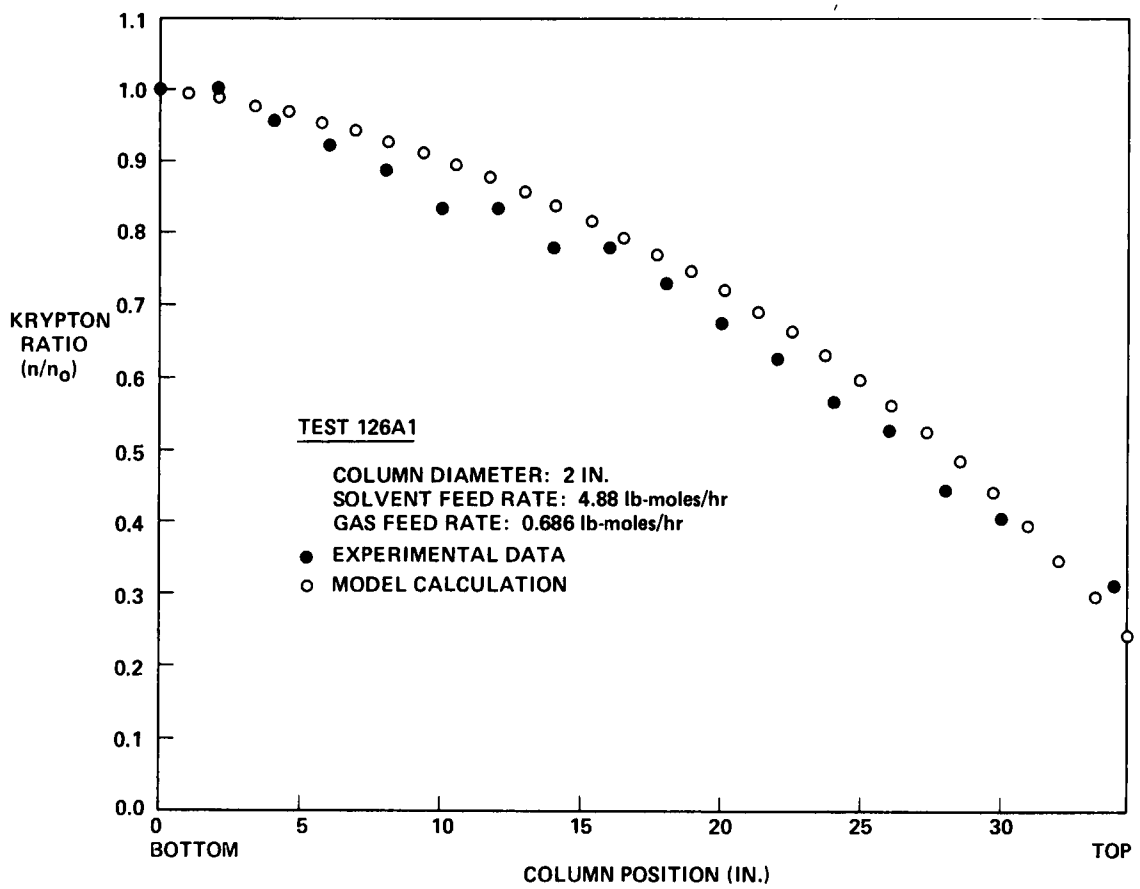

Figure B-41

EXPERIMENTAL AND CALCULATED KRYPTON PROFILES
FOR TEST 126A1

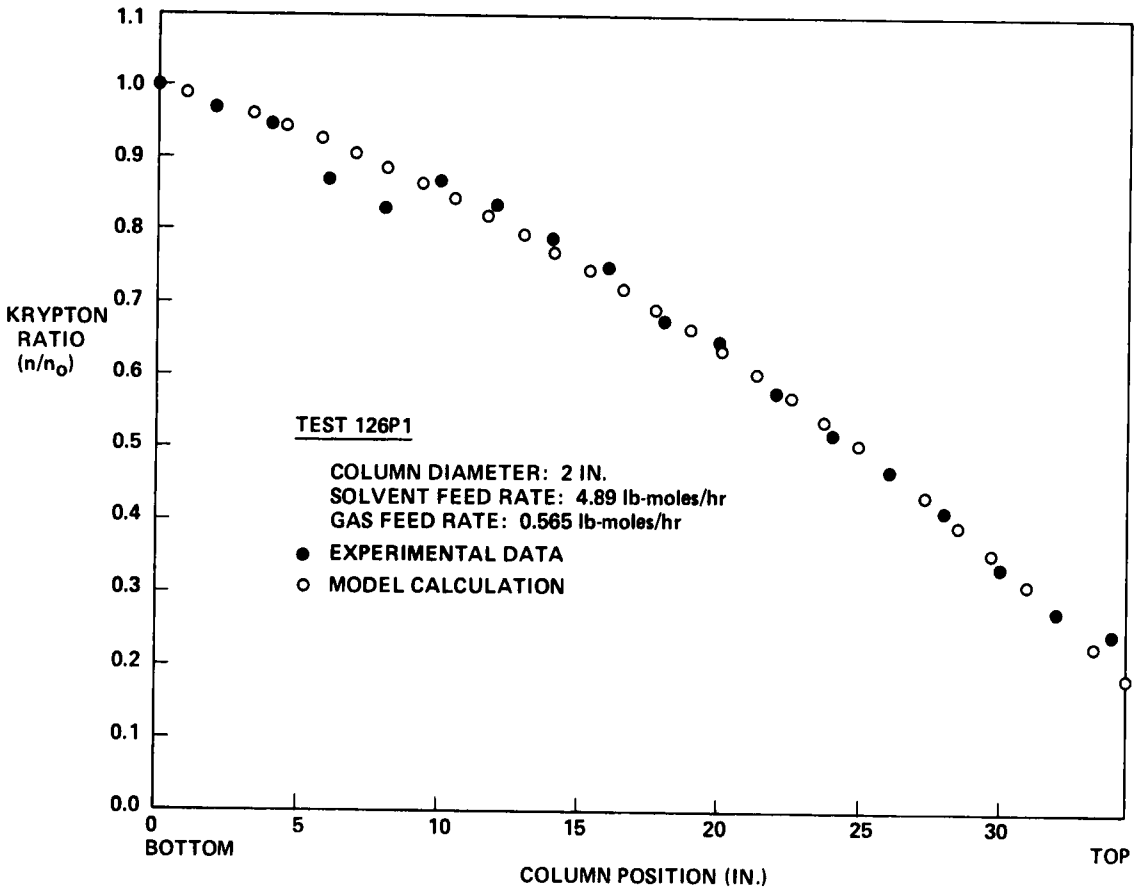

Figure B-42

EXPERIMENTAL AND CALCULATED KRYPTON PROFILES
FOR TEST 126P1

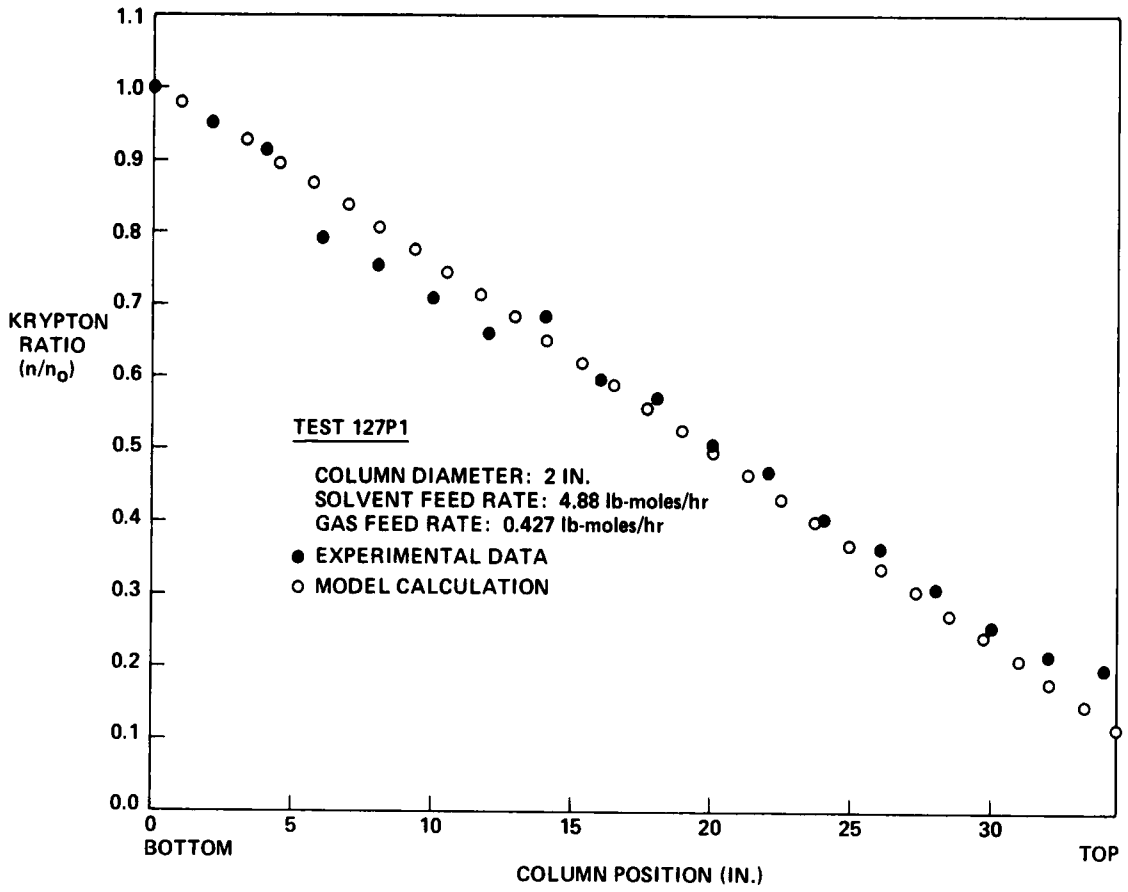

Figure B-43

EXPERIMENTAL AND CALCULATED KRYPTON PROFILES
FOR TEST 127P1

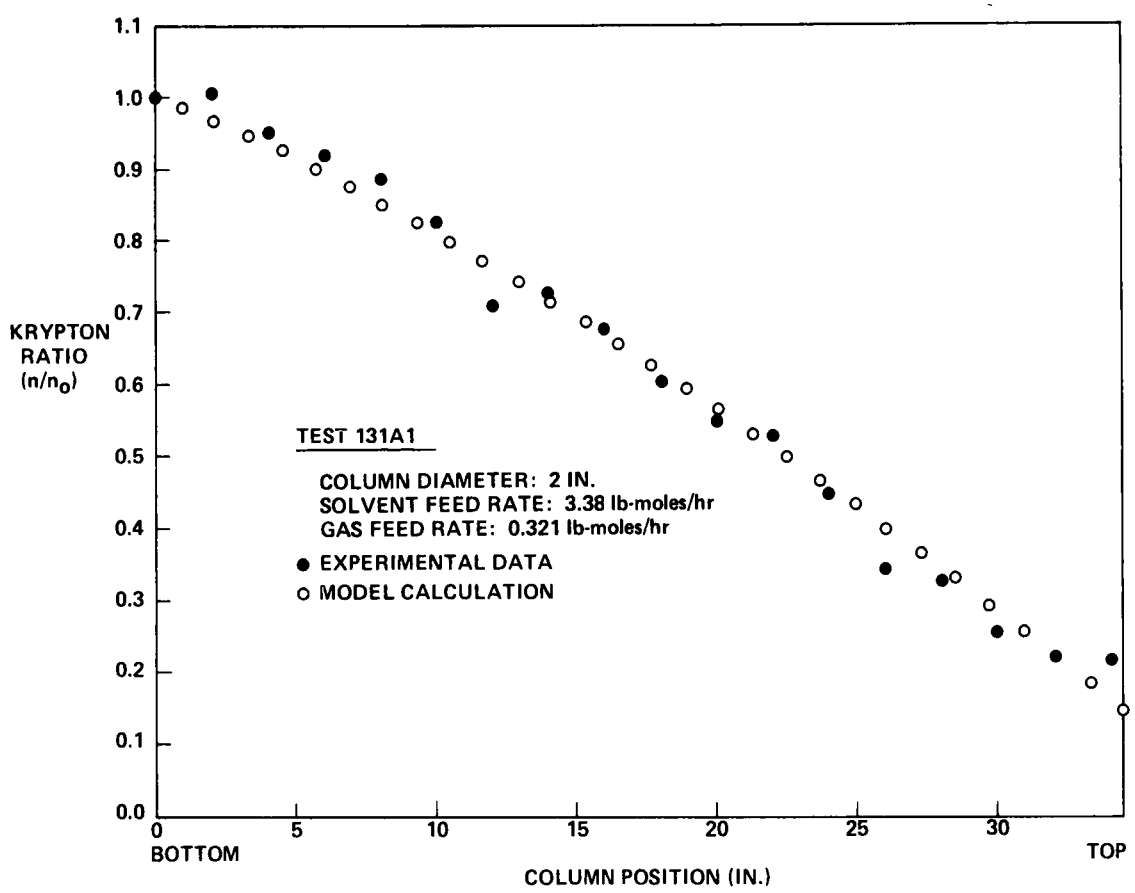

Figure B-44

EXPERIMENTAL AND CALCULATED KRYPTON PROFILES
FOR TEST 131A1

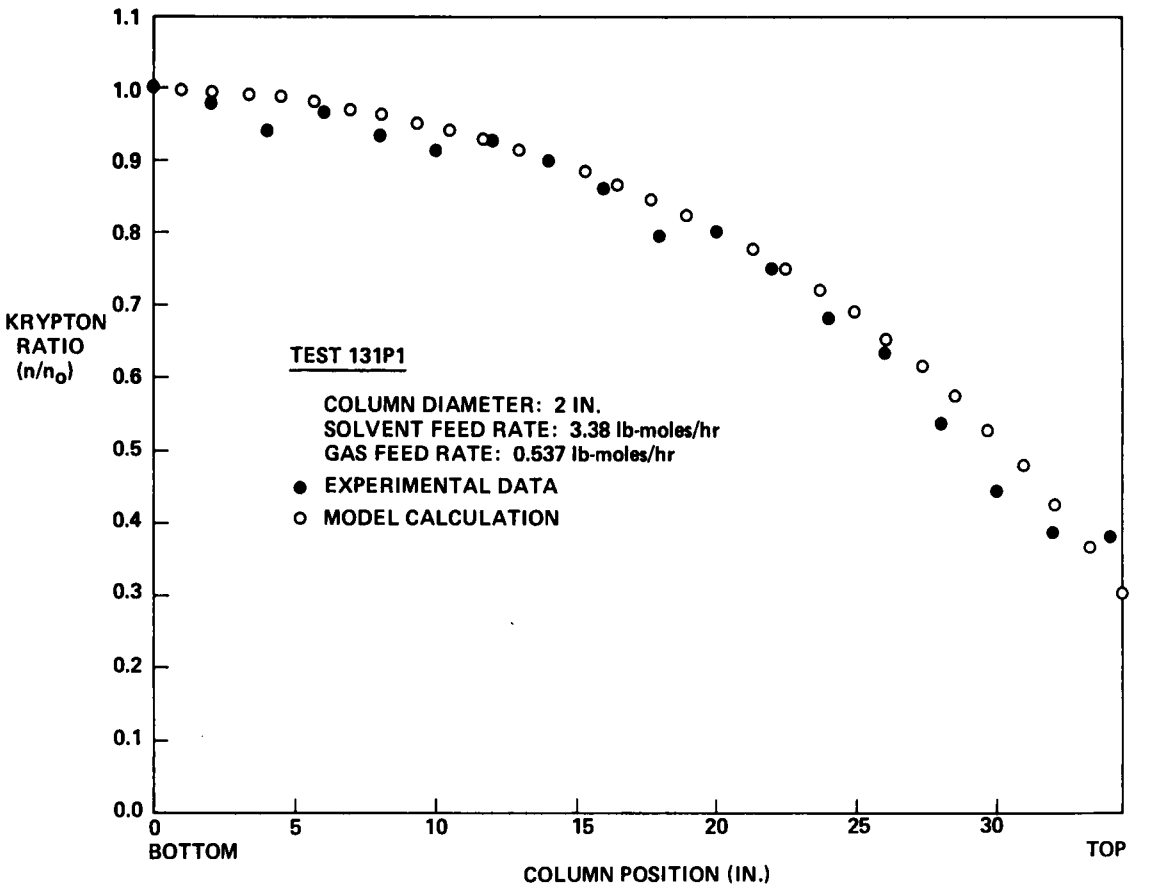

Figure B-45

EXPERIMENTAL AND CALCULATED KRYPTON PROFILES
FOR TEST 131P1

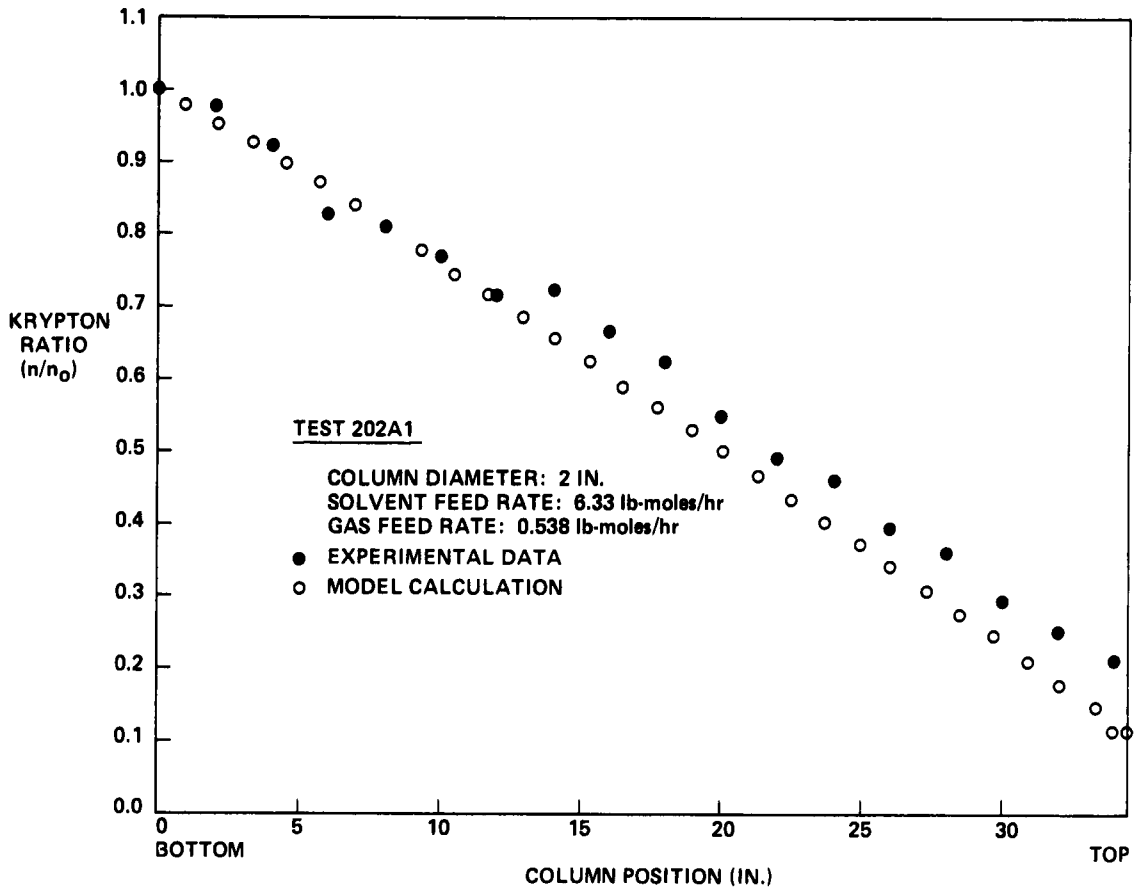

Figure B-46

EXPERIMENTAL AND CALCULATED KRYPTON PROFILES
FOR TEST 202A1

APPENDIX C

OPERATING VOID FRACTION

The operating void fraction of Goodloe packing is required for the calculation of the characteristic length. The method used to estimate this quantity was developed by Stephenson.[43]

The operating void fraction is related to the liquid holdup of the packing by

$$\varepsilon_o = \varepsilon - \Phi_\tau, \qquad \text{C-1}$$

where ε_o = operating void fraction, ft^3/ft^3,

ε = void fraction of dry packing, ft^3/ft^3, and

Φ_τ = total liquid holdup, ft^3 solvent/ft^3 column.

The void fraction of unwetted Goodloe packing, ε, was determined by Choi[8] to be 0.95. The liquid holdup is the sum of the static holdup, Φ_s, the operating holdup, Φ_o, and the holdup due to the vapor upflow, $\Phi_{\Delta P}$,

$$\Phi_\tau = \Phi_s + \Phi_o + \Phi_{\Delta P}. \qquad \text{C-2}$$

Based on the data of Bragg,[6] Stephenson concluded that the static holdup would constitute less than 5% of the total and could safely be neglected. An expression for the operating holdup was developed by fitting the holdup data given by Bragg to the correlating form suggested by Shulman.[40] Thus,

$$\Phi_o = 5.0\ L^{0.415} \mu_L^{0.13} \left(\frac{1}{\rho_L}\right)^{0.84} \left(\frac{\sigma_s}{73}\right)^{0.1}, \qquad \text{C-3}$$

where σ_s = surface tension of R-12, dynes/cm, and

L = liquid flow rate, ft^3/hr.

The holdup due to the vapor upflow, $\Phi_{\Delta P}$, becomes important when the column is operated above the loading point.[39] This quantity is expressed in terms of the pressure drop as

$$\Phi_{\Delta P} = \frac{\Delta P_R}{\rho_L}, \qquad \text{C-4}$$

where ΔP_R = pressure drop in an R-12 system, mm Hg/ft.

The manufacturers of Goodloe packing recommend[28] that the pressure drop in an aqueous system be estimated from

$$\Delta P_W = 2.529\ f^{2.01}, \qquad \text{C-5}$$

where ΔP_W = pressure drop in a water-based system, mm Hg/ft,

f = capacity factor v_{actual}/v_{max}, and

v_{actual} = vapor velocity, ft/sec.

The maximum vapor velocity, v_{max}, can be determined from

$$v_{max} = \psi \frac{0.0942}{\mu_L} \left(\frac{\rho_L - \rho_G}{\rho_G}\right)^{0.57}, \qquad \text{C-6}$$

and the flow correction factor, ψ, is expressed by

$$\ell n\ \psi = -\ 0.2621 - 0.05738\ (L/V) + 0.1049 \cdot 10^{-2}\ (L/V)^2$$

$$-\ 7.014 \cdot 10^{-5}\ (L/V)^3, \qquad \text{C-7}$$

where L = liquid mass velocity, lb/hr, and

V = vapor mass velocity, lb/hr.

As ΔP_R is needed in equation C-4, the relationship

$$\Delta P_R = \Delta P_W \frac{\rho_R}{\rho_W} \qquad \text{C-8}$$

is used to convert between the two systems.

In this work, ε_o calculated with this method showed no significant variation along the packed bed in any given test and only varied from 0.708 to 0.794 between tests.

APPENDIX D

INCREMENT SIZE

The size of the incremental depth of packing, dz, over which the flux calculations are made effects both the convergence of the solution and the computational speed. Very small values of dz generally assure a convergent solution, but require excessive amounts of computational time. The value of dz chosen must therefore represent a compromise.

Figure D-1 demonstrates the effect of increment size on the model solution of a typical data set. The curves presented represent values of the molar krypton ratio at the top of the column and the gas feed rate calculated at various values of dz ratioed to the values obtained with dz = 0.01 foot. Clearly the model solution is essentially convergent with dz <0.01 foot while those with dz >0.5 foot are obviously unacceptable. In this work, an incremental depth of 0.01 foot is used as this value provides an adequately convergent solution with acceptable computational speed.

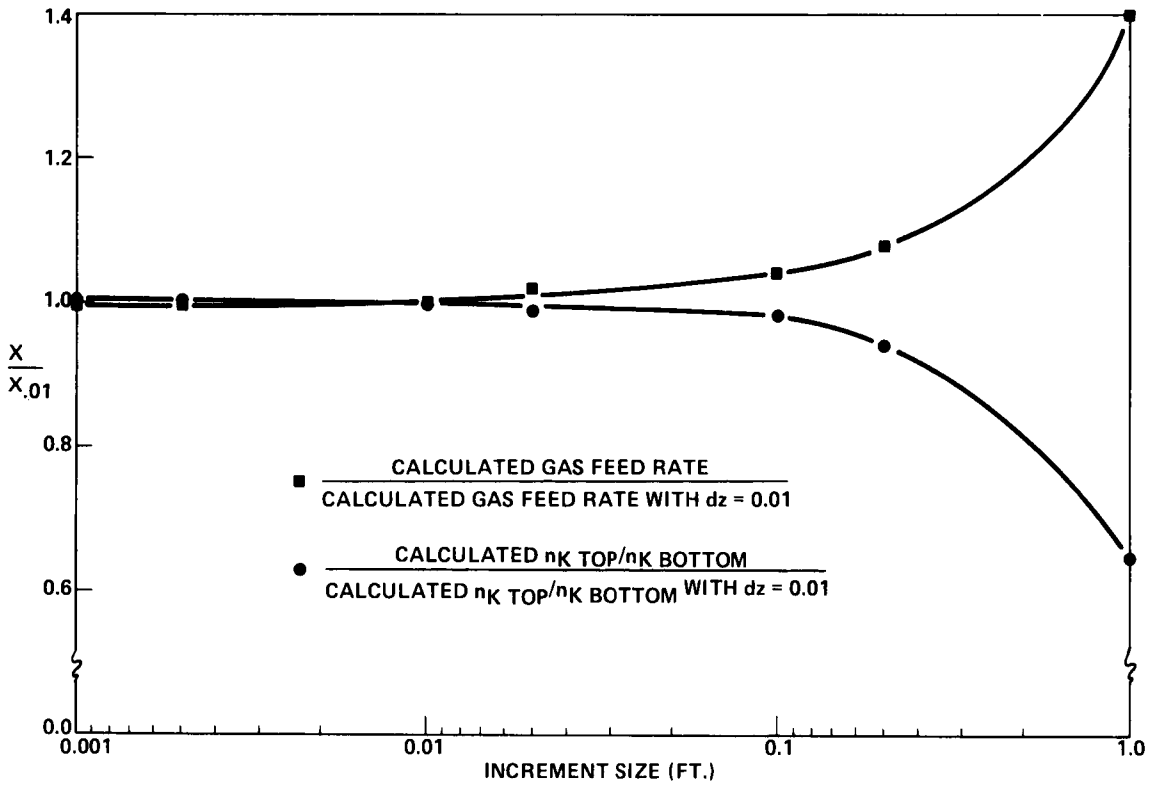

Figure D-1

EFFECT OF INCREMENT SIZE ON MODEL CONVERGENCE

APPENDIX E

FORTRAN CODE OF THE ABSORBER MODEL

Table E-1 is a listing of the Fortran IV computer program used to solve the absorber model equations by the techniques outlined in Chapter V. The version listed assumes that the solvent feed is pure R-12, and the column contains 34.5 inches of Goodloe packing. These values, however, are easily changed. For the model to converge, the variables in the program require a minimum word length of 12 bits. The program is therefore written in double precision. Use of this program requires specification of the number of cases to be calculated and following information for each case:

1. Case identification number,
2. Solvent feed rate, lb moles/hr,
3. Off-gas flow rate, lb moles/hr,
4. Mole fraction of R-12 in off-gas,
5. Mole fraction of krypton in off-gas$\cdot 10^8$,
6. Column pressure, atm,
7. Column temperature, °F,
8. Size of increment dz, ft,
9. Column diameter, in., and
10. Number of increments to be calculated between printouts.

The program is divided into well-identified sections and subprograms, and an attempt was made to use nomenclature in the program that corresponds to that used in the text of this work.

TABLE E-1

FORTRAN CODE OF THE ABSORBER MODEL

```
C*************************************************************************
C*************************************************************************
C*************************************************************************
C          A MULTICOMPONENT GAS ABSORPTION MODEL --- B.E.KANAK
C                          REVISED: 8/25/78
C                            UNCLASSIFIED
C*************************************************************************
C*************************************************************************
C*************************************************************************
C
C
C
C
C
      IMPLICIT REAL * 8 (A-H,O-Z)
      REAL * 8 L,L1,NDG1,NDG2,NDG
      EXP(X) = DEXP(X)
      ALOG10(X) = DLOG10(X)
      ABS(X) = DABS(X)
      B(X) =(DEXP(X/FGA/DZ) * (YNB - XNB) +DEXP(X/FLA/DZ) *
     C (YNI - XNI) -YNI + XNB)/(YNB - XNI)
      F(X) = X - (1.0/(1.0/FLA/DZ + 1.0/FGA/DZ)) * DLOG((DEXP(X/
     C FGA/DZ) * (YNB - XNB) +DEXP(X/FLA/DZ) * (YNI - XNI)
     C - YNI + XNB)/(YNB - XNI))
C
C
C                       KEY
C
      WRITE(6,237)
      WRITE(6,238)
      WRITE(6,239)
      WRITE(6,240)
      WRITE(6,200)
      WRITE(6,201)
      WRITE(6,202)
      WRITE(6,203)
      WRITE(6,204)
      WRITE(6,205)
      WRITE(6,206)
      WRITE(6,207)
      WRITE(6,208)
      WRITE(6,209)
      WRITE(6,210)
      WRITE(6,211)
      WRITE(6,212)
      WRITE(6,213)
      WRITE(6,214)
      WRITE(6,215)
```

TABLE E-1 (Continued)

```
      WRITE(6,216)
      WRITE(6,217)
      WRITE(6,218)
      WRITE(6,219)
      WRITE(6,220)
      WRITE(6,221)
      WRITE(6,222)
      WRITE(6,223)
      WRITE(6,224)
      WRITE(6,225)
      WRITE(6,226)
      WRITE(6,227)
      WRITE(6,228)
      WRITE(6,229)
      WRITE(6,230)
      WRITE(6,231)
      WRITE(6,232)
      WRITE(6,233)
      WRITE(6,234)
      WRITE(6,235)
      WRITE(6,236)
237   FORMAT(1H1,//////,18X,'FLOUROCARBON PROCESS ABSORBER MODEL')
238   FORMAT(28X,'- B. E. KANAK -')
239   FORMAT(28X,'REVISED: 8/25/78')
240   FORMAT(30X,'UNCLASSIFIED')
200   FORMAT(///,30X,'OUTPUT KEY')
201   FORMAT(//,5X,'HT. --- DISTANCE FROM BOTTOM OF PACKED BED',
     C ' (INCHES)')
202   FORMAT(5X,'YRB --- MOLE FRACTION R-12 IN BULK GAS')
203   FORMAT(5X,'YNB --- MOLE FRACTION N2 IN BULK GAS')
204   FORMAT(5X,'XRB --- MOLE FRACTION R-12 IN BULK LIQUID')
205   FORMAT(5X,'XNB --- MOLE FRACTION N2 IN BULK LIQUID')
206   FORMAT(5X,'G ----- TOTAL MOLAR GAS FLOW RATE (LB MOLES/HR)')
207   FORMAT(5X,'L ----- TOTAL MOLAR LIQUID FLOW RATE (LB MOLES/HR)')
208   FORMAT(5X,'AKRT -- TOTAL AMOUNT OF KR (LB MOLES/HR * 1E+08)')
209   FORMAT(5X,'AKRG -- AMOUNT OF KR IN GAS (LB MOLES/HR * 1E+08)')
210   FORMAT(5X,'YKB --- MOLE FRACTION KR IN BULK GAS')
211   FORMAT(5X,'XKB --- MOLE FRACTION IN BULK LIQUID)')
212   FORMAT(5X,'FGA --- MASS TRANSFER COEFFICIENT * INTERFACIAL',
     C ' AREA FOR N2 & R-12 ACROSS GAS')
213   FORMAT(13X,'FILM (LB MOLES/HR/FT)')
214   FORMAT(5X,'FLA --- MASS TRANSFER COEFFICIENT * INTERFACIAL',
     C ' AREA FOR N2 & R-12 ACROSS')
215   FORMAT(13X,'LIQUID FILM (LB MOLES/HR/FT)')
216   FORMAT(5X,'FGK --- MASS TRANSFER COEFFICIENT * INTERFACIAL',
     C ' AREA FOR KR ACROSS GAS')
217   FORMAT(13X,'FILM (LB MOLES/HR/FT)')
218   FORMAT(5X,'FLK --- MASS TRANSFER COEFFICIENT  * INTERFACIAL',
```

TABLE E-1 (Continued)

```
     C ' AREA FOR KR ACROSS')
219   FORMAT(13X,'LIQUID FILM (LB MOLES/HR/FT)')
220   FORMAT(5X,'YKI --- INTERFACIAL GAS MOLE FRACTION OF KR')
221   FORMAT(5X,'XKI --- INTERFACIAL LIQUID MOLE FRACTION OF KR')
222   FORMAT(5X,'REG --- GAS REYNOLDS NUMBER')
223   FORMAT(5X,'REL --- LIQUID REYNOLDS NUMBER')
224   FORMAT(5X,'EPS --- OPERATING VOID FRACTION')
225   FORMAT(5X,'DG ---- TOTAL FLUX FROM GAS TO LIQUID (LB MOLES/HR)')
226   FORMAT(5X,'DGYK -- KR FLUX FROM GAS TO LIQUID (LB MOLES/HR)')
227   FORMAT(5X,'SCG --- GAS SCHMIDT NUMBER FOR N2 & R-12')
228   FORMAT(5X,'SCL --- LIQUID SCHMIDT NUMBER FOR N2 & R-12')
229   FORMAT(5X,'SCGK -- GAS SCHMIDT NUMBER FOR KR')
230   FORMAT(5X,'SCLK -- LIQUID SCHMIDT NUMBER FOR KR')
231   FORMAT(5X,'DGYN -- N2 FLUX FROM GAS TO LIQUID (LB MOLES/HR)')
232   FORMAT(5X,'DGYR -- R-12 FLUX FROM GAS  TO LIQUID (LB MOLES/HR)')
233   FORMAT(5X,'GDRN -- GAS DIFFUSIVITY FOR R-12 & N2 (FT2/HR)')
234   FORMAT(5X,'LDRN -- LIQUID DIFFUSIVITY FOR R-12 & N2 (FT2/HR)')
235   FORMAT(5X,'GDKR -- GAS DIFFUSIVITY FOR KR (FT2/HR)')
236   FORMAT(5X,'LDKR -- LIQUID DIFFUSIVITY FOR KR (FT2/HR)')
C
C
C                  DATA INPUT
C
      READ(5,100) NUMBER
      DO 99 IJKLM = 1,NUMBER
      READ(5,101) MNOP,PONM,POMN
      READ(5,102) L,XNB
      READ(5,103) G,YRB,GRAT
      READ(5,104) PATM,TF,D7,CD,INCRE
100   FORMAT(10X,I2)
101   FORMAT(10X,I4,A1,I1)
102   FORMAT(10X,F10.5,F10.7)
103   FORMAT(10X,F20.10,F10.8,F10.5)
104   FORMAT(10X,4F10.5,I2)
C
C
C               OPERATING PARAMETERS OUTPUT
C
      WRITE(6,106) MNOP,PONM,POMN
      WRITE(6,107) CD
      WRITE(6,108)
      WRITE(6,109) L
      WRITE(6,110) G
      WRITE(6,111) PATM
      WRITE(6,112) TF
      WRITE(6,113)
      WRITE(6,114)
      BBBB = 1.0 - XNB
```

TABLE E-1 (Continued)

```
      WRITE(6,115)XNB,BBBB
      BBBB = GRAT * 1E-8/G
      AAAA = 1.0 - YRB
      WRITE(6,116) AAAA,YRB,BBBB
106   FORMAT(1H1, 9X,'RUN NUMBER:',2X,I4,A1,I1)
107   FORMAT(10X,'COLUMN DIAMETER:',2X,F5.2,1X,'INCHES')
108   FORMAT(10X,'OPERATING PARAMETERS')
109   FORMAT(20X,'LIQUID FEED RATE:',2X,F5.3,1X,'LB MOLES/HR')
110   FORMAT(20X,'OFF-GAS FLOW RATE:',2X,F6.4,1X,'LB MOLES/HR')
111   FORMAT(20X,'COLUMN PRESSURE:',2X,F5.3,1X,'ATM')
112   FORMAT(20X,'COLUMN TEMPERATURE:',2X,F6.2,1X,'DEG-F')
113   FORMAT(20X,'COMPOSITION')
114   FORMAT(37X,'N2',5X,'R-12',7X,'KR')
115   FORMAT(27X,'LIQUID',2X,F5.4,2X,F6.4,3X,'.0000D 00')
116   FORMAT(30X,'GAS',2X,F5.4,3X,F5.4,3X,E9.4)
C
C
C              DISTRIBUTION COEFFICIENTS
C
      DN = EXP(6.097 + .00166 * TF)
      DR = (10**(39.88391727D+0 - 3436.632228D+0/(TF + 460) -
     C 12.47152228D+0 * ALOG10(TF + 460) + .00473044244D+0
     C * (TF + 460)))/14.7D+0
      DK = EXP(5.15586173D+0 + (-65.31695880D+0/
     C (TF + 104.93294275D+0)))
      Z = 2.875
      CSA = 3.141592654D+0 * (CD/24.0D+0)**2.0D+0
C
C
C           INTERFACIAL CONCENTRATIONS
C
      XNI = (PATM - DR)/(DN - DR)
      YNI = DN * XNI/PATM
      XRI = 1.0 - XNI
      YRI = 1.0 - YNI
      WRITE (6,118)
      WRITE(6,119)
      WRITE(6,120)
      WRITE(6,121) YRI,YNI,XRI,XNI
118   FORMAT(//,22X,'INTERFACIAL COMPOSITIONS')
119   FORMAT(23X,'GAS',14X,'LIQUID')
120   FORMAT(18X,'R-12',6X,'N2',6X,'R-12',6X,'N2')
121   FORMAT(17X,4(F6.4,3X))
C
C
C           PRINTOUT
C
      WRITE(6,122)
```

TABLE E-1 (Continued)

```
      WRITE(6,123)
      WRITE(6,124)
      WRITE(6,125)
      WRITE(6,126)
      XRB = 1.0 - XNB
      YNB = 1.0 - YRB
      XKB = 0.0000000000000
      YKB = GRAT/G * 1E-8
      RAT = (L * XKB + G * YKB)/1E-8
      AAAA = Z * 12.0
      WRITE(6,127) AAAA,YRB,YNB,XRB,XNB,G,L,RAT,GRAT
122   FORMAT(//,1X,'HT.',5X,'YRB',5X,'YNB',7X,'XRB',5X,'YNB',7X,
     C 'G',7X,'L',6X,'AKRT',4X,'AKRG')
123   FORMAT(7X,'YKB',7X,'XKB',15X,'FGA',7X,'FLA',7X,'FGK',7X,
     C 'FLK')
124   FORMAT(7X,'YKI',7X,'XKI',15X,'REG',7X,'REL',7X,'EPS')
125   FORMAT(7X,'DG',7X,'DGYK',15X,'SCG',7X,'SCL',6X,'SCGK',
     C 6X,'SCLK')
126   FORMAT(6X,'DGYN',6X,'DGYR',14X,'GDRN',6X,'LDRN',6X
     C ,'GDKR',6X,'LDKR')
127   FORMAT(/,1X,F6.2,2X,3(F6.4,3X),F6.4,2X,F6.3,2X,F6.3,2(2X,F7.4))
C
C
C                DELTA G CALCULATION
C
      ICOUNT = 1.0
      L = L/CSA
      G = G/CSA
      ISTART = 1.0
1     CONTINUE
      CALL COEFF(CSA,TF,XNB,XRB,YNB,YRB,L,G,PATM,FLA,FGA,FLK,
     C REG,REL,SCG,SCL,SCLK,COFDIF,DIFCOF,DIFKRL,
     C FOVKR,FOVKN,DELR,DELN,TK,A,VISGM,DENG,AMWTG,FACT,EPS)
C
C
C              POSITIVE BRACKET
C
      PDG1 = 1.0
      PDG2 = 1.0
15    IF(PDG1/DZ/FGA.LE.200)GO TO 14
      PDG2 = PDG1/2.0
      PDG1 = PDG1/2.0
      GO TO 15
14    IF(F(PDG1).GT.0.0) GO TO 3
      PDG2 = 2 * PDG1
      PDG1 = 2 * PDG1
      GO TO 14
3     CONTINUE
```

TABLE E-1 (Continued)

```
      IF(F(PDG1).LT.0.0) GO TO 4
      IF(PDG1.LT.1E-12) GO TO 5
      PDG2 = PDG1
      PDG1 = PDG1/2
      GO TO 3
4     CONTINUE
      CALL BISECT(PDG1,PDG2,FLA,FGA,DZ,YNB,XNB,YNI,XNI,PDG)
      GO TO 6
5     PDG = 0.0
6     CONTINUE
C
C
C                        NEGATIVE BRACKET
C
      NDG1 = -1.0
      NDG2 = -1.0
7     CONTINUE
      IF(B(NDG1).GT.0.0) GO TO 8
      NDG1 = NDG1/2
      GO TO 7
8     CONTINUE
      IF(F(NDG1).GT.0.0) GO TO 13
      NDG1 = NDG1 - .0001
      GO TO 7
13    NDG2 = NDG1
9     CONTINUE
      IF(F(NDG1).LT.0.0) GO TO 11
      IF(NDG1.GT.-1E-12) GO TO 10
      NDG2 = NDG1
      NDG1 = NDG1/2
      GO TO 9
10    NDG = 0.0
      GO TO 12
11    CALL BISECT(NDG1,NDG2,FLA,FGA,DZ,YNB,XNB,YNI,XNI,NDG)
12    CONTINUE
      IF(ABS(NDG).GT.ABS(PDG)) DG = NDG
      IF(ABS(NDG).LE.ABS(PDG)) DG = PDG
      IF(DG.EQ.0.0) DG = .1D-12
C
C
C                                FLUX
C
      DGYN = (YNI * DG  - YNB * DG  * EXP(DG /FGA/DZ))/
     C (1.0 - EXP(DG /FGA/DZ))
      DGYR = (YRI * DG  - YRB * DG  * EXP(DG /FGA/DZ))/
     C (1.0 - EXP(DG /FGA/DZ))
      CALL FLUXK(FOVKR,FOVKN,DELR,DELN,TK,PATM,ISTART,DIFKMX,
     C YKB,YNB,YRB,DG,DGYR,DGYN,A,   REG,VISGM,DENG,AMWTG,FACT,
```

TABLE E-1 (Continued)

```
     C DZ,XKB,DK,FLK,FGK,DGYK,SCGK,YKI)
C
C
C          LIQUID PHASE FLUX
C
      DL =  DG
      DLXN =  DGYN
      DLXR =  DGYR
      DLXK = DGYK
C
C
C               NEXT INCREMENT
C
      G1 = G + DG
      L1 = L + DL
      YRB = (G * YRB + DGYR)/G1
      XNB = (L * XNB + DLXN)/L1
      YNB = 1.0 - YRB
      XRB = 1.0 - XNB
      YKB = (G * YKB + DGYK)/G1
      XKB = (L * XKB + DLXK)/L1
      RAT = CSA * (L1 * XKB + G1 * YKB)/1E-8
      GRAT = CSA * G1 * YKB/1E-8
      G = G1
      L = L1
      IF(Z.LE.DZ) DZ = Z
      Z = Z - DZ
      IF(Z.LE..00001) GO TO 2
      IF(ICOUNT.NE.INCRE) GO TO 20
      AAAA = 12.0 * Z
      BBBB = G * CSA
      CCCC = L * CSA
40    WRITE(6,127) AAAA,YRB,YNB,XRB,XNB,BBBB,CCCC,RAT,GRAT
      WRITE(6,128)YKB,XKB,FGA,FLA,FGK,FLK
      AAAA = YKI * PATM/DK
      WRITE(6,129) YKI,AAAA,REG,REL,EPS
      WRITE(6,128)DG,DGYK,SCG,SCL,SCGK,SCLK
      WRITE(6,128)DGYN,DGYR,COFDIF,DIFCOF,DIFKMX,DIFKRL
      ICOUNT = 0.0
20    ICOUNT = ICOUNT + 1.0
      GO TO 1
2     CONTINUE
      AAAA = 12.0 * Z
      BBBB = G * CSA
      CCCC = L * CSA
      WRITE(6,127) AAAA,YRB,YNB,XRB,XNB,BBBB,CCCC,RAT,GRAT
      WRITE(6,128)YKB,XKB,FGA,FLA,FGK,FLK
      AAAA = YKI * PATM/DK
```

TABLE E-1 (Continued)

```
      WRITE(6,129) YKI,AAAA,REG,REL,EPS
      WRITE(6,128)DG,DGYK,SCG,SCL,SCGK,SCLK
      WRITE(6,128) DGYN,DGYR,COEDIF,DIFCOF,DIFKMX,DIFKRL
128   FORMAT(3X,2(E9.3,1X),7X,4(2X,E8.3))
129   FORMAT(4X,2(E8.3,2X),6X,3(2X,E8.3))
99    CONTINUE
      STOP
      END
C
C
C              MASS TRANSFER COEFFICIENTS
C
      SUBROUTINE COEFF(CSA,TF,XNB,XRB,YNB,YRB,L,G,PATM,FLA,FGA,FLK,
     C REG,REL,SCG,SCL,SCLK,COEDIF,DIFCOF,DIFKRL,
     C FOVKR,FOVKN,DELR,DELN,TK,A,VISGM,DENG,AMWTG,FACT,EPS)
      IMPLICIT REAL * 8 (A-H,O-Z)
      REAL * 8 L
      EXP(X) = DEXP(X)
C
C
C                  LIQUID REYNOLDS NUMBER
C
1000  TR = TF + 460.0
      TK = TR/1.8
      AMWTL = XNB * 28.0 + XRB * 121.0
      VISRL = (EXP(-3.099 + 933.0/TR)) * 2.419
C
C
C                  GAS REYNOLDS NUMBER
C
1010  AMWTG = YNB * 28 + YRB * 121
      VISRV = .00372 + .164E-4 * TR
      VISNV = (30.43 + .4989 * TK - 109.3E-6 * (TK)** 2.0)
     C * 1E-4
      PHIIJ = 1.0/8.0**.5 * (1.0 + (VISNV/VISRV) ** .5 *
     C (121.0/28.0) ** .25) ** 2.0/(1.0 + 28.0/121.0) ** .5
      PHIJI = 1.0/8.0**.5 * (1.0 + (VISRV/VISNV) ** .5 *
     C (28.0/121.0) ** .25) ** 2.0/(1.0 + 121.0/28.0) ** .5
      VISGM = VISNV/(1.0 + YRB/YNB * PHIIJ) +
     C VISRV/(1.0 + YNB/YRB * PHIJI)
C
C
C                  LIQUID SCHMIDT NUMBER
C
1020  DENRL = 34.84D+0 + .02696D+0 * (693.3D+0 - TR) + .834921D+0
     C * (693.3D+0 - TR) ** .5D+0 + 6.02683D+0 * (693.3D+0 - TR)
     C **(1.0D+0/3.0D+0) - 6.55549D-6 * (693.3D+0 - TR) ** 2.0D+0
      DIFCOF = 7.4E-8 * TK * 11/(VISRL * 31.2 ** .6) * 60.0
```

TABLE E-1 (Continued)

```
     C * .00107639D+0 * 60.0D+0 * 2.419D+0
      SCL = VISRL/(DENRL * DIFCOF)
C
C
C                    GAS SCHMIDT NUMBER (N2 - R-12)
C
      SIMPLE = YRB * PATM * 14.7
1030  CALL FREPRO(TR,SIMPLE,DENGR)
      DENGN = PATM * YNB * 28.0/.7302/TR
      DENG = DENGR + DENGN
      EOVKR = 302
      EOVKN = 91.5
      DELR = 4.95
      DELN = 3.681
      EOVKRN = (EOVKN * EOVKR) ** .5
      DELRN = (DELR + DELN)/2.0
      OMEGA  = 1.06036D+0 /(TK/EOVKRN) ** .1561D+0 + .193D+0/EXP(
     C .47635D+0 * (TK/EOVKRN)) + 1.03587D+0/EXP(1.52996D+0 * (
     C TK/EOVKRN)) + 1.76474D+0/ EXP(3.89411D+0 * (TK/EOVKRN))
      B1 = .00214D+0 - .000492D+0 * ((121.0D+0 + 28.0D+0)/
     C (121.0D+0 * 28.0D+0)) ** .5D+0
      COFDIF = B1*TK ** (3.0/2.0)/PATM/DELRN ** 2.0/
     C OMEGA *((121.0 + 28.0)/(121.0 * 28.0)) ** .5 * 60.0 *
     C .00107639D+0 * 60.0D+0
      SCG = VISGM/DENG/COFDIF * 2.419
C
C
C                    OPERATING VOID FRACTION
C
1035  EL = L * AMWTL / DENRL * CSA
      SURTEN = 11.8 * ((693.3 - TR)/193.6) ** 1.25
      EPS2 = 5 * (EL) ** .415 * (VISRL/2.419) ** .13 * (1.0/DENRL)
     C ** .84 * (SURTEN/73) ** .1
      ZL = L * CSA * AMWTL
      ZG = G * CSA * AMWTG
      IF(ZL/ZG.GT.50.0) GO TO 1036
      ZZ = EXP(-.2621D+0 - .05738D+0 * (ZL/ZG) + .001049D+0 * (ZL/ZG)
     C ** 2.0D+0 - .7014D-5 * (ZL/ZG) ** 3.0D+0)
      UMAX = .0942/(VISGM) ** .33 * ((DENRL - DENG)/DENG) ** .57
      CORMAX = UMAX * ZZ
      SG = G/DENG * AMWTG/60.0/60.0
      CF = SG/CORMAX
      DELP = 2.529 * CF ** 2.01
      EPS1 = .0464 * DELP
      GO TO 1037
1036  EPS1 = 0.0
1037  EPS = .949 - EPS1 - EPS2
      FACT = 6.0 / (1.0 - EPS) / 585.0
```

TABLE E-1 (Continued)

```
      REL = FACT * L * AMWTL/VISRL
      REG = FACT * G * AMWTG/VISGM/2.419
C
C
C                  LIQUID SCHMIDT NUMBER (KR)
C
1040  DIFKRL = 7.4E-8 * TK * 11/(VISRL * (92.? * .38) ** .6) * 60.0
     C * .00107639D+0 * 60.0D+0 * 2.419D+0
      SCLK = VISRL/(DENRL * DIFKRL)
C
C
C               MASS TRANSFER COEFFICIENTS
C
1060  FL = DIFCOF * REL ** .45 * SCL ** .5 *8.0 * DENRL/AMWTL/FACT
      FG = COFDIF * REG ** .40 * SCG ** (1.0/3.0) *2.3 * DENG/AMWTG/FACT
      FLKR =8.0 * DIFKRL * REL ** .45 * SCLK ** .5 * DENRL/AMWTL/FACT
1065  A =REG ** .605
      FLA = FL * A
      FGA = FG * A
      FLK = FLKR * A
      RETURN
      END
C
C
C            ROUTINE FOR DENSITY OF R-12 VAPOR
C
      SUBROUTINE FREPRO(T,P,DG)
      IMPLICIT REAL * 8 (A-H,O-Z)
      EXP(X) = DEXP(X)
      ABS (X) = DABS(X)
900   B1 = 0.0065093886D+0
      TR = T/693.3
      XK = -5.475
      F = EXP(XK*TR)
      A = -0.088734D+0 * T
      B = 3.409727134D+0 - 1.59434848D-3 * T + 56.76276710+0 * F
      C = -0.06023944654D+0 + 1.879618431D-5 * T - 1.311399084D+0 * F
      D = 5.48737007D-4
      F = -3.468834D-9 * T + 2.54390678D-5 * F
      VS = 10.731 * T/P/120.93
      VS = VS - B1
910   THETA = P + (A/VS+1.0/VS*(B/VS+1.0/VS*(C/VS+1.0/VS*(D/VS
     C +1.0/VS*(F/VS)))))
      DTHETA = -1.0/VS*(A/VS+1.0/VS*(2.0*B/VS+1.0/VS*(3.0*C/VS
     C +1.0/VS*(4.0*D/VS+1.0/VS*(5.0*F/VS)))))
      VNEW = VS - THETA/DTHETA
      DEL = VNEW - VS
      IF(ABS(DEL).GT.0.0001) GO TO 920
```

TABLE E-1 (Continued)

```
      GO TO 930
920   VS = VNEW
      GO TO 910
930   VG = VNEW+B1
      DG = 1.0/VG
      RETURN
      END
C
C
C                  BISECTION ROUTINE
C
      SUBROUTINE BISECT(DG1,DG2,FLA,FGA,DZ,YNB,XNB,YNI,XNI,DG)
      IMPLICIT REAL * 8 (A-H,O-Z)
      ABS (X) = DABS(X)
      EXP(X) = DEXP(X)
      F(X) = X - (1.0 /(1.0/FLA/DZ + 1.0/FGA/DZ)) * DLOG
     C((DEXP(X/FGA/DZ) * (YNB - XNB) +DEXP(X/FLA/DZ) *
     C ( YNI - XNI) - YNI + XNB)/(YNB - XNI))
      T = 0.0
800   DG = (DG1 + DG2)/2.0
      IF(F(DG1) * F(DG2).GT.0.0) WRITE(6,805)
805   FORMAT('ROOT NOT IN INTERVAL')
      IF(F(DG) * F(DG1) .LE.0.0) DG2 = DG
      IF(F(DG) * F(DG2).LT.0.0) DG1 = DG
      IF(ABS(1.0 - T/DG) .LE..0001) GO TO 810
      T = DG
      GO TO 800
810   CONTINUE
      RETURN
      END
C
C
C                     KR FLUX ROUTINE
C
      SUBROUTINE FLUXK(EOVKR,EOVKN,DELR,DELN,TK,PATM,ISTART,DIFKMX,
     C YKB,YNB,YRB,DG,DGYR,DGYN,A    ,REG,VISGM,DENG,AMWTG,FACT,
     C DZ,XKB,DK,FLK,FGK,DGYK,SCGK,YKI)
      IMPLICIT REAL * 8 (A-H,O-Z)
      EXP(X) = DEXP(X)
      ABS (X) = DABS(X)
700   B10(X) =(DEXP(DG/X/DZ) * (YKB - XKB - YKB *DEXP(DG/FLK/DZ))
     C + XKB)/((DEXP(DG/FLK/DZ) * (PATM/DK - 1.0 - PATM/DK * DEXP
     C (DG/X/DZ))) + 1.0)
      B20(X,Y) = DG * (YKB *DEXP(DG/X/DZ) - Y)/(DEXP(DG/X/DZ)
     C - 1.0)
      B30(X) = (X - YKB * (DGYN + DGYR))/((1.0/DIFKR *
     C (YRB * X - YKB * DGYR)) + (1.0/DIFKN * (YNB * X
     C - YKB * DGYN)))
```

TABLE E-1 (Continued)

```
      FG(X) = A * 2.3  * X * REG ** .40 * (VISGM/DENG/X * 2.419)
     C ** (1.0/3.0) * DENG/AMWTG/FACT
C
C
C                    GAS PHASE SCHMIDT NUMBER
C
710   EOVKK = 190
      DELK = 3.61
      EOVKRK = (EOVKR * EOVKK) ** .5
      EOVKNK = (EOVKN * EOVKK) ** .5
      DELRK = (DELR + DELK)/2.0
      DELNK = (DELN + DELK)/2.0
      OMEGAR = 1.06036D+0 /(TK/EOVKRK) ** .1561D+0 + .193D+0/EXP(
     C .47635D+0 * (TK/EOVKRK)) + 1.03587D+0/EXP(1.52996D+0 * (
     C TK/EOVKRK)) + 1.76474D+0/ EXP(3.89411D+0 * (TK/EOVKRK))
      OMEGAN = 1.06036D+0 /(TK/EOVKNK) ** .1561D+0 + .193D+0/EXP(
     C .47635D+0 * (TK/EOVKNK)) + 1.03587D+0/EXP(1.52996D+0 * (
     C TK/EOVKNK)) + 1.76474D+0/ EXP(3.89411D+0 * (TK/EOVKNK))
      BR = .00214D+0 - .000492D+0 * ((121.0D+0 + 84.0D+0)
     C /(121.0D+0 * 84.0D+0)) ** .5D+0
      BN = .00214D+0 - .000492D+0 * ((28.0D+0 + 84.0D+0)
     C /(28.0D+0 * 84.0D+0)) ** .5D+0
      DIFKR = BR * TK ** (3.0/2.0)/PATM/DELRK ** 2.0/
     C OMEGAR * ((121.0 + 84.0)/(121.0 * 84.0)) ** .5 * 60 *
     C .00107639D+0 * 60.0D+0
      DIFKN = BN * TK ** (3.0/2.0)/PATM/DELNK ** 2.0/
     C OMEGAN * ((28.0 + 84.0)/(28.0 * 84.0)) ** .5 * 60 *
     C .00107639D+0 * 60.0D+0
C
C
C                DIFFUSIVITY ITERATION
C
720   IF(ISTART.EQ.2) GO TO 724
      DIFKM1 = (1.0 - YKB)/(YNB/DIFKN + YRB/DIFKR)
      ISTART = 2.
      GO TO 725
724   DIFKM1 = DIFKMX
725   DFLUX = DG/(DGYR/DIFKR + DGYN/DIFKN)
      IF(DIFKM1.GT..1) DIFKM1 = (DIFKM1+DFLUX)/2.0
      IXXXZ = 20
      SAVE = 10.0
726   FGK = FG(DIFKM1)
      YKI = B10(FGK)
      DGYK1 = B20(FGK,YKI)
      DIFKM2 = B30(DGYK1)
      IF(DIFKM2.LE.0.0) GO TO 798
      FGK = FG(DIFKM2)
      YKI = B10(FGK)
```

TABLE E-1 (Continued)

```
      DGYK2 = B20(FGK,YKI)
      IF(ABS(1.0 - DIFKM1/DIFKM2).LT..001) GO TO 790
      DIFER = ABS(DIFKM1 - DIFKM2)
      IF(DIFER.GT.SAVE) GO TO 799
      IF(IXXXZ.EQ.1) GO TO 799
      SAVE = DIFER
      DIFKM1 = DIFKM2
      GO TO 726
798   IF(DIFKM2.LT.DIFKM1) DIFKM1 = .999 * DIFKM1
      IF(DIFKM2.GT.DIFKM1) DIFKM1 = 1.001 * DIFKM1
      GO TO 726
799   IF(DIFKM2.LT.DIFKM1) DIFKM1 = 1.001 * DIFKM1
      IF(DIFKM2.GT.DIFKM1) DIFKM1 = DIFKM1 * .999
      SAVE = DIFER
      IXXXZ = 1
      GO TO 726
790   DIFKMX = DIFKM1
      SCGK = VISGM/DENG/DIFKMX * 2.419
      FGK = FG(DIFKMX)
      YKI = B10(FGK)
      DGYK = B20(FGK,YKI)
      RETURN
      END
```

VITA

Brant E. Kanak was born in Chicago, Illinois, on May 29, 1954. He attended elementary and secondary schools in Broadview and Maywood, Illinois, graduating from Proviso East High School in 1972. He then entered the University of Illinois at Urbana and was graduated in May of 1976 with a B. S. degree in chemical engineering.

Since that time, he has been employed by the Nuclear Division of Union Carbide Corporation in Oak Ridge, Tennessee, where he is currently in the Systems and Equipment Technology Department of the Enrichment Technology Division at the Oak Ridge Gaseous Diffusion Plant. During this employment, the author pursued a graduate program through the University of Tennessee and received a M. S. degree in chemical engineering in August of 1979.

He is an associate member of the American Institute of Chemical Engineers.